

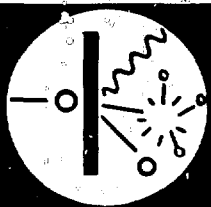
137  
8/29/78

Dr 410

LBL-7950

CONF-771075--

**MASTER**



Proceedings of the  
**SIXTH ANNUAL CONFERENCE  
OF THE INTERNATIONAL NUCLEAR  
TARGET DEVELOPMENT SOCIETY**

October 19-20, 1977



Lawrence Berkeley Laboratory  
University of California  
Berkeley, California

DISTRIBUTION OF THIS DOCUMENT IS UNLIMITED.

Proceedings of the  
**SIXTH ANNUAL CONFERENCE  
OF THE INTERNATIONAL NUCLEAR  
TARGET DEVELOPMENT SOCIETY**

Held at  
Lawrence Berkeley Laboratory  
University of California  
Berkeley, California  
October 19-20, 1977

Compiled by  
Gordon Steers

NOTICE  
This report was prepared as an account of work sponsored by the United States Government. Neither the United States nor the United States Department of Energy, nor any of their employees, nor any of their contractors, subcontractors, or their employees, makes any warranty, express or implied, or assumes any legal liability or responsibility for the accuracy, completeness or usefulness of any information, apparatus, product or process disclosed, or represents that its use would not infringe privately owned rights.

August 1978

file

## FOREWORD

The Sixth Annual Conference of the International Nuclear Target Development Society was held at the Lawrence Berkeley Laboratory, University of California, Berkeley, California, on October 19-21, 1977. There were 34 registrants, 26 from the United States and 8 from foreign countries.

The discussion covered nuclear target preparation by evaporation, reduction of oxides, electrodeposition, reactive sputtering, rolling, gas jets, and related techniques.

The participants were welcomed to the conference by Dr. Bernard Harvey, a director of the Lawrence Berkeley Laboratory. A plan to incorporate the Nuclear Target Development Society, presented by President Dan Riel and the society officers, was approved by the members. Officers elected were: Dan Riel, president; Joanne Heagney, secretary-treasurer; and Don Ramsay, vice president. The board of directors includes: Peter Maier-Komor, Judith Gursky, Jack Stinson, and George Thomas. Munich, Germany, was chosen as the site of the next conference, with Peter Maier-Komor and Hans Maier of the Technical University of Munich and the University of Munich, respectively, as co-hosts.

Dr. Richard Lemmon, Lawrence Berkeley Laboratory, was the featured speaker at a banquet held on the second day of the conference. Dr. Lemmon spoke on prebiological synthesis. On the third day, tours were conducted of the Stanford Linear Accelerator and the Lawrence Berkeley Laboratory.

These proceedings contain 23 conference papers; as noted in the text, some of the papers were not presented orally. Papers are reproduced as received from the authors.

I wish to thank Paul Hernandez and Tom Lewis of the Lawrence Berkeley Laboratory for their initial approval and generous support of the conference program and for publishing these proceedings.

Gordon Steers  
Conference Chairman

TABLE OF CONTENTS

	<u>Page</u>
<u>Session A</u>	
<i>Chairman, Edward Kobilsk</i>	
A-1 Preparation and Characterization of $^{241}_{95}\text{Am}$ and $^3_1\text{H}$ Targets H. L. Adair . . . . .	1
A-2 Lifetimes of Carbon Stripping Foils G. E. Thomas, P. K. Den Hartog, J. J. Bicek, and J. L. Yntema . . . . .	17
A-3 Rolling Thin Uranium Foils and Other Exotic Isotopic Metals E. Kellner and P. Maier-Komor . . . . .	27
A-4 A Simple, Efficient Method for Reducing Small Quantities of Zinc Oxide J. M. Heagney and J. S. Heagney . . . . .	35
<u>Session B</u>	
<i>Chairman, Peter Maier-Komor</i>	
B-1 Optimum Collection Time for Short-Lived Isotopes Jerome Lerner . . . . .	37
B-2 Hydriding of Titanium Cones for a Sputter-Ion Source Judith C. Gursky and Boyd A. Sherwood . . . . .	53
B-3 Nitrogen Targets Produced by Reactive Sputtering of Tantalum and Titanium J. D. Stinson . . . . .	59
B-4 Uranium Sandwich Targets of 0.1 to 100 $\text{mg}\cdot\text{cm}^{-2}$ Prepared by Electron Beam Gun Evaporation Helmut Folger and Josef Klemm . . . . .	69
B-5 Preparation of 3/4" Dia. Self Supporting $^{182}\text{W}$ and $^{184}\text{W}$ Targets for Cyclotron Bombardment C. E. Ellsworth . . . . .	79
B-6 A High Density Windowless Gas Jet Target W. Tietsch, H. Feist, K. Bethge, and E. Schopper . . . . .	81

Session C*Chairman, Judith Gureky*

C-1	Gallium Rich Ga <sub>2</sub> O Targets for Use at Room Temperature from Isotopic Ga <sub>2</sub> O <sub>3</sub> Starting Material William D. Riel . . . . .	101
C-2	Preparation of Isotopically Enriched, Self Supporting Chromium Targets H. U. Friebe, Dagmar Frischke, R. Großmann and H. J. Maier . .	105
C-3	A Dry Powder Technique for the Preparation of Carbon Foils W. R. Lozowski . . . . .	115
C-4	A Heavy Ion Sputtering System With A Penning-Ion-Source H. Baumann and H. L. Wirth . . . . .	121
C-5	Preparation of Self-Supporting Platinum Targets by Electrodeposition M. A. Saettel . . . . .	129
C-6	Preparation of Rare Actinide Targets for Accelerator Bombardment Ron Loughheed . . . . .	*
C-7	Preparation of Targets By Electrodeposition T. L. Morgan . . . . .	139

Session D<sup>†</sup>*Chairman: Dan Riel*

D-1	A Method for the Preparation of Cadmium Isotopic Targets J. L. Gallant and D. Yaraskavitch . . . . .	141
D-2	Thin Carbon Foil Breakage Times Under Ion Beam Bombardment A. E. Livingston, H. C. Berry and G. E. Thomas . . . . .	149
D-3	Distribution of Carbon Surface Density Evaporated by a Carbon Arc V. Olivas, J. O. Stoner, Jr., and S. Bashkin . . . . .	159
D-4	Mounting a Very Large Carbon Foil John O. Stoner, Jr. and Stanley Bashkin . . . . .	165
D-5	Calibration of Surface Densities of Metal Films by Optical Transmittance Mark Rhoads, John O. Stoner, Jr., and Stanley Bashkin . . . . .	169

	<u>Page</u>
D-6 Vacuum Tight <sup>208</sup> Pb Foils A. Meens . . . . .	173
<u>List of Registrants</u> . . . . .	181

---

\*Manuscript not received in time for publication.

†Indicates papers not given orally.

PREPARATION AND CHARACTERIZATION OF  $^{241}_{95}\text{Am}$  AND  $^3_1\text{H}$  TARGETS\*

H. L. Adair

Oak Ridge National Laboratory  
Oak Ridge, Tennessee 37830

## INTRODUCTION

The Isotope Research Materials Laboratory (IRML) at the Oak Ridge National Laboratory (ORNL) was established in 1960 to provide high-purity materials (usually isotopic) for various areas of research. The samples range from very thin to very thick backed or self-supporting stable or radioactive materials. Our initial emphasis was on stable isotopic materials, but the demand for radioactive samples of various forms has, in the past two years, exceeded the demand for stable targets. This was brought about mainly as a result of increased emphasis on reactor technology. Many actinide deposits have been required for determining precise neutron cross sections for fuel burn-up and neutron dosimetry applications. High purity actinide metals have been required for material property studies.

A large part of the radioactive sample preparation by IRML involves the fabrication of tritium targets. The tritium targets are used by researchers as a source of 14 MeV neutrons which are obtained from the D-T reaction  $[^3_1\text{H} (^1_1\text{H}, ^1_0\text{n}) ^4_2\text{He}]$ . The 14 MeV neutrons are normally used in materials irradiation and testing experiments.

---

\* Research sponsored by the Department of Energy under contract with Union Carbide Corporation.

Procedures for fabricating americium oxide, americium metal, and both small and large area tritium targets are described. Performance data for some of the larger area tritium targets are presented.

#### ACTINIDE TARGET PREPARATION

The fabrication of actinide deposits is easily accomplished by the vacuum evaporation of the actinide oxides. (1, 2) The material to be deposited, whether it be  $\text{AmO}_2$  or any of the other actinide oxide compounds, is pressed into approximately 0.5-in. diameter pellets and placed in the crucible of an electron beam gun as shown in Fig. 1. The electron beam gun is located in a vacuum system which is contained in a glove box system as shown in Fig. 2. The glove box is operated at  $\geq 0.35$  in. negative pressure with respect to the laboratory to prevent the escape of highly radioactive material to the laboratory environment. The targets are properly masked and rotated directly above the source. The uniformity requirements dictate the source to substrate distances. Since most of the material evaporated is in short supply and is very expensive, the material that is not deposited on the substrate can be chemically reclaimed from the substrate mask and quartz cylinder positioned between the source and substrate.

The amount of material deposited on substrate materials of aluminum and titanium has varied from a few  $\mu\text{g}/\text{cm}^2$  to  $\geq 5 \text{ mg}/\text{cm}^2$ . The amount of material deposited is determined both by directly weighing the target or by low geometry alpha counting. The  $^{241}\text{AmO}_2$  deposits are normally counted in a low geometry alpha counting system in which the geometry factor can be varied from  $10^{-2}$  to  $10^{-7}$ . The geometry factor is determined either by using standard sources or by destructively analyzing a target of the same material and dimensions of

interest. This permits the  $^{241}\text{Am}$  content in the  $^{241}\text{AmO}_2$  targets to be defined to  $\leq \pm 1\%$ .

High purity actinide metals from those materials which have a reasonable vapor pressure at their melting points can be prepared by a vacuum reduction-distillation technique. One major advantage of this technique over, for example, the bomb reduction technique is that a purification of the final product metal can be achieved by first distilling away the more volatile components before distilling the desired material. This reduction-distillation technique has been previously described, thus I will only briefly summarize the steps involved.<sup>(3, 4)</sup> The actinide oxide is mixed with ~25-50 percent stoichiometric excess of a suitable reductant such as thorium. The material is pressed into a pellet and placed inside a tantalum still. Radiofrequency heating is used to heat the still in a vacuum of  $10^{-6}$  torr and drive off the desired metal component which is collected in a quartz dome. The resultant metal is easily removed from the quartz. A typical distillation experiment is shown in Fig. 3.

During the past year a large quantity of high purity  $^{241}\text{Am}$  was needed for material property measurements. This metal was prepared by the vacuum reduction-distillation technique described above. A total of 187.6 g of  $\text{AmO}_2$  was reduced with a 30% excess of thorium during a total of seven reduction-distillation operations. The product metal was arc melted and cast into a

1.8-cm diameter copper mold. The rough casting was then machined to 1.75-cm diameter x 2.30-cm long (Fig. 4). The final  $^{241}\text{Am}$  cylinder weight was 73.69 g which gave a density of  $13.29 \text{ g/cm}^3$ . A total of 165.0 g of metal was collected from the starting 187.6 g of  $\text{AmO}_2$  which gave a reduction efficiency of 76%.

#### TRITIUM TARGET PREPARATION

For several years IRML has been preparing large area (~23 cm diameter) tritium targets for use in materials experiments being conducted at Lawrence Livermore Laboratory (LLL). These targets are used to provide an intense source of 14 MeV by the D-T reaction [ $^3_1\text{H} (^2_1\text{H}, ^1_0\text{n}) ^4_2\text{He}$ ]. Even larger targets (~51 cm diameter) are needed in the future to evaluate component materials that will be used in controlled thermonuclear reactor environments. Since 1960, IRML has prepared tritium targets using various base materials such as zirconium, titanium, as well as most of the rare earth materials including erbium. In terms of average neutron output and target lifetime, titanium appears to be the best base material.

The titanium is evaporated onto the appropriate substrate material by electron bombardment heating. A schematic of the setup used for the LLL 23 cm targets is shown in Fig. 5. The sequence of steps in the evaporation

process after the substrate has been installed in the vacuum system and the system pumped down to  $\leq 10^{-6}$  torr are:

- 1) Heat the rotating substrate to  $\sim 400^{\circ}\text{C}$ .
- 2) Obtain a steady titanium evaporation rate and then open the shutter.
- 3) Evaporate titanium until the quartz oscillating crystal thickness monitor indicates that the proper titanium thickness has been obtained.
- 4) Cool the system down and let it up to atmospheric pressure with argon.

The copper alloy titanium coated targets are then removed from the vacuum system and transferred (in an argon atmosphere) to the tritium system. A schematic of the tritium system is shown in Fig. 6. The target is installed in the all-metal vacuum pumped tritium system and evacuated to  $\leq 10^{-8}$  torr. The target is then heated to  $450^{\circ}\text{C}$ , the pump is valved off and a tritium chamber pressure of  $\geq 300$  mm is obtained by heating tritium storage traps, which are filled with uranium, to  $500-600^{\circ}\text{C}$ . The target chamber is then valved off and the target is left at  $450^{\circ}\text{C}$  for one hour in the tritium atmosphere. After one hour the target heaters are turned off and the target is allowed to cool to  $< 200^{\circ}\text{C}$  before the uranium storage traps are opened to absorb the remaining residual tritium. The system is then let up to atmosphere with

argon. The resulting tritium targets are removed from the vacuum chamber, inspected to see that the base material has not blistered during the tritiation process, and then the uniformity of the tritium absorbed by the titanium is measured with an ion chamber. The ion chamber has a small opening (~1.3 cm diameter) and by placing it at various locations on the surface of the target and reading the corresponding ion current produced by the beta disintegrations from the tritium, the uniformity of the absorbed tritium in a thin titanium surface layer can be obtained. A typical uniformity measurement of one of the LLL 23 cm targets is shown in Fig. 7. The amount of tritium contained in each target can be determined quantitatively by destructively analyzing small test targets that are prepared simultaneously with the large targets. In most every case, the tritium to titanium atom ratio is  $\geq 1.5$  to 1.

The performance of thirty-one 23-cm diameter LLL tritium targets bombarded with 400 keV at a current of 15 mA has been monitored and some important parameters are shown in the table below.

IRML Tritium Targets Provide High Intensity Neutrons for  
Long Time Periods\*

<u>Target No.</u>	<u>Initial Yield N/μA</u>	<u>Average Yield N/μA (x 10<sup>15</sup>)</u>	<u>Total Target Neutron Yield (x 10<sup>18</sup>)</u>	<u>Target Usage μA-hrs</u>
1	3.5 x 10 <sup>11</sup>	0.91	1.58	1700
2	2.15 x 10 <sup>11</sup>	0.87	2.98	3400
3	2.6 x 10 <sup>11</sup>	0.78	1.22	1550
4	2.9 x 10 <sup>11</sup>	0.85	1.50	1780
5	2.6 x 10 <sup>11</sup>	0.78	0.95	1225
6	3.0 x 10 <sup>11</sup>	0.90	1.90	2100
7	2.55 x 10 <sup>11</sup>	0.85	1.30	1500
8	2.65 x 10 <sup>11</sup>	0.93	1.10	1100
9	4.20 x 10 <sup>11</sup>	0.82	0.80	1025
10	3.10 x 10 <sup>11</sup>	0.96	1.20	1225
11	2.50 x 10 <sup>11</sup>	0.80	1.91	2400
12	2.40 x 10 <sup>11</sup>	0.78	0.95	1225
13	2.20 x 10 <sup>11</sup>	0.77	0.20	300
14	2.80 x 10 <sup>11</sup>	0.70	0.80	1100
15	3.15 x 10 <sup>11</sup>	0.91	1.19	1300
16	2.30 x 10 <sup>11</sup>	0.63	0.80	1225
17	2.25 x 10 <sup>11</sup>	0.72	0.75	1000
18	2.20 x 10 <sup>11</sup>	0.70	0.82	1190
19	2.90 x 10 <sup>11</sup>	0.89	1.00	1125
20	2.50 x 10 <sup>11</sup>	0.76	0.90	1150
21	2.15 x 10 <sup>11</sup>	0.74	2.20	2980
22	2.40 x 10 <sup>11</sup>	0.76	1.12	1450
23	2.85 x 10 <sup>11</sup>	0.85	1.29	1500
24	2.40 x 10 <sup>11</sup>	0.82	1.04	1290
25	3.10 x 10 <sup>11</sup>	0.91	2.30	2500
26	3.35 x 10 <sup>11</sup>		0.60	500
27	2.65 x 10 <sup>11</sup>	0.85	1.59	1850
28	2.85 x 10 <sup>11</sup>	0.95	1.05	1100
29	2.75 x 10 <sup>11</sup>	0.90	0.90	1000
30	2.50 x 10 <sup>11</sup>	0.83	0.95	1100
31	2.80 x 10 <sup>11</sup>	0.83	1.12	1325

\* Data supplied by C. Logan, LLL.

IRML is well aware that the tritium targets produced probably are not optimum. There are many variables involved and the procedure presently being used has evolved over the past sixteen years of tritium target fabrication. At present, funding is not available to conduct a systematic study to try to optimize tritium target fabrication.

#### SUMMARY

Many radioactive samples are prepared by IRML to support various areas of research. This paper describes actinide oxide deposits in support of reactor technology, high purity  $^{241}\text{Am}$  metal fabrication for material property studies and tritium target fabrication in support of materials research conducted at LLL.

#### REFERENCES

1. H. L. Adair, J. R. Gibson, E. H. Kobisk, and J. M. Dalley, "Vapor Deposition of Large Area  $\text{NpO}_2$  and  $\text{UO}_2$  Deposits," Presented at the 5th Annual Conference, International Nuclear Target Development Society, LASL, Oct. 19-21, 1976, Los Alamos, New Mexico.
2. H. L. Adair, Nucl. Inst. and Methods 113 (1973) 545-548.
3. E. H. Kobisk and W. B. Grisham, Mater. Res. Bull. 4, 651 (1969).
4. H. L. Adair, J. Inorg. Nucl. Chem., 1970, Vol. 32, pp. 1173-1181.

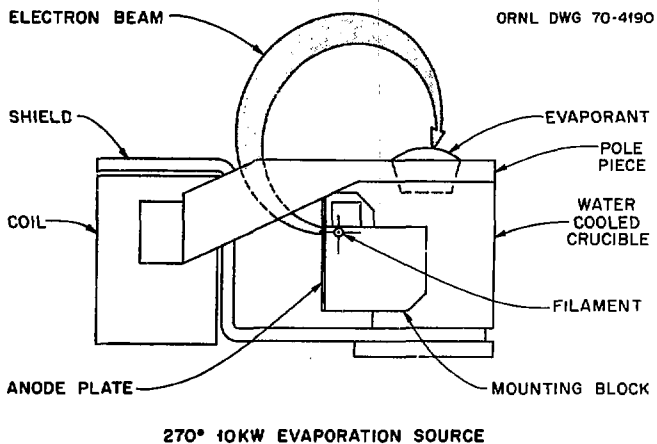


Figure 1. Commercial electron beam gun used for fast evaporation of actinide oxides.



Figure 2. Radioactive glove box system used for containing actinide oxide materials from laboratory environment.

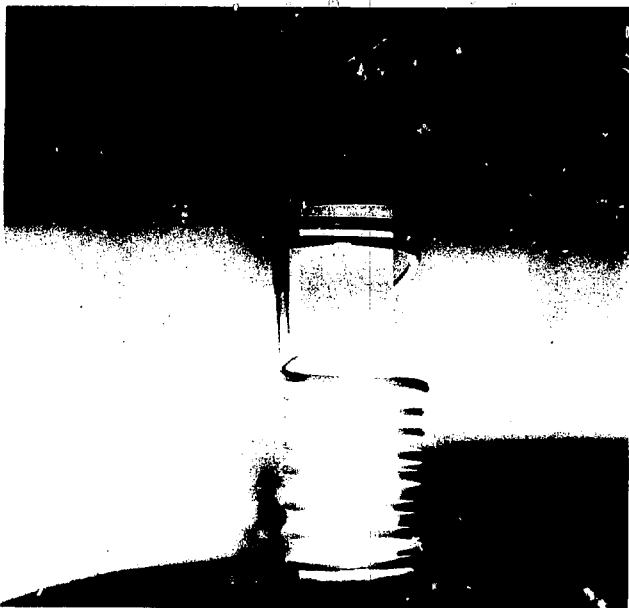


Figure 3. Vacuum reduction distillation procedure requires minimal equipment.



Figure 4. High purity  $^{241}\text{Am}$  metal cylinder machined in protective atmosphere.

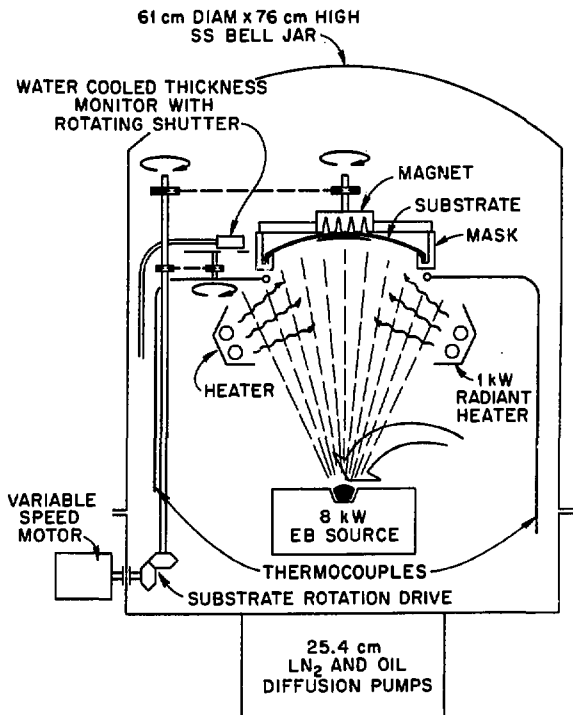


Figure 5. Evaporation system used for preparing adherent, uniform titanium deposits.

ORNL-DWG 77-18073

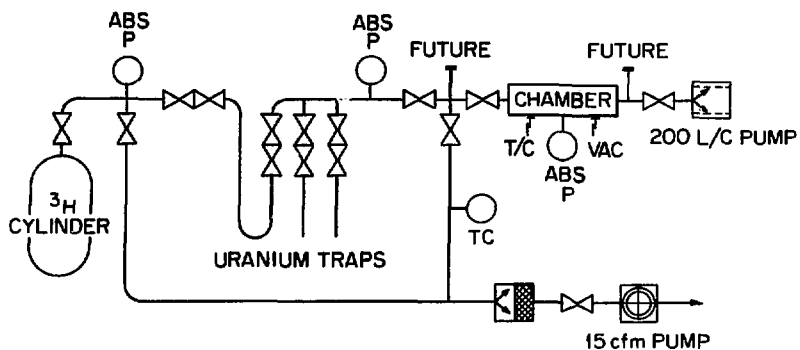


Figure 6. Tritium system used for preparing large area tritium targets.

ORNL-DWG 77-18072

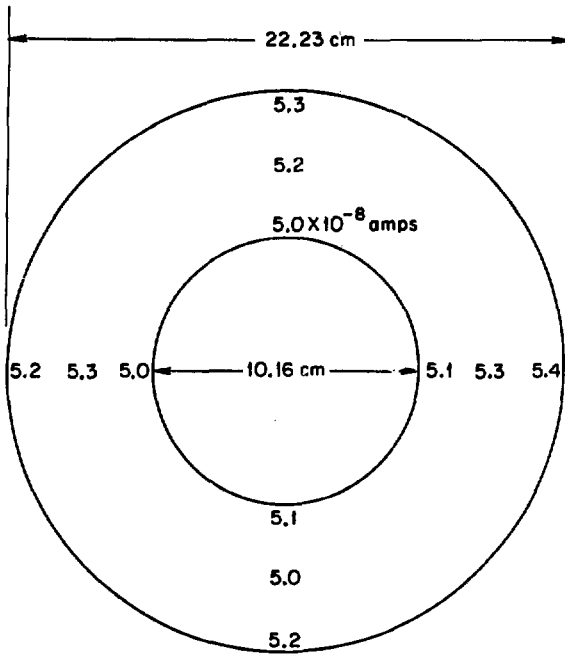


Figure 7. Ion chamber measurements indicate homogeneous tritium distribution in large area LLL targets.

### Lifetimes of Carbon Stripping Foils

G. E. Thomas, P. K. Den Hartog, J. J. Bicek, and J. L. Yntema  
Argonne National Laboratory, Argonne, Illinois 60439\*

Measurements have been made to determine the lifetimes of  $5 \mu\text{g cm}^{-2}$  carbon targets when bombarded by 3-MeV  $\text{Kr}^+$  ions. Stationary, orbiting, and heated targets were tested using both constant and intermittent beams. Preliminary results indicate some lifetime amplification by the use of these devices. There will be an informal discussion of these results.

#### Introduction

It has been previously pointed out by Yntema,<sup>1-3,6,7)</sup> Dobberstein and Henke,<sup>4)</sup> Whitmell et al.,<sup>5)</sup> Frick et al.,<sup>8)</sup> Yntema and Nickel,<sup>9)</sup> and others, that the use of heavy ion particles with accelerators may seriously reduce the lifetimes of carbon stripper foils. It has become increasingly evident that it is quite important to either find a method to extend the carbon foil lifetime when using heavy ion beams or to develop a new type of stripping foil. Progress has been made in developing a system using a fine spray of carbon as a stripper.<sup>10)</sup> Also, carbon stripper foil arrays have been designed using as many as  $\sim 900$  foils in one loading.<sup>11)</sup> However, this does not totally eliminate the problem of having the beam frequently interrupted while a foil is changed.

At Argonne, Yntema has found a significant increase in lifetime by either foil heating, giving it a slow circular motion, or a combination of both. Others such as Dobberstein and Henke,<sup>4)</sup> and Whitmell et al.<sup>5)</sup> have had less success with these methods of increasing foil lifetime. In this paper we report results of additional experiments done at this laboratory.

### Experiment

In the basic experimental arrangement shown schematically in Fig. 1, the Argonne Dynamitron was used as a source of 3-4 MeV ions of either Argon, Nickel, or Krypton. A four-jaw slit was used to collimate the beam to a size of  $\sim 2 \times \sim 2$  mm as seen on a quartz plate at the Faraday cup at the rear of the experiment. The Faraday cup was used first to measure the unstripped beam current and then to monitor the current while determining the lifetime of the foil. During each run there was a darkening of the foil in the area hit by the beam and a corresponding increase in current, indicating a possible thickening of the foil. This is due either to carbon contamination in the beam line or may also result from migration of the carbon within the foil toward the beam spot, or radiation damage. When the foil broke there was a sudden drop in current due to the change in the charge state distribution. The current measurement was also used as a method to determine the time when the stripping effectiveness was reduced to 75% of its initial value. Using the T. V. camera, the foil could be viewed remotely. Coincident with the current drop, the tear in the foil appeared on the T. V. screen as a bright spot.

An annular furnace was used to heat the foil to a given temperature. The optical pyrometer and thermocouple used measured the temperature of the furnace and its environment, but not necessarily that of the foil itself.

The motor used to move the foil with a slow circular motion had a speed of one revolution per minute.

### Results

The experimental results are summarized in Table I. The reduced lifetime of a foil in a stationary position and in a room temperature environment is 0.4 - 0.5 min. Two sets of measurements using different experimental parameters were made. These results are in good agreement with those obtained earlier in experiments by Yntema.<sup>3)</sup>

Two important observations concerning the method of foil breakage were observed. Firstly, an unheated foil usually broke completely and instantly. Secondly, a heated foil in most cases initially had a small tear appear near its edge, gradually increasing in size until the foil was no longer useable.

Heating the carbon foil and graphite support frame to an ambient temperature of  $450 \pm 150^\circ \text{C}$  increased its lifetime by about a factor of 4. Moving the foil with a circular motion so that the beam progressed around the edge of the foil at a speed of about one revolution per minute extended its lifetime by about a factor of 3. It is possible that moving the foil at a different speed might further increase its lifetime.

Simultaneously heating the foil and moving it with a circular

motion extended its lifetime by about a factor of 6. It is important to note that this value is the initial breaktime and not that for 75% stripping effectiveness. As the beam crossed the torn area the measured current dropped significantly and then returned to normal when the torn area was rotated out of the beam path. For any particular experiment, it must be determined if, or to what extent, this periodicity is tolerable. As a result, the lifetime could either be extended greatly or not at all beyond that mentioned above.

Experiments have been performed in which the beam was on and off for equal times. Periods of sixty seconds have produced encouraging results while six second periods showed very little improvement in foil lifetimes. The longer cycling times may afford the foil a relaxation time. This relaxation time may also be a contributing factor in the increased lifetimes for foils which are moved. This is in addition to the larger foil area one obtains when moving the foil.

#### Summary

Although this work is not complete and there is much yet to be done, there are several important results to be reported. First, room temperature foils tend to break suddenly and over most of the area while heated foils tear along an edge and the tear increases gradually in size. Heating or moving carbon foils or a combination of both significantly increases their lifetime. The explanation of our differences in lifetime versus those obtained in earlier work by Yntema for a combination of

heating and moving the foils with a circular motion may be that in the earlier work the particular foil did not tear in a place seen by the beam or that their interpretation of when it was still a useable foil was different than in this experiment. Also, having the beam on and off for sixty second periods does increase the foil lifetime.

Footnotes and References

\* Work performed under the auspices of the U. S. Department of Energy.

1) J. L. Yntema, Nucl. Instrum. Methods 98, 379 (1972).

2) J. L. Yntema, Nucl. Instrum. Methods 113, 605 (1973).

3) J. L. Yntema, IEEE Trans. Nucl. Sci. NS-23 (2), pp. 1133-1136  
(April 1976).

4) P. Dobberstein and L. Henke, Nucl. Instrum. Methods 119, 611 (1974).

5) D. S. Whitmell, B. H. Armitage, D. R. Porter, and A. T. G. Ferguson  
in Proceedings of International Conference on the Technology of Electrostatic  
Accelerators, Daresbury, 4-7 May 1973, Edited by W. T. Aitken and  
N. R. S. Tait (Science Research Council, Daresbury Nuclear Physics  
Laboratory, 1973) pp. 265-274.

6) J. L. Yntema in Proceedings of the Fourth Annual International Conference  
of the Nuclear Target Development Society, Argonne National Laboratory,  
Sept. 30, Oct. 1-2, 1975, Edited by G. E. Thomas and F. J. Karasek  
(Argonne National Laboratory, 1976 Report ANL/PHY/MSD-76-1) pp. 188-192.

7) J. L. Yntema,

8) G. Frick, V. Chaki, B. Heusch, Ch. Richard, P. Wagner, Stripping Experiments in Carbon Foils With Heavy Ions in the Energy Range of 0.4–0.9 MeV/A, Centre de Recherches Nucleaires, Strasbourg, France, CRN/PN 77-9 (1977).

9) J. L. Yntema and F. Nickel, to be published.

10) D. R. Burch, J. S. Cramer, and P. B. Cramer, Annual Report University of Washington at Seattle (1975) pp. 18–20.

11) I. Fergenbaum, Brookhaven National Laboratory, private communication.

CARBON STRIPPER FOIL LIFETIMES

Mode	Number of Runs	Dynamitron Voltage <sup>(a)</sup> (Me V)	I PμA mm <sup>-2</sup>	Initial Break Time (min)	75% Stripping Time (min)	
					Actual	Reduced <sup>(b)</sup>
Stationary Room Temp. Series I	2	3.5	0.2	2	2	0.4
Stationary Room Temp. Series II	8	3.0	0.125	4	4	0.5
Stationary Heated	4	3.5	0.2	5	8	1.6
Orbited	6	3.0	0.125	9.5	9.5	1.2
Orbited and Heated	3	3.0	0.125	21 <sup>(c)</sup>		2.6

(a) Krypton Beam

(b) Actual 75% stripping time x I

(c) See text

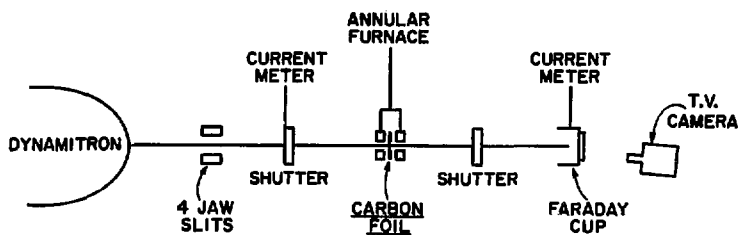


Figure 1. Schematic drawing of the experimental arrangement used for determining carbon foil lifetimes. The source of particles was the Argonne Dynamitron.

## ROLLING THIN URANIUM FOILS AND OTHER EXOTIC ISOTOPIC METALS

E. Kellner, P. Maier-Komor

Physik-Department, Techn. Universität München, Germany

## ABSTRACT

Rolled target foils withstand due to their crystalline structure longer a heavy ion beam than evaporated targets. This fact is important for experiments with very heavy ions available now at the SUPER HILAC at Berkeley or at the UNILAC at Darmstadt, Germany. Because the crystalline disorientation of the targets by the heavy ion beam requires a frequent target exchange to prevent a deterioration of the energy resolution, we developed a method to produce large quantities of rolled targets with thicknesses below  $1\text{mg}/\text{cm}^2$ .

As an example results of some new techniques for producing rolled uranium metal foils will be reported. The metal has been purified by zone melting using a well focused electron beam, a softer metal practically without local defects due to impurities has been obtained. Ductility, crystalline structure and low surface roughness of special stainless steel jackets lead to a more uniform pressure during the rolling process and therefore to a high homogeneity of the foils. The number of pinholes in the targets caused by dust particles is reduced using a laminar flow box. Humidity and oxygen content are decreased by using dry nitrogen in the laminar flow box to prevent oxidation of the foils.

With these techniques Uranium targets below  $1\text{mg}/\text{cm}^2$  were obtained. First results about their behavior in a heavy ion beam will also be reported.

## INTRODUCTION

Due to their crystalline structure rolled target foils can withstand longer a high energy heavy ion beam than evaporated targets. This is an important fact for experiments with very heavy ions available now at the Super Hilac in Berkeley or at the Unilac in Darmstadt, Germany.

What is the reason for this difference in lifetime?

Usually the target material is evaporated on a substrate which is held at temperatures below  $700^{\circ}\text{K}$ . This temperature however is in most cases too low to allow the atoms to migrate enough and thus prevents the formation of complete crystals. So there are regions in evaporated targets which show a highly disordered crystalline structure. The atoms in these regions have many degrees of freedom. The phonon excitation in the crystals stimulated by the huge energy loss of the heavy ions leads to crystalline transformations in the more amorphous regions. Some areas of the target contract others expand due to this crystalline distortion. The wrinkles in the foil around the beam spot finally result in a destruction of the target. For rolled target foils however the destruction occurs at a much higher dose of heavy ions. The explanation of this effect is, that the structure of the rolled target foils is more crystalline and therefore the density of Frenkel defects is much lower. To knock out an atom from its lattice place the Wigner energy is needed. This is for metals between 10 and 40eV, and is much higher, than the energy to throw out atoms from interstices or scatter atoms in Frenkel holes.

The idea to heat the substrates to much higher temperatures to overcome this crystal structure problem in evaporated targets must be disregarded, because the diffusion of the target material in the parting substance produces high impurities, which besides lead to a very brittle target.

Because of this remarkable difference between evaporated and rolled targets, experiments with intense heavy ion beams should be done with rolled target foils. We therefore tried to improve the old methods of rolling targets, for making better and thinner targets with lower expenditure of time.

#### EXPERIMENTAL

Before starting the rolling procedure it is very important to have as raw product a metal bead of the target material free from impurities. The first procedure is converting the isotopic compound to its metallic form. The standard methods of reduction are used. The next point is to clean and solidify the metals. For metals with high vapor pressure below the melting point, one can use the distillation-condensation method described by Ed Kobisk for Magnesium on the Harwell Conference in 1965. But the first 10% of the material should evaporate through the open hole to get rid of impurities with still higher vapor pressures. Then the evaporation temperature should be held as low as possible to keep the impurities with higher vapor pressures in the crucible. Metals with low vapor pressures at the melting point should be melted with the induction levitation melting technique or which is much easier in a water cooled copper crucible with an electron gun.

The older method of pressing the metal powder and sintering it under vacuum shows severe disadvantages. The defects at the grain boundaries set an early limit during the rolling process. Arc melting has disadvantages to, there maybe many gaseous impurities in the processed metal bead, which can be explained by a simple comparison:

An extreme clean gas for arc melting with an impurity of only 1ppm is comparable to a poor vacuum of  $10^{-3}$  Torr.

The metals are melted in portions from 50 to 500 mg in a water cooled copper crucible with an electron gun keeping the temperature just above the melting point. It will be observed with a quartz crystal thickness monitor at a distance of about 10 cm when the metal droplet is nearly free of contaminations with higher vapor pressures. To get also rid of impurities with lower vapor pressures we tried several modified zone melting techniques. For Uranium we milled a 2 mm wide 2 mm deep and 30 mm long groove in the water cooled copper crucible of an electron gun with magnetic deflection. Reducing the current in the coil we swept the 2 mm long electron beam over an Uranium rod with 2 mm in diameter, which was lying in the groove. But with every sweep the Uranium rod became shorter and shorter. The final result was a droplet. No zone refining took place, because the surface tension of Uranium and most liquid metals is too high to succeed with this method.

With the second method we had more success: We used a gun with an electrostatic deflected electron beam with 70% of the power concentrated on a 2 mm diameter spot. After melting the pressed metal powder into a droplet the power of the electron gun has been very slowly reduced. In doing so the drop solidified starting with the zone nearest to the water-cooled crucible. The part of the drop which solidified last was formed like a stalagmite and was highly enriched with impurities. After venting with argon this stalagmite can be cut away and the procedure can be repeated. For Uranium we did this about 10 times. The result was an Uranium bead, shiny like nickel for several days.

Rolling and pack rolling are two completely different methods.

With a normal sheet-rolling mill and assuming the mill is accurately designed the homogeneity of the machined foil is practically only a function of the solid state data of the processed metal piece.

In pack rolling for target fabrication the situation is much more complex: The machined metal piece does not see the two rolls, but it notices every inhomogeneous area on the sandwich foils. The standard sandwich sheets for rolling most isotopic metals are stainless steel. But there are a multitude of different kinds of stainless steel. For rolling metals with a ductility lower than nickel or iron one should take as sandwich material a stainless steel with a high carbon content named spring steel band. This material has a higher temper due to its carbon content of about 0.1%. All other stainless steel sandwiches should be made of a Chrom-Nickel steel with extreme low carbon content. There are some materials available with a carbon content below 0.03%.

What should be the thickness of the stainless steel sheets ?

We noticed that material with a thickness of 0.5 mm or below gave the best results. This can be explained by the industrial selection process of materials for sheet with small thicknesses: Even stainless steel with the same material number behaves different when machined on cold rolling-mill trains. An expert decides which charge can subsequently worked into the thinnest sheets.

So these sheets have the highest homogeneity. This material should be bright-annealed in an inert gas atmosphere and be dressed in a temper pass mill, to get a highly polished oxide-free surface. The surface roughness for the best quality material is of the order of 0.05 to 0.1  $\mu$  which means the peak heights are for example 100  $\mu\text{g}/\text{cm}^2$  thick for nickel or 200  $\mu\text{g}/\text{cm}^2$  for gold.

This surface roughness may be reduced by electropolishing in a galvanic bath. We tried this method, but in our case the rolled foils with electropolished sandwiches did not show a significant better structure. A higher polished sandwich gives not automatically a more homogeneous target. Rolling a target in a stainless steel jacket one will notice

that after a few reduction passes the surface roughness of the sandwich will have increased, the surface looks in a magnifying glass like the peel of an orange with no significant indication on the original surface roughness. The so called grain disintegration is caused by the high pressure during the rolling process and means that the axes of the small crystals have different angles relative to the surface. The compressibility is a function of this angle.

This grain disintegration is large for stainless steels with high carbon content and small for stainless steels with low carbon content. That is the reason why we suggest to use stainless steels with low carbon content.

When rolling it was often noticed especially when a target foil has been already very thin that it was suddenly divided into two or more pieces by a line on the sandwich in the original rolling direction of the sandwich sheet.

These lines are strictly parallel and always along the texture of the sheets, which can be seen when electro-polishing the stainless steel sheets. The source of these inhomogeneities are the scales which remained on and in the ingot before machining it to cold rolled band steel. Vacuum melted stainless steel does not have these impurities. Cold rolled stainless steel band made of vacuum melted material is commercially available for the qualities with very low carbon content. We use it for the inner part of our double sandwich.

The rolling procedure is described for the example of uranium: First the uranium bead prepared as described before is pelletized under vacuum in a pressing tool with a hydraulic pressure of  $10^5$  N/cm<sup>2</sup>. Then the rolling procedure is started on a work bench for a six rolls mill and a two rolls mill, which is a part of a laminar flow box against dust

particles. To reduce oxidation of the uranium foils we blow dry nitrogen through a hose coupling in the input of the laminar flow blower. The dry nitrogen is produced by heating liquid nitrogen.

After cleaning the stainless steel bands in an ultrasonic bath the stainless steel jackets are produced in the left side of the laminar flow box. First the steel band is cut with pneumatic driven guillotine shears to suitable sizes. Then two pieces each 0.5 mm thick are spot welded on one side cleaned again from dust by blowing Argon with a pistol-type nozzle into the jacket. The pellet or the foil is placed in the center of the jacket, which is then closed on all sides by spot welding. This jacket can be passed through the rolling mill and reduced by about 3 to 10% per pass. When the jacket increased its size by approximately a factor of two the foil is placed in a new jacket. When the Uranium foil has a thickness of 5 to 10 mg/cm<sup>2</sup> the double sandwich method is used. We prepare a smaller jacket with a thickness of 0.1 to 0.2 mm of the vacuum melted stainless steel sheets in which the uranium foil is enclosed. This jacket is then placed in a 0.5 mm sheet jacket which is also closed by spot welding, and the rolling process continues. Also in this case the increase in the size of the jacket should not exceed the factor of 2.

If oxidation on the surface of the Uranium foil is observed it should be etched with diluted nitric acid of the best quality, because all metal impurities in the acid will be caught by the Uranium foil due to its very negative electro-chemical potential of -1.8 volts. After cleaning in oxygen free distilled water and ethanol the foil is annealed between two Tantalum sheets which are heated by an alternating current. The annealing lasts for

about half an hour in a vacuum of  $10^{-7}$  Torr at a temperature below  $930^{\circ}\text{K}$ , which was chosen to prevent phase transitions. With these methods we obtained Uranium foils with a thickness of at least  $800 \mu\text{g}/\text{cm}^2$ .

To give another example how good this technique works, we produced also  $130 \mu\text{g}/\text{cm}^2$  Molybdenum foils, and this without any hot rolling.

In the first experiments the Uranium foils were destroyed by a heavy ion beam during the first 1 or 2 hours. The monitor spectrum showed almost pure Uranium oxide. In the beginning we could not explain this effect, because the Uranium foils looked metallic when they left our lab. in a vacuum container. The problem was a poor vacuum of  $10^{-5}$  Torr in the scattering chamber which allowed oxidation similar to the effect in an ion getter pump. In the next experiment the vacuum was in the  $10^{-6}$  Torr range due to an additional cryo-pump and the targets lived much longer, but one could see still in the monitor spectrum, that oxidation took place.

To overcome the problems of oxidation of the chemical active metals we will install a rolling mill in a leak tight aluminium box, which can be filled with a continuously highly purified Argon. With this improvement we hope to obtain rolled Uranium foils and other exotic foils with thicknesses below the limit given above.

A SIMPLE, EFFICIENT METHOD FOR REDUCING  
SMALL QUANTITIES OF ZINC OXIDE

J. M. Heagney and J. S. Heagney  
MicroMatter Co., Seattle, WA.

ABSTRACT

The requirement of reducing several small, separate batches of  $^{70}\text{ZnO}$  for rolling thin metal foils led to the development of a technique which proved to be considerably more efficient than previous methods. A simple acetate plating bath was used. The metal was collected on a hard cathode and subsequently scraped free. Consolidation of the zinc metal into a bead for rolling was accomplished by melting under inert gas.

- - - - -

The need to reduce three separate, small (15 mg or less) quantities of  $^{70}\text{ZnO}$  of different isotopic enrichments led us to examine alternative methods of electrowinning. The usual plating geometries and cyanide or sulfate baths lead to contamination of the deposit and sometimes to troublesome adherence to the cathode. Since zinc oxide is soluble in dilute acetic acid, an acetate solution of approximately one milliliter for fifteen milligrams of  $^{70}\text{Zn}$  is made by dissolving the oxide in 5% acetic acid in the original ORNL isotope bottle. The solution is then pipetted to a small platinum crucible. The platinum crucible forms the anode of an electroplating circuit as shown in figure 1. The cathode of this circuit is a hardened tool steel alloy rod, which can be scraped to remove the zinc metal without contaminating the deposit. The current density is kept high (greater than  $4 \text{ ma/cm}^2$ ) to ensure a dendritic deposit of poor adherence. Towards the end of the plating time (approx. 2-3 times that required by Faraday's Law), the current will decrease due to the very low conductivity of the zinc depleted solution and the current can be allowed to decrease.

After plating, the cathode is scraped to free the metallic zinc, which is collected and pellet pressed to reduce the surface area. In order to prepare a bead suitable for rolling, the pellet is melted in a vitreous carbon crucible in a slightly over-one-atmosphere pressure of argon.<sup>1</sup> Using a temperature just slightly higher than the melting point, a bead is formed with negligible loss of material due to vaporization. This technique is superior to the usual melting under flux (ammonium chloride, etc.) in that losses are minimized; however, only very clean, pure zinc will yield beads under such conditions.

Using these techniques, efficiencies of 80-90% from oxide to metal bead can be achieved with quantities in the 10 mg range. The reduction of isotopic cadmium oxide has also been accomplished using this technique. We recently reduced 4.6 mg of  $^{106}\text{CdO}$  with a yield of 3.6 mg of metal for an efficiency of 90%.

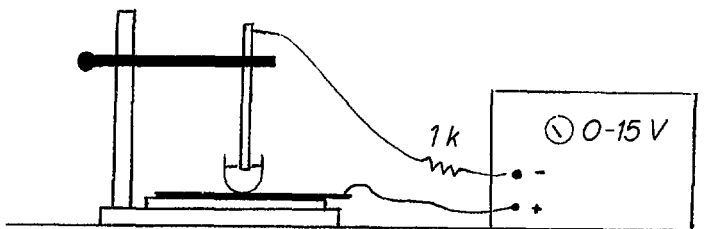


Figure 1. Electroplating setup.

#### REFERENCES

1. F. Karasek, Argonne National Laboratory, private communication.

## OPTIMUM COLLECTION TIME FOR SHORT-LIVED ISOTOPES\*

JEROME LERNER

*Chemistry Division**Argonne National Laboratory, Argonne, Illinois 60439*

In dealing with an isotope whose half-life is comparable to the processing time, the target-maker wishes to terminate the procedure at a point that will maximize the amount of the desired material on the target. This cut-off time is not always easy to determine; while it is true that fresh material is constantly being deposited, the isotope previously laid down is steadily decaying, and in addition the rate at which fresh material is applied is usually decreasing. The purpose of this paper is to determine a rule-of-thumb that can be used by the operator, during the deposition process, to yield the maximum amount of collected isotope.

---

\*Work performed under the auspices of the Division of Basic Energy Sciences of the Department of Energy.

## INTRODUCTION

Although the original investigation was specifically intended to guide the operator of an isotope separator, the conclusions are valid for other processes as well; for example, a vacuum evaporator. We assume that the desired isotope is prepared by some kind of batch process, then placed in the source of the target-producing apparatus (an ion-source in the case of an isotope separator, the furnace of an evaporator, etc.). The isotope is then transferred to the target at a rate that varies with time. It is assumed initially that the decay half-life is known.

Certain points are self-evident. If the half-life is long relative to the processing time (e.g. several hours) then the operation should continue until the source is essentially exhausted. Similarly, if the half-life is very short (i.e., a few minutes) then speed is essential and everything possible must be done to curtail processing time (minimum carrier, high temperature, etc.).

If the material is being generated in the source at a constant rate (e.g., daughter of a long-lived parent, or in an on-line isotope separator), then equilibrium is reached after a few half-lives and there is no difficulty in determining the optimum time. Finally, it is sometimes possible to monitor the radioactivity of the target during its preparation, and here also there is no problem in locating the best termination time.

The cases under consideration are thus those where the half-life is of the order of the processing time (e.g.,  $^{233}\text{Th}$ ,  $^{239}\text{U}$ ,  $^{241}\text{Np}$ ,  $^{235}\text{Pu}$ ,  $^{247}\text{Am}$ ,  $^{256}\text{Es}$ ;  $T_{1/2} \approx 20$  m) and it is not practical to measure directly the amount of the isotope on the target or the rate at which it is being deposited. It is assumed initially, however, that an indication of the transfer rate as a function of time is available. For example, in an isotope separator there is often a relatively stable isotope of the same element whose ion current can be measured, or in the case of an evaporator there may be previous experience correlating temperature and deposition rate for the same or a similar element.

#### Basic Equation

The differential equation for the process is easily written:

$$\frac{dN}{dt} = N_0 e^{-\lambda t} \cdot K I_t - \lambda N$$

where  $N$  is the amount of material presently on the target,  $N_0$  is the quantity initially deposited in the source,  $I_t$  is a measure of the rate of transfer (assuming no decay),  $K$  incorporates the transfer efficiency and the factor for converting "I" units to "N" units,  $\lambda$  is the radioactive decay constant, and  $t$  is time. In the differential equation  $N_0 e^{-\lambda t}$  is the amount in the source at time "t",  $K I_t$  is the transfer rate at this time, and  $\lambda N$  is the decay rate of the material already on the target.

The solution is:

$$N e^{\lambda t} = K N_0 \int I_t dt + C$$

where the integration constant can be evaluated by noting that  $N$  is zero when  $t$  is zero. Clearly, in order to evaluate  $N$  it is necessary to know the source-to-target transfer ( $I_t$ ) as a function of time. In the sections that follow some idealized transfer functions will be considered. Since we are primarily interested in determining the optimum time for termination, the curve amplitudes will be normalized so that the peaks all occur at  $N = 1$ , and the unit along the time axis will be the mean-life ( $= 1/\lambda = 1.44 T_{1/2}$ ). While these curves are useful for determining the optimal termination time, it should be noted that the non-normalized value for  $N$  varies directly as  $K$ ,  $N_0$  and  $I_0$ .

### Constant Carrier

The simplest case is constant transfer function for at least several half-lives. Then  $I_t = I_0$  and the solution is

$$N = K N_0 I_0 t e^{-\lambda t} \quad (\text{Figure 1})$$

The maximum occurs at the mean-life and its location depends only upon the decay constant of the collected isotope. The peak is a broad one, however; stopping at one half-life (0.7 mean lives) or two half-lives yields roughly 95% of the maximum, and even 50% of a half-life or three half-lives yields better than 2/3 of optimum.

Linear Rise

A simple alternative to a constant level is the case where the transfer function increases linearly. Then  $I_t = I_0 t$  and

$$N = K N_0 I_0 \frac{t^2 e^{-\lambda t}}{2} \quad (\text{Figure 2})$$

This curve is also independent of the parameters of the transfer function; however, the peak occurs at two mean-lives. The normalized curve is also a broad one, so that at two or four half-lives the yield is approximately 90%. It should be noted that the value of  $N$  in the non-normalized curves varies directly as the slope  $I_0$ .

Interrupted Linear Rise

In general transfer functions do not increase indefinitely; a more realistic approximation to reality would be an interrupted linear rise. If  $t_0$  is the point at which the rise levels off, then

$$N = K N_0 I_0 \frac{t^2 e^{-\lambda t}}{2 t_0} \quad \text{for } t \leq t_0$$

$$= K N_0 I_0 (t - 0.5 t_0) e^{-\lambda t} \quad \text{for } t > t_0 \quad (\text{Figure 3})$$

It is evident that if  $t_0$  is very large compared to the mean-life (i.e., long, slow rise in transfer function), then Figure 2 applies and the optimum is at two mean-lives. Conversely, if  $t_0$  is very small then the transfer function rises immediately to a steady state and Figure 1, with peak at one mean-life, applies. One would expect the curves to peak in between for intermediate values of  $t_0$ , and that is precisely the case. For all values

of  $t_0$ , however, the region in the neighborhood of two half-lives (about 1.5 mean-lives) yields 90% or better of the maximum. It is interesting to note that the yield curves are smooth at the points where the slope of the transfer curve shifts abruptly.

### Growth Curve

In general the transfer function does not rise linearly and then abruptly level off. A more reasonable approximation to experimental conditions would be a curve of the form:

$$I_t = I_0 (1 - e^{-\lambda_0 t})$$

similar to the rise to equilibrium of the short-lived daughter of a long-lived parent. Notice that  $\lambda_0$  is part of the transfer-rate time-constant, and is not related to the radioactive decay constant  $\lambda$ . The solution is:

$$N = K N_0 I_0 [t - (1 - e^{-\lambda_0 t}) / \lambda_0] e^{-\lambda t} \quad (\text{Figure 4})$$

As might be expected, the curves are very similar to the previous case. For very small values of  $\lambda_0$  (i.e., long rise time) the current is essentially linear with time and Figure 2 applies; for large values of  $\lambda_0$  (rapid rise time) the current is essentially constant and Figure 1 applies. For intermediate values of  $\lambda_0$  the location of the peak shifts between one and two mean-lives. As before, terminating the collection time at two half-lives yields 90% or better of the maximum.

Other curves have been studied in which the transfer function rises and then levels off, and all give essentially the same result: a relatively broad peak located in the interval between one and two mean-lives. *A suitable rule-of-thumb seems to be to collect for two half-lives in order to obtain at least 90% of the optimum.*

### Linear Decay

In the next two sections we shall consider cases where the transfer function starts at a non-zero value or reaches its peak in a time very short compared to the half-life, then decreases steadily. This might be true in an isotope separator, for example, when there is little or no carrier, or in an evaporator where the target is initially shielded while an impurity is vaporized.

If we assume linear decay from an initial value  $I_0$  to zero at  $t_0$ , then

$$I_t = I_0 (1-t/t_0)$$

and the solution is

$$N = K N_0 I_0 (t-t^2/2t_0) e^{-\lambda t} \quad \text{for } 0 \leq t \leq t_0$$

$$N = K N_0 I_0 \frac{t_0 e^{-\lambda t}}{2} \quad \text{for } t \geq t_0 \quad (\text{Figure 5})$$

As expected, for large values of  $t_0$  (i.e., slowly decaying current) the curve is essentially Figure 1, with peak at one mean-life. For shorter values of  $t_0$  (faster decay of transfer rate) the peaks move toward zero. Obviously the previous rule-of-thumb does not apply.

Exponential Decay

It we presume that  $I_t = I_0 e^{-\lambda_0 t}$  (where again  $\lambda_0$  is not related to the radioactive decay constant  $\lambda$ ) then the solution is

$$N = K N_0 I_0 \frac{1 - e^{-\lambda_0 t}}{\lambda_0} e^{-\lambda t} \quad (\text{Figure 6})$$

The curves do not differ significantly from the linear decay case; the peak locations vary from zero (rapid decay) to one mean-life (slow decay). For cases in which the transfer functions fall off at other rates (i.e., hyperbolic, parabolic, etc.) the curves are essentially similar.

We can formulate a rule-of-thumb that applies when the transfer function peaks immediately and then drops off: *stop collection after one mean-life or when the transfer rate drops to 20% of its peak value, whichever occurs first.* Examination of many different transfer drop-off rates indicates that this will yield at least 90% of maximum.

Half-Life Not Accurately Known

In some cases the half-life is known only roughly or is estimated from systematics. Fortunately, the curves (in those circumstances that require knowledge of the half-life) are relatively broad (as already noted) so that selecting an acceptable collection time is generally not a critical decision.

Much more difficult is the case where the half-life is essentially unknown, as for example when searching for new isotopes. Preliminary Monte Carlo calculations have not yielded a clearly defined rule-of-thumb that can be easily summarized; however, it seems to be true, broadly speaking, that short collection times are preferable to long ones. This seems intuitively correct -- doubling the collection time, for example, can at best double the yield (on the rising part of the curve), but can also reduce the yield by a large factor on the decaying part of the curve.

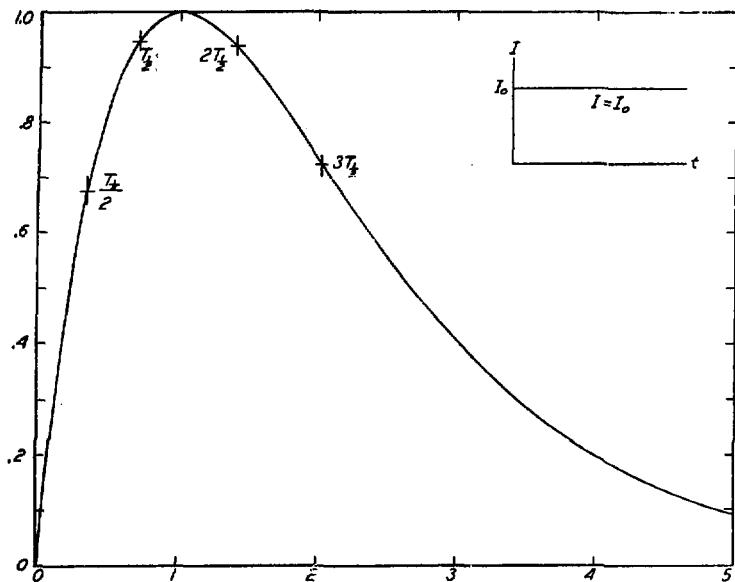


Figure 1. Normalized target activity for constant transfer function. Horizontal time axis in units of mean-life ( $= 1/\lambda$ ).

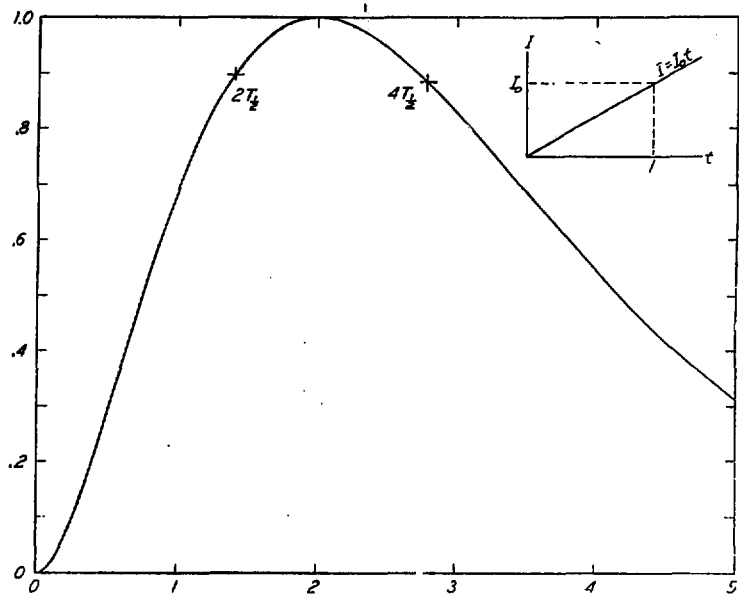


Figure 2. Linearly increasing transfer function.

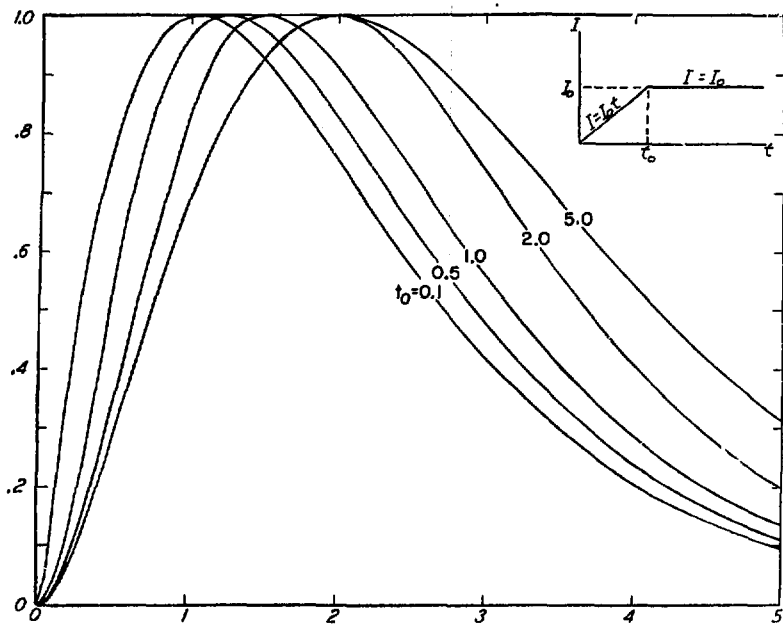


Figure 3. Interrupted linear rise transfer function.

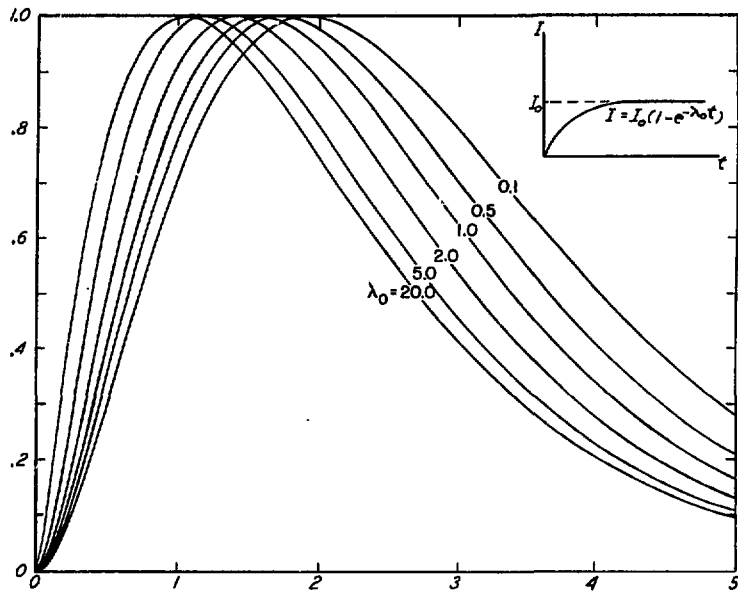


Figure 4. Growth curve transfer function.

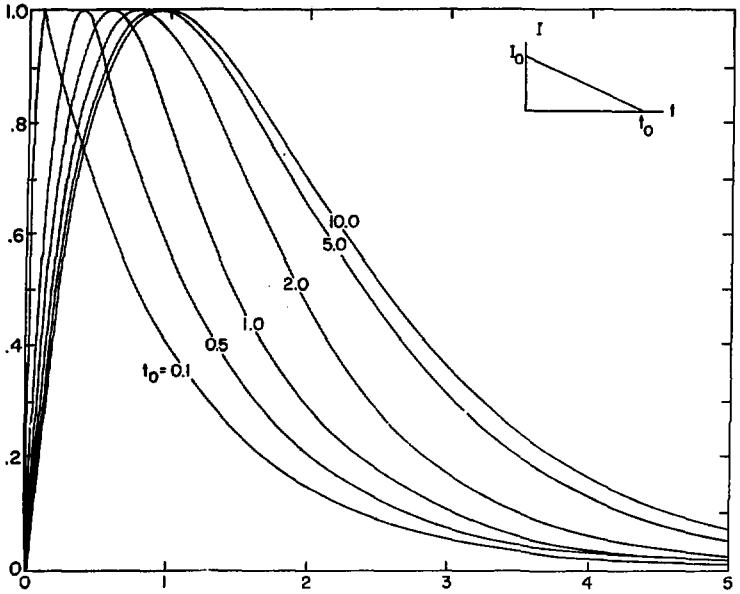


Figure 5. Linear decay transfer function.

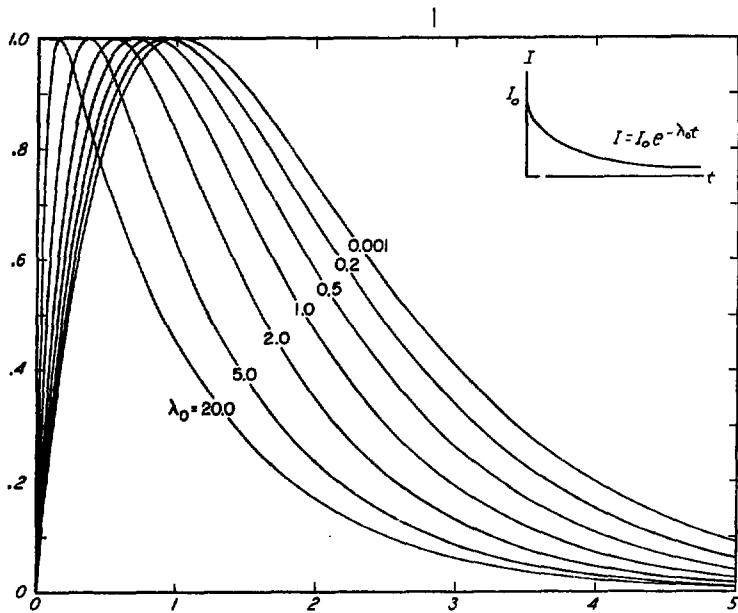


Figure 6. Exponential decay transfer function.

copy

## HYDRIDING OF TITANIUM CONES FOR A SPUTTER-ION SOURCE

by

Judith C. Gursky and Boyd A. Sherwood

Los Alamos Scientific Laboratory  
University of California  
Los Alamos, New Mexico 87544

The Los Alamos Scientific Laboratory recently purchased a General Ionex sputter-ion source for the vertical machine at the Van de Graaff facility. Figure 1 shows the source developed by Roy Middleton and Charles Adams<sup>1</sup> at the University of Pennsylvania, which is the basis of the General Ionex source. The cesium vapor is converted to positive Cs ions by the surface ionization tube. The ions are accelerated in order to sputter material from one of the hollow cones mounted in a wheel that can be rotated. In addition to producing heavy ions directly from a cone of the desired species, such as calcium, copper, or nickel, cones of titanium can be filled with gas such as hydrogen sulfide, oxygen, or hydrogen to produce S<sup>-</sup>, O<sup>-</sup>, and H<sup>-</sup> ions.

It is desirable to be able to produce protons and deuterons from the sputter cones to avoid the lengthy job of changing to a gas-fed source. In addition, a major advantage is the possibility of producing tritium beams without handling tritium gas in the accelerator. This paper describes a simple, small-scale method for absorbing hydrogen and deuterium into titanium cones.

Titanium has the property of absorbing hydrogen gas at elevated temperature and/or pressure. Our procedure is called hydriding for convenience, but it is actually absorption rather than true hydriding. It operates at about 650°C at less than atmospheric pressure so that standard vacuum seals can be used. The dimensions of the cones are shown in Fig. 2.

The history and cleanliness of the cones determine whether they will absorb hydrogen. These cones were cleaned ultrasonically in detergent solution, followed by trichloroethylene.

Figure 3 shows the system. It is attached to a flange and slide-valve on the side of an existing small, diffusion-pumped vacuum system. It was designed

to use available glass culture tubes and flasks. The lip of the flask was sawed off, and a ring of epoxy was applied to keep it from sliding into the vacuum fitting. A glass-epoxy insulating disk keeps the rf coil from touching the brass fitting. The coil slips over the neck of the flask. The two cones rest inside a quartz sleeve in the neck of the flask. The additional volume of the bulb of the flask is needed to keep the pressure well under one atmosphere. The volume of the system was calculated including all the tubing and the internal volume of the gauge.

The rf induction coil is water-cooled and is powered by a Lepel 2.5-kW supply at 450 kHz. The hydrogen or deuterium gas is passed through a deoxygenating cartridge and through a liquid-nitrogen trap. The trap is essential; the gas is not absorbed otherwise. An infrared pyrometer is focused through the flask on the small hole in the cone, which is close to blackbody condition.

The cones are first outgassed in vacuum at about 800°C. After cooling we close the slide-valve and introduce enough hydrogen or deuterium to supply 130 cm<sup>3</sup> to each of the cones, with some to spare. We measure the take-up of gas by the cones on the differential pressure gauge as their temperature is raised. Absorption of the desired amount is measured by the calculated pressure drop. Figure 4 shows an absorption cycle. In this case the system volume is 442 cm<sup>3</sup>. The volume of gas to be absorbed is 260 cm<sup>3</sup>. The system was filled to 547 mm, that is,  $547/760 \times 442 = 318$  cm<sup>3</sup> of H<sub>2</sub> at STP was introduced. The pressure change,  $\Delta P$ , was 447 mm, therefore  $447/547 = 0.817$  of the available gas was absorbed, or 260 cm<sup>3</sup>, 130 cm<sup>3</sup> to each cone.

The absorption goes fairly slowly at about 650°C and requires about two hours for absorption and slow cooling. If the cones do not absorb all the gas required, the system is pumped out. The cones are heated to 800°C to dehydride them and another cycle is done. So far, one or two cycles have been enough.

Our sputter-ion source is not yet operational, but the hydrogen cones have worked well at the University of Pennsylvania, including tritium cones.<sup>2</sup> The basic procedure is the same for tritium, but much more elaborate equipment is required because of the radioactivity and biological hazard of tritium.

1. R. A. Middleton and Charles T. Adams, *Nucl. Instr. and Meth.* 112, 329-336 (1974).
2. R. A. Middleton, Symposium of Northeastern Accelerator Personnel, Los Alamos, New Mexico, October, 1977.

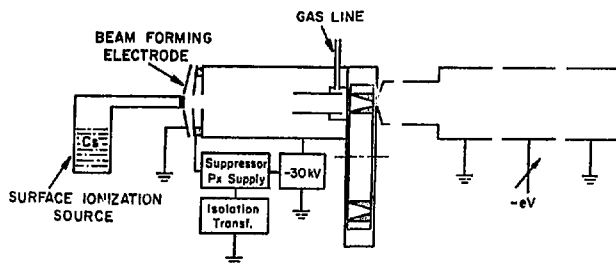


Figure 1. Sputter-ion source.

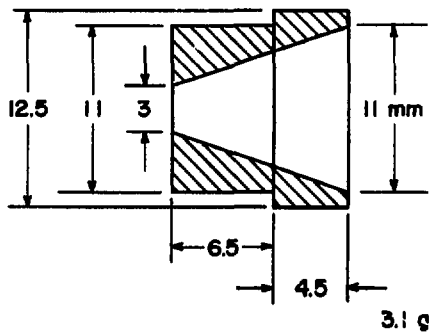


Figure 2. Titanium cone.

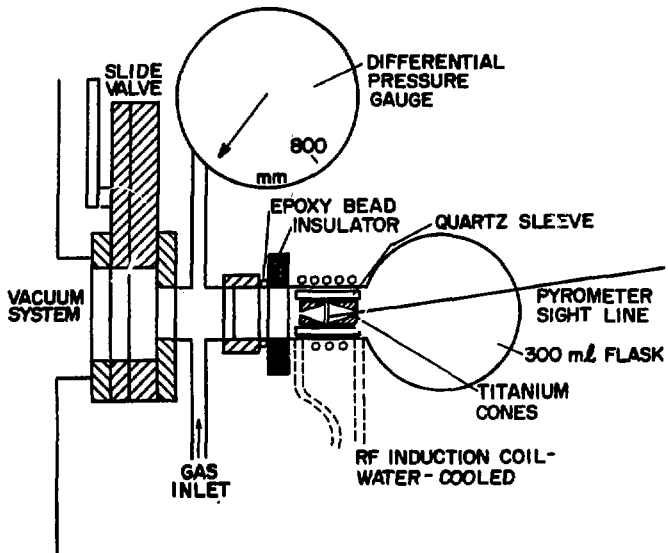


Figure 3. Apparatus for hydrogen absorption.

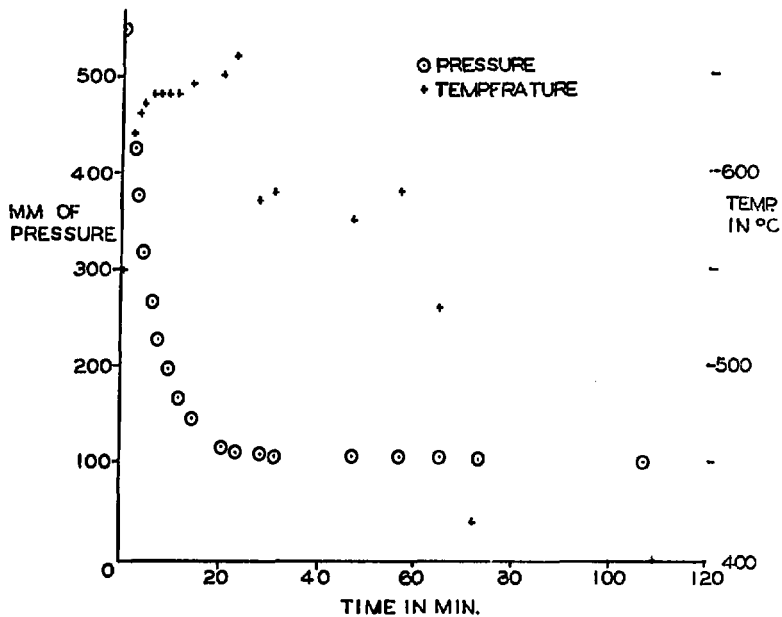


Figure 4. Hydrogen gas take-up by titanium cones.

## Nitrogen Targets Produced By Reactive Sputtering of Tantalum And Titanium

by

J.D. Stinson  
Division of Physics, National Research Council  
Ottawa, Canada

A method for the preparation of nitrogen targets by the reactive sputtering of tantalum and titanium is described. Targets in the range of  $5 \mu\text{g}/\text{cm}^2$  to  $120 \mu\text{g}/\text{cm}^2$  have been produced. A discussion of the equipment and electrical requirements is included.

### Introduction

The reactive sputtering of tantalum in oxygen and nitrogen to provide thin films for the production of resistors and capacitors has been employed in industry for many years. The binary compounds of tantalum and nitrogen, TaN and TaN<sub>2</sub>, can be selectively produced by process control and have been extensively studied<sup>(1)</sup> for purity, chemical composition and crystal structure. Others<sup>(2)(3)</sup> have successfully used the process to provide both backed and self supporting nuclear targets.

Researchers in our laboratory use water cooled nitride targets to study the  $^{15}\text{N}(\alpha\gamma)^{19}\text{F}$  reaction and apply  $\alpha$  beams of 2 to 5 MeV at 10  $\mu\text{A}$  current. Target requirements consist of good adhesion of the nitride film to the substrate, and purity of both the film and the substrate material.

Until one year ago, nitrogen targets were made in this laboratory by evaporating titanium and reacting the deposit in nitrogen at 750 to 800°C, as described in a previous presentation<sup>(4)</sup> to the society. The

targets were of inferior purity and gave poor background spectra which interfered with the reaction being studied. The introduction of these impurities, mainly carbon with some low Z elements, in the titanium film was caused by oil vapour present in the vacuum system, and residual atmospheric gases. In addition, the tantalum substrate which was used contributed its share of interfering impurities. Gold substrates were tried instead of tantalum but produced poorly defined targets. It is believed that the deposited titanium layer and the nitrogen diffused into the gold when the coated substrate was heated to the reaction temperature.

To overcome these difficulties, we built the necessary equipment to produce nitride targets by reactive sputtering, and by using gold substrates of 4-9's purity. The first targets produced were tantalum nitride, and later titanium nitride. The titanium nitride targets gave an increase in reaction yield as compared to the tantalum nitride targets. It was expected that TiN should give approximately the same yield as TaN<sub>2</sub>. This raises the question as to whether the tantalum nitride was the preferred TaN<sub>2</sub> or TaN. Spark spectroscopy analysis of the tantalum nitride film is planned and will resolve this question.

#### Vacuum System

The choice of vacuum equipment was determined from the need to have a clean system free of hydrocarbons. Hydrocarbons crack during the sputtering process and deposit carbon or form carbides with the refractory metals used.

A carbon vane pump and two sorption pumps were chosen for the roughing system. The carbon vane pump serves a dual purpose. It is used to exhaust the system to 125 mm pressure and also serves as a compressor forcing air through the sorption pumps to remove water, during the first stage of regeneration. During the second stage of regeneration the carbon vane pump exhausts residual moisture and gas. The sorption pumps produce a vacuum of  $10^{-4}$ mm and are used one at a time with one pump being held in reserve.

A 110 l/s, noble gas, sputter-ion pump is used to attain the high vacuum in the sputtering chamber. Pressures as low as  $5 \times 10^{-8}$ mm have been observed. Since the sputter-ion pump is not required to handle heavy gas loads, it is found to be adequate for this purpose. A six inch gate valve isolates the sputter-ion pump during the roughing and processing procedures.

Materials used in the system construction were stainless steel, copper, silicon bronze, 95-5 solder and ceramic sealed electrode inputs. Conflat type flanges with copper seals were used for assembly where possible, with some viton "O" rings being used to facilitate easy dismantling. In fabrication, inert gas welded joints were used in preference to silver brazing.

### The Chamber

The sputtering chamber, made of stainless steel, is closed at the top with a bolted flange and "O" ring seal. For loading and unloading the chamber, this type of seal permits easy access. Fastened to this top flange is the cathode shield, and the high voltage connector feeding the

cathode. The cathode assembly is comprised of the cathode, a disc of tantalum or titanium which is 7.5 cm in diameter, a collar welded to the disc, and the support rod. Both the centre pin of the high voltage connector and the support rod are threaded to facilitate positioning of the assembly.

The cathode shield also serves as a cold trap and is supported by two tubes which are used for filling the trap with liquid nitrogen. Close spacing, 0.5 cm, between the cathode shield and cathode assembly was designed to prevent a glow discharge from occurring in this region, and limits the discharge to the cathode - anode gap. Similarly the water cooled platform defines the cathode to anode volume and prevents the discharge from occurring farther down the chamber.

The anode consists of two parts; the heatable tantalum platform and the surrounding water cooled platform. The heatable portion of the anode is an inverted "U" of 0.25 mm tantalum which provides a square receiving surface 5.1 cm x 5.1 cm, for heating the substrates prior to the coating process. Two copper ceramic feed-through electrodes, which are water cooled, supply high current at low voltage to the tantalum platform.

The shutter mechanism is actuated by a bellows type rotary feed-through. The shutters are used in the closed position to shield the substrates during a pre-sputter clean up.

A viewing window in the chamber wall, not shown in the illustration, permits visual inspection during processing.

Nitrogen gas stored in a lecture cylinder is fed to the chamber using a needle valve. A plug valve with higher conductance than, and parallel to, the needle valve, permits preliminary evacuation of the gas manifold to the cylinder valve.

### Instrumentation

Vacuum measurements are made by two gauges. A hot filament ionization gauge monitors the chamber for high vacuum measurements and a thermocouple gauge measures roughing and sputtering gas pressures.

Two power units fulfill the electrical requirements of the target processing. A variable a.c. supply with a 3 kVA capability feeds 250 amperes to the heated anode. A d.c. supply with a 2 kVA, 5000 volt capability feeds 30 mA of current at minus 3000 volts to the cathode.

### The Sputtering Process

The dc sputtering process is initiated by striking an electrical discharge between two electrodes in gas at low pressure. Electrons emitted from the cathode ionize the gas and these gas ions in turn strike the cathode at high kinetic energy. In this way atoms of material are removed from the cathode and are deposited on the anode. The gas pressure in the chamber determines the voltage and current parameters. Inert gas is used in the sputtering deposition of metals and is pumped through the chamber with the desired pressure being maintained. Because high purity nitrogen is expensive, the gas used in reactive sputtering is captive, and is replenished at the same rate it is consumed by the reaction.

### Processing

Clean gold substrates of 4-9s purity are placed on the heatable tantalum anode. The tantalum anode will accept four of our substrates which are 2.5 cm x 2.5 cm in size and are 0.25 mm thick. When the substrates and cathode are in place, the chamber is closed and evacuated to  $10^{-7}$ mm or better. We usually pump overnight to outgas the system.

The tantalum anode heater current is increased to the point that the gold substrates exhibit a dull red incandescence with the room lights out. We estimate this temperature to be in the order of 700°C. Outgassing of the chamber and substrates is indicated by a rise in vacuum pressure. After a 10 minute heating period, the chamber is allowed to cool for 20 minutes to restore the low pressure in the system. The gate valve is then closed to isolate the chamber from the sputter-ion pump.

A 15 minute preliminary sputtering period with the shutters closed is the next stage of the process. The pre-sputtering outgasses the cathode assembly and the cathode shield and exposes a new surface of cathode material. The cathode shield or cold trap is heated by radiant energy and, for this reason, is not filled with liquid nitrogen. To initiate the pre-sputtering, the plug valve and needle valve are closed, and the sputtering gas manifold is pressurized with nitrogen by opening and closing the cylinder valve. By carefully opening the needle valve, the chamber is pressurized to 80  $\mu$ m. The cathode voltage is increased so that the current is 30 mA. The pressure in the chamber is either decreased or increased to obtain a reading of 3000 volts and 30 mA of current. With some experience the needle valve can be set so that the voltage and current remain relatively constant. To complete the pre-

sputtering stage we rid the chamber of the impure gas by sorption pumping to less than 1  $\mu\text{m}$ .

To conclude the target preparation process, the shutters are opened and the cold trap is filled with liquid nitrogen. Chamber pressures and electrical parameters are adjusted to the same values as previously described. Target thickness is determined by the length of time the sputtering process is allowed to proceed. After a cooling period of one hour the chamber is back filled with commercial grade nitrogen to permit target removal. Exact target thicknesses are measured by weighing and from observed widths of alpha-capture resonances.

Tantalum nitride targets with a thickness of 36  $\mu\text{g}/\text{cm}^2$  were produced by sputtering for eight minutes. Titanium nitride targets of the same thickness required 32 minutes. Assessing the targets we have made, we find the sputtering rates range from 1 to 1.5  $\mu\text{g}/\text{cm}^2\cdot\text{min}$  for tantalum nitride, and from 3 to 4.5  $\mu\text{g}/\text{cm}^2\cdot\text{min}$  for titanium nitride. Because the cathode is not water cooled, the longer sputtering times required for thick targets produce higher temperatures, and higher rates. A non-linear relationship between deposition time and thickness therefore exists, and explains the spread in the rate figures quoted.

#### General Comments

Nitrogen targets produced by reactive sputtering are of superior quality compared to those made by resistive heating techniques. The important advantages are the cleanliness of the process with low light element contamination, and the freedom of the researcher to choose backing materials suited to the experiment. Even, tough films, easy thickness

control and production of self supporting targets are other advantages inherent to the process.

A large part of this paper has been devoted to a description of the processing apparatus. Proper equipment is essential for purity attainment and good processing techniques. Though some target makers may find the equipment expensive, it should be kept in mind that the same apparatus can be used to reactively sputter such metals as vanadium, niobium and zirconium. Our future plans include the production of isotopically enriched oxygen targets.

The author gratefully acknowledges the assistance and encouragement of Dr. W.R. Dixon and Dr. D.W.O. Rogers. A special thanks is also due to Mr. W.H. Taylor and staff members of the Physics Machine Shop for their engineering expertise in producing the equipment drawings and machined parts.

#### References

- (1) David J. Wilmott, J. Appl. Phys. 43, 4865 (1972).
- (2) M.R. Wormald, B.Y. Underwood and K.M. Allen, Nucl. Instr. & Meth. 107, 233 (1973)
- (3) H.W. Fulbright and H. Freiesleben, Nucl. Instr. & Meth. 115, 83 (1974)
- (4) J.D. Stinson, Proc. 5th Annual Confer. Intern. Nucl. Target Devel. Soc. 85 (1976).

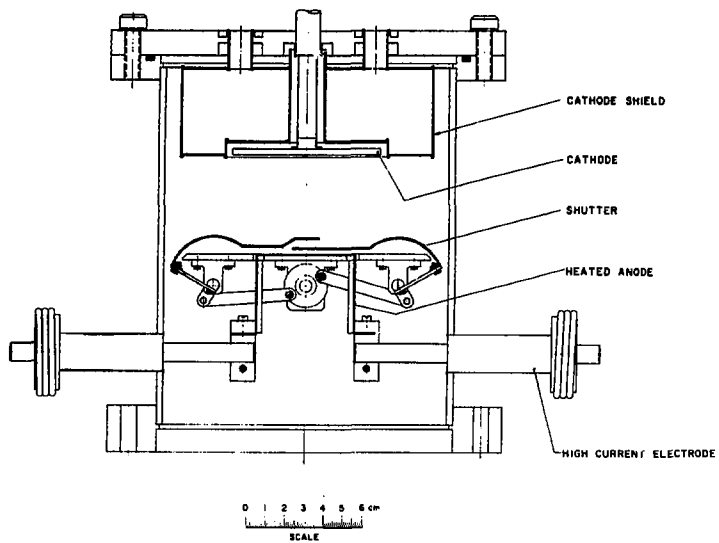


Figure 1. Reactive sputtering chamber.

URANIUM SANDWICH TARGETS OF 0.1 TO 100 mg·cm<sup>-2</sup> PREPARED  
BY ELECTRON BEAM GUN EVAPORATION

Helmut Folger and Josef Klemm

Gesellschaft für Schwerionenforschung, Darmstadt, Germany

1. ABSTRACT

Metallic uranium layers of 0.1 to 100 mg·cm<sup>-2</sup> between different backings and protecting layers were prepared for bombardments with heavy ions such as argon, krypton, xenon, lead, or uranium at energies of up to 8 MeV/u at the UNILAC of the GSI.

An experimental set-up for the preparation of thick and oxygen-free sandwich targets using a 6 kVA electron beam gun was installed in a high vacuum apparatus. Then deposition and evaporation rates for uranium were investigated as a function of the electron beam gun power. It turned out that reproducible evaporation rates of up to 7 mg·s<sup>-1</sup> were achieved when uranium pieces of 20 to 40 grams were used. Specific evaporation rates and vapor pressures for different temperatures were calculated. Some of these data are compared to measured values, especially evaporation rates at the evaporation point.

The preparation, composition, and usage of uranium sandwich targets is described in detail. It concerns uranium layers of 0.1 to 100 mg·cm<sup>-2</sup> deposited onto backings of carbon, titanium, nickel, gold, or glass. Evaporated films of carbon, titanium, nickel, or gold of 0.01 to 0.2 mg·cm<sup>-2</sup> are used to protect the uranium layers from oxidation.

## 2. APPARATUS

Uranium targets are very sensitive to oxygen and moist air. In order to handle vacuum evaporated targets in an oxygen-free atmosphere a glove-box was attached to an evaporation apparatus (fig.1). It mainly consists of a plastic foil with gloves and a small plastic bag used as a pass-through-chamber. All targets are transferred in dry argon atmosphere to sample vials for further handling, i.e. weighing or mounting to target holders in a separate glove-box.

The high vacuum system, type VE-770-A of Veeco, Plainview, N.Y., is equipped with an oil diffusion pump of  $2000 \text{ l}\cdot\text{s}^{-1}$ . It has a combined water and liquid nitrogen cooled chevron baffle. The apparatus can be operated in the pressure range of  $10^{-7}$  to  $10^{-6}$  mbar. On top of the rack (left side of fig.1) there is a quartz crystal deposition rate and thickness control monitor type QM-331 of Kronos. The rack below contains power supplies and control units for an electron beam gun evaporator of Leybold-Heraeus, Hanau, Germany.

The 6 kVA electron beam gun ESV-6 shown in fig.2 may be operated with an acceleration voltage of 6,8,10, or 12 kV at up to 0.5 amps beam current. It works at a deflection angle of  $180^\circ$ . The vertically entering beam can be moved or oscillated over the evaporant material in x- and y-direction. The beam intensity, and thus the evaporation rate, is regulated electronically by an emission current constanter. A turnable water cooled copper block with 4 hearths of  $4 \text{ cm}^3$  volume each is used to prepare sandwich targets in one vacuum cyclus. Nearly the same evaporation system has already been described by H.J.Maier and R.Großmann<sup>1)</sup> for the preparation of  $\alpha$ -radioactive isotope targets.

The apparatus, prepared for a special run, is shown in fig.3. In the center there is one crucible of the electron gun, surrounded by a shield which keeps uranium contaminations low in the whole system. The turnable shutter on the right side has a hole being covered with a microscopic slide so that prefiring can be observed and regulated. Glow discharge electrodes with aluminum foils are on both sides. The target holder in the center keeps 7 targets each having 25 mm of diameter; it can be water cooled or heated by an infrared radiator, the latter was turned up to get a better survey. The evaporation rate is observed by a water cooled quartz crystal located above a hole in the target holder. The entire evaporation assembly is surrounded by a metal cylinder serving as x-ray and contamination shield.

### 3. DEPOSITION AND EVAPORATION RATES AND YIELDS

In connection with the production of uranium targets some experiments were performed to measure deposition rates of uranium with the quartz thickness control monitor at a source distance of 20 cm as a function of the electron beam power (fig.4). The weight of the evaporant material was changed in this series from 0.1 to 40 grams. The deposition rate was extremely low when samples beyond 1 gram were inserted, mainly, because the relatively large electron beam spot of  $5 \cdot 8$  mm heated up the cooling water of the gun. Even a sample of 8 grams of uranium could not be evaporated as effectively as expected. The best results were achieved by using pieces of 22, 40, and 37 grams. Here the difference in the deposition behaviour was not significant when the electron acceleration voltage was changed from 10 to 12 kV, as can be seen from the measured values given in fig.4.

Normal deposition rates of  $10^{-4}$  to  $10^{-3}$   $\text{mg}\cdot\text{cm}^{-2}\cdot\text{s}^{-1}$  at a distance of 20 cm - taken in many target preparation procedures - were gained with an electron beam gun power of 1.7 to 2.5 kVA. Further increase in the power input at constant size of the beam spot raised the deposition rate only slightly. The weak raise seems to be due to beam intensity consuming effects as increases in heat radiation and thermal heat conductivity of the evaporant material, increase in the production of charged particles above the uranium surface, etc. At about 4.6 kVA sparking occurred as a result of gas discharge processes so that the evaporation was interrupted.

A measured evaporation yield of  $0.1 \text{ \%}\cdot\text{cm}^{-2}$  at 20 cm from the source is taken to compare rates of deposition and evaporation. It can be seen from fig.4 that depositing uranium at  $10^{-3}$   $\text{mg}\cdot\text{cm}^{-2}\cdot\text{s}^{-1}$  (left scale) corresponds to an evaporation rate of about  $1 \text{ mg}\cdot 0.4 \text{ cm}^{-2}\cdot\text{s}^{-1}$  (right scale). Layers of  $1 \text{ mg}\cdot\text{cm}^{-2}$  can thus be produced in about 17 minutes. - Uranium targets of  $20 \text{ mg}\cdot\text{cm}^{-2}$  and more were prepared at a source-to-substrate distance of 8 cm yielding in a deposition rate of  $0.55 \text{ \%}\cdot\text{cm}^{-2}$ . In about 1 hour targets of  $20 \text{ mg}\cdot\text{cm}^{-2}$  were prepared. The same time was required to build up layers of around  $100 \text{ mg}\cdot\text{cm}^{-2}$  of uranium, which was obtained by increasing the input power to about 3.8 kVA thus accelerating the deposition by a factor of about 5.

### 4. SPECIFIC EVAPORATION RATE, VAPOR PRESSURE, AND TEMPERATURE

The process of evaporation can be explained by an atomistic model, in which the evaporation rate  $\Gamma$  is caused by the number of molecules  $dN_e$  of a mass  $m$

evaporating from a surface area  $A_e$  during the time interval  $dt$ . The kinetic theory of gases describes this phenomenon using the equilibrium pressure  $p$  and the absolute temperature  $T$  in the following relation where  $k$  is the Boltzmann constant

$$\Gamma = m \frac{dN_e}{A_e \cdot dt} = \left( \frac{m}{2 \cdot \pi \cdot k \cdot T} \right)^{1/2} \cdot p \quad (1)$$

This yields an equation for the specific evaporation rate of uranium for vapor pressure values in torr (1 torr = 1.333 mbar)

$$\Gamma_{\text{uranium}} = 9.0 \cdot 10^2 \cdot T^{-1/2} \cdot p_{\text{torr}} \quad \text{mg} \cdot \text{cm}^{-2} \cdot \text{s}^{-1} \quad (2)$$

In fig.5 the specific evaporation rate of uranium is plotted versus the temperature (dashed curve). It has to be pointed out that the curvature depends on thermodynamic data characterizing the vapor pressure as

$$\log p = - \frac{\Delta_v H}{2.303 \cdot R \cdot T} + \text{const.} \quad (3)$$

( $\Delta_v H$  = molar heat of vaporization;  $R$  = gasconstant).

Taking the values from G.G.Schlessinger's compilation<sup>2)</sup> with  $\Delta_v H = 106836 \text{ cal} \cdot \text{mol}^{-1} \cdot \text{degr}^{-1}$  and  $\text{const} = 8.587$  the vapor pressure of uranium can be calculated for different temperatures from the equation

$$\log p_{\text{uranium}} = - 2.335 \cdot 10^4 \cdot T^{-1} + 8.587 \quad \text{torr.} \quad (4)$$

A corresponding vapor pressure curve is plotted in fig.5 (full line). The pressure is given in torr, a dimension used in the available literature. It should be mentioned - without discussing it - that values calculated with equation (4) may in some cases differ from literature values; e.g. vapor pressures given by R.E.Honig and D.A.Kramer<sup>3)</sup> are about 7% higher.

The evaporation pressure of  $10^{-2}$  torr is reached at a temperature of 2205 K and the specific evaporation rate at this point is  $0.18 \text{ mg} \cdot \text{cm}^{-2} \cdot \text{s}^{-1}$  (fig.5). This is in rather good agreement with the measured value of  $0.1 \text{ mg} \cdot 0.4 \text{ cm}^{-2} \cdot \text{s}^{-1}$  belonging to a deposition rate of  $10^{-4} \text{ mg} \cdot \text{cm}^{-2} \cdot \text{s}^{-1}$  at 20 cm (fig.4). As the evaporation of uranium begins at 1.7 kVA it can be assumed that this power corresponds to a temperature of uranium of about 2200 K. In a future series of uranium depositions the evaporation temperature will be measured directly.

## 5. SANDWICH TARGET PREPARATION

For the preparation of all uranium targets metallic uranium-238 with a contents of 0.4% of uranium-235 was used as supplied by the Nukem, Hanau, Germany. The material is molten and refined by an intensive prefiring with the electron beam prior to an evaporation. After the target backings are brought into the apparatus, the evaporation chamber is evacuated to about  $10^{-6}$  mbar. Then a glow discharge cleaning is initiated for 15 minutes at about 0.05 mbar of argon pressure before the system is pumped down thoroughly. The substrate then is heated to about 600 K and, after a prefiring of some minutes, uranium is evaporated by means of the electron beam gun as already described. In most cases a period of 50 minutes is sufficient to cool down the apparatus before the turnable copper block of the electron gun is moved to the next crucible, and a protecting film of a selected material thus can be deposited to the uranium surface.

## 6. COMPOSITION AND USAGE OF THE TARGETS

The composition of some uranium sandwich targets which were prepared for heavy ion bombardments at the UNILAC of the GSI are listed in tab.1.

Different carbon-uranium-carbon targets were prepared for investigations of the straggling of uranium on uranium. This type of target was also taken in Coulomb excitation experiments using particle-gamma coincidence techniques. Titanium-uranium-titanium and nickel-uranium-nickel systems were needed either as combined window/target foils in a gas jet system or as targets in a gas jet chamber; in both cases recoils from nuclear reactions were collected for  $\alpha$ -spectroscopy and time-of-flight measurements. Thick nickel backings with uranium layers and thin nickel surfaces (tab.1, type 4) were taken to investigate K-shell ionisation effects in heavy-ion/atom collisions by observing x-rays.

Thick gold layers (type 5) or copper chips ignition-plated with gold (type 6) were coated with uranium and then covered with gold. These sandwich targets were prepared to measure excitation functions for fission and transfer reactions in the system xenon on uranium at energies below the Coulomb barrier. As the Coulomb barrier for reactions of xenon with light elements as oxygen, nitrogen, or carbon is smaller than the barrier for xenon bombardments on uranium, especially the oxygen contents had to be kept very low in this system in order to depress the amount of fission and transfer products from the reactions of xenon on oxygen; they would have disturbed the other measurements.

Our thickest uranium layers of 20 and 100  $\text{mg}\cdot\text{cm}^{-2}$  were evaporated onto 2 mm thick copper chips of 25 mm of diameter to measure production cross sections for heavy elements. These targets did not get a protecting surface.

Type	Backing		Uranium	Protecting Layer	
	substance	$\text{mg}\cdot\text{cm}^{-2}$		$\text{mg}\cdot\text{cm}^{-2}$	substance
1	C	0.03-13.0	0.1-1.0	C	0.02-0.05
2	Ti	1-7	1-3	Ti	0.05
3	Ni	3-7	1-3	Ni	0.05
4	Ni	25	1.0	Ni	0.05
5	Au	50	1.5	Au	0.05
6	Cu/Au	2/0.5 mm	1.5	Au	0.05
7	Cu	2 mm thick	20-100	-	-
8	glass	5 mm thick	1.5	Ni	0.05

Tab.1. Composition of uranium sandwich targets.

Finally it may be seen from the table that uranium was also evaporated to glass. This was done to investigate 3- and 4-prong-fission events in special metaphosphate glasses.

All these investigations are described in detail elsewhere<sup>4)</sup>.

## 7. CONCLUDING REMARKS

The preparation of sandwich targets containing uranium layers is easily accomplished by electron beam gun evaporation in very clean high vacuum systems. It should be mentioned, however, that reproducible evaporation rates, temperatures, or deposition rates strongly depend on the amount and purity of the uranium, on the size and form of the electron beam spot, on geometric factors, and on the substrate temperatures.

## REFERENCES

- 1) H.J. Maier and R. Großmann,  
ANL/PHY/MSD - 76 - 1, Argonne National Laboratory,  
1976, p. 167
- 2) G.G. Schlessinger, in: Handbook of Chemistry and Physics,  
CRC-Press, Cleveland, Ohio,  
ed. R.C. Weast, 1973, tab. D-182
- 3) R.E. Honig and D.A. Kramer,  
RCA Review, Vol 30. No. 2, 185 (1969)
- 4) GSI-Jahresbericht 1977, J - 1 - 78, Mai 1978,  
GSI - Darmstadt, Germany



Fig. 1. High vacuum evaporation apparatus and electron gun power unit.

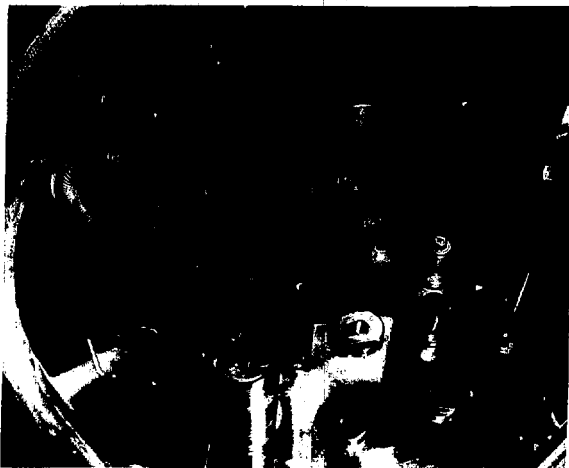


Fig. 2. 6 kVA electron beam gun evaporator.

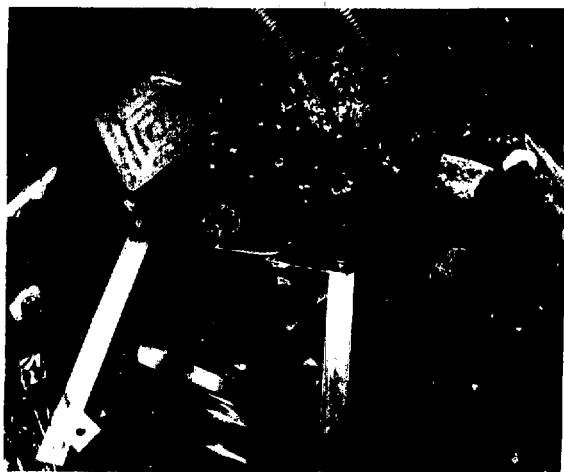


Fig. 3. Evaporation assembly for the production of uranium targets.

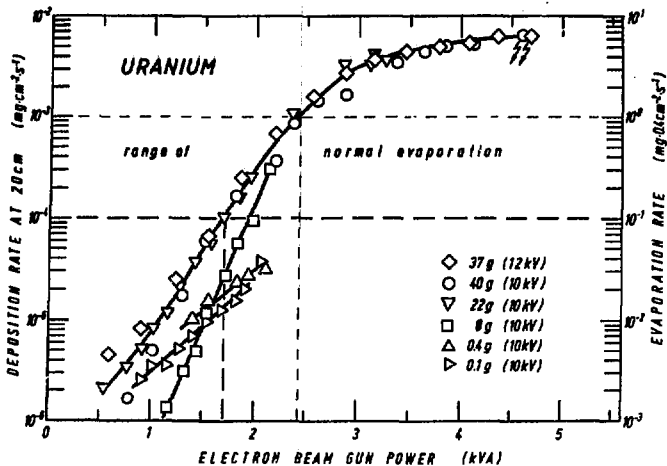


Fig. 4. Deposition and evaporation values for uranium measured as a function of the electron beam gun power.

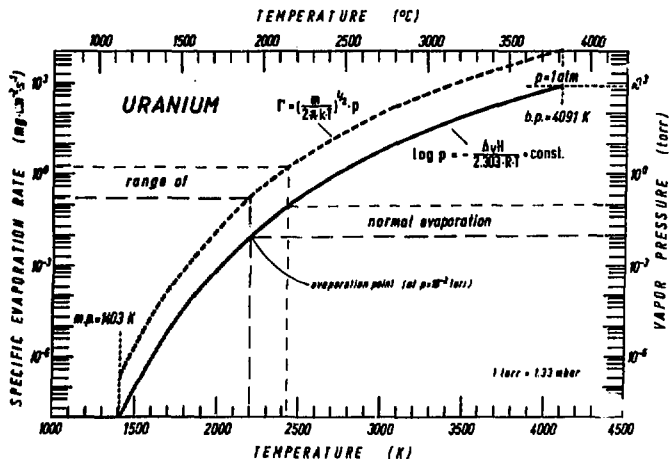


Fig. 5. Specific evaporation rate and vapor pressure of uranium as a function of the temperature.

PREPARATION OF 3/4" DIA. SELF SUPPORTING  
 $^{182}\text{W}$  and  $^{184}\text{W}$  TARGETS FOR CYCLOTRON BOMBARDMENT

C. E. Ellsworth

Lawrence Berkeley Laboratory  
University of California  
Berkeley, California 94720

ABSTRACT

A technique for production of thin (0.1 to 0.3 mg/cm<sup>2</sup>) self supporting cyclotron targets 3/4" diameter from small amounts of material (300-500 mg) by vacuum evaporation using an electron gun.

The usual method of evaporating from a molten W ball in a water cooled copper crucible produced highly stressed targets with short shelf life. There was a high mortality rate of both the targets and tungsten ball.

The first step in the technique developed was to melt 400-500 mg of isotope powders to form an outgassed ball weighing 300-400 mg. 100 mg being the average loss from outgassing. Next a tungsten rod, 1/8" diameter, one inch long, was pressed into a water cooled copper crucible. The tip of the rod was melted to outgas the tungsten, which was then ground flat to form a pedestal. The isotope ball was then spot welded to the rod using a 50 watt second discharge.

The W ball was heated by electron bombardment from a simple loop filament 3/8 to 1/2 inch dia. placed 1/4 to 1/2 inch above the ball. 6 KV at 130 ma produced an average evaporation rate. Evaporation rate and target thickness were controlled by a quartz crystal monitor. Experience determines the maximum rate that will prevent the ball from wetting the rod. With care 3 to 4 runs may be made before the ball finally wets to rod and the enrichment is lost.

Two types of substrate were used. 1/4 mil Al foil etched with Na OH gave some success. Best results were obtained with 10 mil stainless sheet coated with NaCl and heated 400 to 600 °F.

Rate of evaporation affected the target structure. Higher rates gave less stressed targets but with the risk of the isotope wetting the natural tungsten rod resulting in its loss. Tank pressure above  $4 \times 10^{-6}$  torr made the targets more brittle and shortened their shelf life.

The successful targets were stored in air for months with no apparent degradation.

## A HIGH DENSITY WINDOWLESS GAS JET TARGET

W. Tietsch, H. Feist, K. Bethge, E. hopper  
Institut für Kernphysik der Universität Frankfurt am Main  
6000 Frankfurt/M 90, Germany

## ABSTRACT

A high density gas target has been developed making use of certain characteristics of supersonic flows: A gas jet under-expanding from an axisymmetric Laval nozzle shows focussing effects. Under constant pressure conditions the first density knot of the supersonic free-jet is spatially fixed and well defined and can thus be used as a gas target. Its length is about 5mm and the cross-sectional average diameter is 3mm. By variation of the inlet gas pressure of the nozzle a variation of the target thickness can be obtained from less than one  $\mu\text{g}/\text{cm}^2$  through over 100  $\mu\text{g}/\text{cm}^2$ . Since window foils are avoided the secondary gas load has to be reduced by a three stage dynamic pumping system which is built concentrically around the gas jet and which allows a 360° access to the target area.

## INTRODUCTION

The increasing interest in heavy ion collision studies involves the development of new experimental methods, since the requirements for heavy ion physics are drastically different from those in conventional light projectile nuclear and atomic research. Most of the arising problems are related with the much larger energy loss of the heavy ions penetrating through matter due to the electronic stopping which is proportional to  $Z_{\text{eff}}^2$ . This considerable energy loss causes a sharp temperature increase in the beam spot region of the target. From calculations /1/ it was known that in cases of poor heat conduction temperatures up to 3000°C occur and exceed therefore the melting points of most of the usual target materials.

Charge exchange effects and the intensified electron stripping due to the large number of remaining electrons of the heavy projectiles causes charging of the target. Highly charged non-conductive targets thus often break under electric forces. Furthermore under heavy ion bombardment solid targets show structured rearrangements which induce mechanical effects such as strain and peeling of evaporated target layers and sputtering, blistering and the formation of voids which finally cause a severe shortening of the target lifetime. Therefore a target, nuclear physicists long for, is an almost unbreakable target, which resists heavy ion beams with intensities up to  $10^{13}$  particles per second, a target, which is well confined and of high purity. Often a variability in the thickness during the experiment run is desired with respect to time saving and the high cost of accelerator operation time.

Most of these requirements can be met with a gastarget.

A gaseous target, which is spatially well defined and operates continuously in vacuum without any separating window foils can be produced by a focussing supersonic gas jet perpendicular to the ion beam. A differential pumping system controls the secondary gas load. The average velocity of the gas particles of the jet in the direction of the ion beam, according to their low temperature is small compared to their axial velocity component. Consequently the jet itself generates a high density gradient at its boundary so that window foils are not necessary.

Several models of gas jet targets have been proposed /2/ but they all are using exclusively the free jet region in the very vicinity of the nozzle exhaust. Unfortunately, however, this is just the part of the flow where the steep gradient of the axial density causes a considerable inhomogeneity of the target. It should be mentioned that the secondary gas flow through the orifice of the first pumping section is still considerable, because of the strong expansion of the jet leaving the nozzle.

From earlier investigations /3/ it was known that in an under-expanded supersonic free-jet produced by a Laval nozzle periodic contraction occur under certain pressure conditions. The first

contraction, a section of the gas flow of increased density will be used as target zone in the present development. Fig. 1 presents an Argon free-jet visualized by its afterglow which was excited by a forgoing electron impact /3/. The figure shows a longitudinal section along the centerline of the jet and the density distribution in the section plane. The jet itself has rotational symmetry.

#### FREE-JET EXPANSION AND GASDYNAMICAL FOCUSING

The gasdynamics of a supersonic nozzle flow and the subsequent free-jet flow field needs for quantitative discussions an extended mathematical apparatus. Here, however, we will discuss the gas-conditions of dynamical focussing only qualitatively; for more details we have to refer to the literature on gas dynamics /4/.

Generally the characteristics of axisymmetric nozzle flows vary with the nozzle shape, the expansion ratio  $p_0/p_1$ , the ratio of the pressure at the nozzle entrance to the pressure in the expansion chamber respectively, and finally the ratio of the specific heat  $\kappa$  of the gas. The nozzles which produce self-focussing underexpanded free-jets are Laval nozzles and are characterized by a set of gas-dynamical variables, due to the ratio of the nozzle cross-section  $F^*/F_1$  and to the related flow conditions in the nozzle exit plane, for example the particle number density  $\rho_1$ , the Mach number  $M_1$  and the flow velocity  $v_1$ . The index 1 refers to quantities in the nozzle exit.  $F^*$  is the cross-sectional area at the point of the "critical" flow velocity, geometrically roughly the narrowest nozzle cross section.

For approximate calculations of gas flows in slim shaped Laval nozzles a onedimensional steady flow model is sufficiently exact compared to the accuracy of the experimental measuring techniques. In this simplified model the flow field inside the nozzle is described by the well known area relationship

$$\frac{F^*}{F} = \left(\frac{\kappa+1}{2}\right)^{\frac{1}{\kappa-1}} \left(\frac{p}{p_0}\right)^{\frac{1}{\kappa}} \frac{1}{\kappa} \left[ \frac{\kappa+1}{\kappa-1} \left(1 - \left(\frac{p}{p_0}\right)^{\frac{\kappa-1}{\kappa}}\right) \right]^{\frac{1}{2}} = \frac{\rho}{\rho_0} \left[1 - \left(\frac{\rho}{\rho_0}\right)^{\kappa-1}\right]^{\frac{1}{2}} \left(\frac{2}{\rho+1}\right)^{\frac{-1}{\kappa-1}} \left(\frac{\kappa+1}{\kappa-1}\right)^{-\frac{1}{2}}$$

Once the flow velocity having reached the sonic velocity at  $F^*$ , either a further acceleration or a deceleration of the gas occurs in the divergent part of the nozzle. This alternative process is controlled by the back pressure  $p'$  at the nozzle exit. If this pressure is smaller than  $p_1$ , which is determined by the area ratio  $F^*/F_1$  and by  $p_0$ , then the subsequent free-jet is said to be under-expanded. Thus for a given ratio  $F^*/F_1$  an isentropic, that is a shockfree gas flow through the nozzle is attainable only for back pressures

$$p'_1 \leq p_1$$

Underexpanding nozzles generate an additional expansion of the free-jet. The principle of the expansion is illustrated in figure 2. The streamlines, leaving the nozzle exhaust continue unaffected by the ambient pressure conditions ( $p'_1$ ) until they meet the first Mach-line. Then penetrating the rarefaction fan, built by an ensemble of Mach-lines which start the rim of the exhaust, the streamlines are changing their direction. The result is a jet expansion until the ambient pressure is reached at the jet boundary and therefore a decrease of the gas density in the vicinity of the jet's centerline. Because of the condition of constant pressure along the boundary the streamlines are bent back to the jet axis. Many compression waves, which are formed at the intersection of the expansion waves with the boundary are sent back into the center of the flow. These waves of the same family coalesce together to form the intercepted shock. For slightly underexpanded flows this interception shock is cambered and bent towards the centerline and meets there its symmetrical counterpart, thus forming the head of the density knot, as we call this region of enlarged density; it is confined downstream by a rotational symmetric system of reflected shocks.

Increase of the pressure ratio  $p_0/p_1$  and, connected with it, of the amount of intensity of underexpansion, however, yields that the interception shocks no longer meet at the jet axis, but are connected with a plain shock perpendicular to the direction of the jet, the so-called Mach-disk. The resultant yield of target thickness

in the original "focus" region is in that case considerably smaller compared to the flow of the focussing type. As a final result one finds, that for a given ratio of the nozzle cross-sections there exists a corresponding maximum of the expansion ratio. Up to this value one gets a strong focussing; otherwise the flow is underexpanded too much and not usable as a target. Fortunately the expansion ratios and the linear jet dimensions are constant for a fixed pumping speed of the connected roughing pump and are therefore independent of the entrance pressure  $p_0$ . The target density for the focussing flow thus is only a linear function of  $p_0$ ; variations in a large range of thickness are very easy to perform, without taking any care of the expansion ratio.

#### METHODS FOR MEASURING SHAPE AND DENSITY DISTRIBUTIONS OF FREE JET

It is important for all applications of jet targets to know the target thickness exactly. This can be achieved mainly by three methods, which shall be discussed briefly; for an extended study we refer to the literature /5/. To measure the shape and the density distributions we can use an electron beam attenuation probe, an electron beam fluorescence probe, or large angle single scattering of an electron beam.

The principles of all three methods are quite simple. A general sketch of the probes is given in fig. 3.

A well collimated electron beam of 20 KeV and 0.5 mm in diameter penetrates the test section. The beam is produced by a commercial television tube gun with an intensity variable from few nA to 1 mA. A three stage dynamical pumping device allows to shoot the beam into the gas section without applying any window foil. The current density of the beam penetrating the gas jet is attenuated by multiple small angle scattering. The result is a diffuse broadening of the beam; only those electrons which are not affected by the gas particles are collected in a Faraday cage. The measured residual current is correlated to the density of the traversed target layer. With static density-calibration and with some geometrical corrections the

density distribution of the jet is known (fig.4). The nozzle can be moved in the jet direction; the corresponding attenuated center-line current can be recorded automatically. A density drop of the current can be seen directly after the nozzle or in the focus region at a distance of about 30 mm from the nozzle exit, just in those parts of the flow, where the density is increased. The probe gives an almost linear output over an extended range of the entrance pressure, as it is shown in fig. 5. Here the target thicknesses in the density knot and in the nozzle exhaust are plotted versus  $p_0$ , compared to the theoretical values. The limits of the density measurements depend on the electron energy as well as on the spatial resolution required. In our case the accessible range extended from 0.5 to 100  $\mu\text{g}/\text{cm}^2$ . This type of probe gives an integrated value from which local densities cannot be extracted.

The electron beam fluorescence technique gives the local gas densities in the flow field directly (see again fig.3). About 50% of the electron-atom interactions are due to elastic scattering. In inelastic collisions the atoms of the gas are excited. The de-excitation of the jet particles gives rise to fluorescence. This fluorescence is mainly confined to a cylindrical region around the beam. The beam is then visible as a thin line with a more or less developed surrounding halo (fig.1).

By focussing the luminescence onto an optical pin hole aperture which is at right angles both to the beam and to the jet, the light emitted from a small gas volume can be detected by a multiplier. A narrow-band interference filter rejects all background light, except the one within a 25 Å region of the spectral line of interest. The photo current measured is a direct indication of the gas density in the volume of emission. Since the fluorescence arises from a direct excitation - spontaneous emission sequence, there exists an upper limit of gas density indicating the onset of collisional quenching. This limit varies for different gases and also for each emission line, because of different lifetimes. The density limit for Argon was found to be about 50  $\mu\text{g}/\text{cm}^3$ , whereas the method for

Nitrogen is good up to about  $20 \mu\text{g}/\text{cm}^3$ . The lower limit depends on the sensitivity of the optical detector and its signal-to-noise ratio and is about  $0.5 \mu\text{g}/\text{cm}^3$  for Argon and  $0.02 \mu\text{g}/\text{cm}^3$  for Nitrogen. The spatial resolution of the optical device is about  $0.1 \text{ mm}^3$ . Calibration runs were performed in static gas targets.

The third method of density measurement applied, is the large angle scattering gage, which is an integrating method too. The principle is shown in fig. 3. From each segment of the beam path a few electrons will be scattered into the direction of the electron detector. The scattering probability is a strong function of the gas density and the scattering angle and drops down only an order of magnitude in a range of scattering angles between  $60^\circ$  to  $120^\circ$ . In this angular range the probe is not particularly sensitive to small changes in the geometrical alignment. By sweeping the beam with the aid of deflection coils so that it intersects the jet, it is possible to measure density distributions across the profile of the jet, integrated over the path of the electron beam. Having gained sufficient confidence in the described methods by foregoing tests all techniques were used to deduce the density distribution of the focussed free-jets; especially the optical beam probe was used to study the geometrical properties of the free-jet expansion.

## RESULTS

In order to find the most suitable nozzle for the production of well-typed jets we investigated a series of differently shaped Laval nozzles under different pressure ratios. The geometrical dimensions of the nozzles investigated have been varied as follows: diameter of the smallest cross-section from 0.32 to 0.9 mm, area ratio from 3.44 to 100. Nozzles made from brass and lucite (fig.6) were produced on a lathe; nozzles of glass were blown from glass capillaries. We found, however, no significant dependence of the quality of the focussed jets from the nozzle material, expected because of the different heat conductivity of the materials.

The mass throughput, on the contrary, is strongly affected by the geometrical shape of the nozzle in the vicinity of the narrowest cross-section, just at that point, where the flow becomes sonic. A smooth transition into this region causes a mass flux identical with the theoretically computed value. An edgy transition, however, as it is inevitable with turned nozzles, causes a mass flux about 20% smaller than the corresponding theoretical value for the cross-sectional area and the given entrance pressure.

The important characteristic linear dimensions of the free-jets are the diameter  $D_a$  of the largest extension of the flow, the diameter of the focussed flow portion  $D_{di}$ , and the axial distances of the head of the knot  $L_{kn}$  and of the point of highest density  $L_{di}$  from the nozzle exit, respectively. These values, plotted versus the square root of the ratio of the expansion pressures are shown in fig. 7. The dependence is almost linear, as is known from a free-jet expanding from a sonic orifice /6/. The linear dimensions can also be expressed analytically

$$\begin{aligned} (D_a/\bar{d}_1) - 1 &= ((p_1/p_1')^{1/2} - 1) A \\ D_{di} &= \epsilon D_a \\ L_{di} &= \bar{d} * ((p_0/p_1')^{1/2} - B) C \end{aligned}$$

where A, B and C depend upon the nozzle parameters and upon the ratio of the specific heats of the gases.  $\epsilon$  depends slightly on the strength of focussing and is about 0.4.

To measure the density distributions similar runs were performed with all nozzles at different entrance pressures and at the highest expansion ratio which could be obtained with respect to the pumping speed of the foreline pump. The aim of this was to look for target densities as high as possible for a given mass throughput, or in other words, to look for the best efficiency. The measurements were made automatically, using digitally controlled stepping motors for the motion of the nozzle and of the analyser, and simultaneous recording of the data. Examples of density profiles recorded in such manner are shown in the following figures. Fig. 8 gives the result

of the integrating large angle scattering probe; fig. 9 presents the local density distribution of the same free-jet received by the fluorescence method. Fig. 10 and 11 exhibit the density distribution of a sonic free-jet and of a focussed Laval jet, compared by means of density contour lines. This way of display demonstrates very clearly the obvious difference between both types of supersonic flows. By integrating these data graphically, the axial target thickness in  $\mu\text{g}/\text{cm}^2$  can be obtained. The ratio of the integrated axial density to the target thickness in the exit plane of the nozzle (fig.12) is independent from the actual entrance pressures. With respect to this distribution a focussing factor of about 0.6 could be reached. This factor depends on the ratio of the nozzle cross-sections and has a maximum of about 0.7 for a monatomic gas and about 0.5 for a diatomic gas, both values for a given pumping speed of  $200 \text{ m}^3/\text{h}$  of the attached roughing pump. As a final result we can state that the target thickness in the knot region of the flow depends linearly upon the mass flux through the nozzle. A thickness of  $250 \mu\text{g}/\text{cm}^2$  per unit mass throughput could be reached for Argon and of  $170 \mu\text{g}/\text{cm}^2$  per unit mass throughput for nitrogen. The geometrical dimensions of the nozzle which is able to produce a focussed free-jet with the best focussing factor we found to be

$$d^* : 0.5 \text{ mm}$$

$$d_1 : 1.65 \text{ mm}$$

opening angle of the divergent part of the nozzle:  $6.3^\circ$

#### THE MECHANICAL LAYOUT OF A JET TARGET

The whole target device consists of a scattering chamber of 300 mm in diameter and a two stage differential pumping system mounted concentrically around the gas jet perpendicular to the ion beam direction. To obtain a  $360^\circ$  access in the reaction plane a variable slit is left so that the density knot can be fixed in the plane and exposed to the ion beam (fig.13). For this purpose the Laval nozzle could be moved by means of a threaded spindle which is to be seen on top of the apparatus in fig. 14. The reaction products can be

detected either inside the chamber or in a long tube which can be revolved in the reaction plane and is flanged to a metal-band sealed connecting piece. A measured pressure profile along the ion beam is shown in fig. 15. An overall pressure reduction by a factor of more than  $10^6$  is attainable at the incoming side of the beam and of about  $10^5$  at the detector side. More than 90% of the integrated target thickness is contained in the density knot, a 3mm region. A general view of the complete target device is shown in fig. 16.

#### SUMMARY

It is shown that a high density windowless, spatially limited, gas target can be realized by using a focussed supersonic free-jet produced by a Laval nozzle. To measure both, linear dimensions and the density distribution of the jet three different electron beam probes were successfully tested. To apply the target with an ion beam, a universal target chamber has been built with a three stage dynamical pumping system in order to reduce the secondary gas load. The pressure reduction was found to be high enough so that more than 90% of the target thickness is confined to the jet.

#### ACKNOWLEDGMENTS

We would like to thank GSI at Darmstadt/Germany for the support of this project.

## REFERENCES

- /1/ F. Nickel, GSI-Bericht 73-7 (1973), 1  
F. Nickel, Nucl. Inst. Meth. 134 (1976), 11
- /2/ K. Bethge, G. Günther, Z. angew. Phys. 17 (1964), 548  
J. Ulbricht, G. Clausnitzer, G. Graw, Nucl. Inst. Meth. 102  
(1972), 93
- /3/ A. E. Grün, Z. Naturforschung 9a (1954), 833  
A. E. Grün, E. Schopper, B.W. Schumacher, Z. angew. Phys. G  
(1954), 198 J. appl. Phys. 24 (1953), 1527
- /4/ A.H. Shapiro, The Dynamics and Thermodynamics of  
Compressible Fluid Flow, Vol.1 and 2, (1953), Ronald Press, N.Y
- /5/ W. Tietsch, Dissertation, Frankfurt 1976  
J.J. Grodski, B.W. Schumacher, ISA Transactions 6 (1967), 103  
E. O. Gadamer, UTIA Report No. 83 (1962)
- /6/ H. Ashkenas, F. S. Sherman, Rarefied Gasdynamics, Vol.2 (1966)  
84, Academic Press, N.Y.

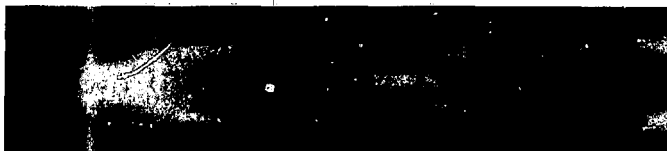


Figure 1. Afterglowing argon free-jet. The fluorescence is stimulated by electron bombardment of the jet just having left the Laval nozzle /3/.

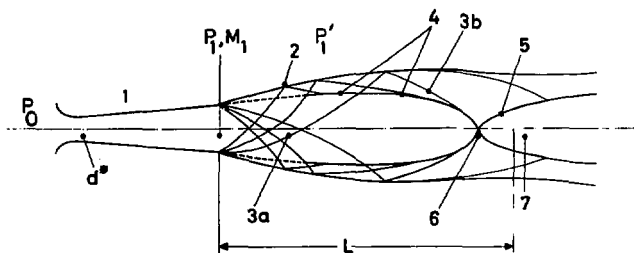


Figure 2. Schematic presentation of an underexpanded focussed free-jet produced by a Laval nozzle. (1). Throat diameter:  $d^*$ , entrance pressure  $p_0$ , exit pressure and nozzle Mach number  $p_1$  and  $M_1$ , resp., (2) jet boundary, (3a) rarefaction waves, (3b) reflected compression waves, (4) intercepted shock, (5) reflected shock, covering the zone of enlarged density (7), (6) head of the density knot.

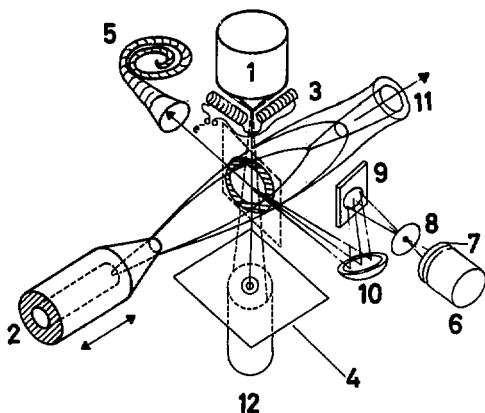


Figure 3. General sketch of the electron beam density probes

- |                                       |                         |
|---------------------------------------|-------------------------|
| (1) Electron gun device               | (7) Interference filter |
| (2) Laval nozzle                      | (8) Pinhole aperture    |
| (3) Sweeping magnet                   | (9) Plane mirror        |
| (4) Aperture                          | (10) Concave mirror     |
| (5) Electron detector,<br>channeltron | (11) Supersonic jet     |
| (6) Multiplier                        | (12) Faraday cage       |

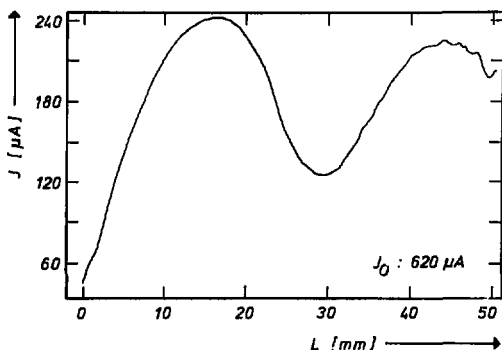


Figure 4. Alternation of the axial current density of an electron beam with an original beam current of  $J_0 = 620 \mu\text{A}$ , which has penetrated a focussed free-jet.

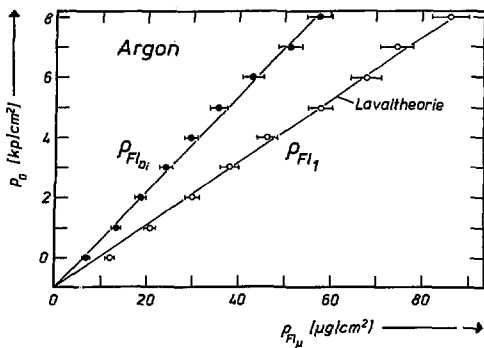


Figure 5. Target thickness in the exit plane of the nozzle and in the density knot as a function of the entrance pressure  $p_0$ . The measured exit values are compared to the theory.

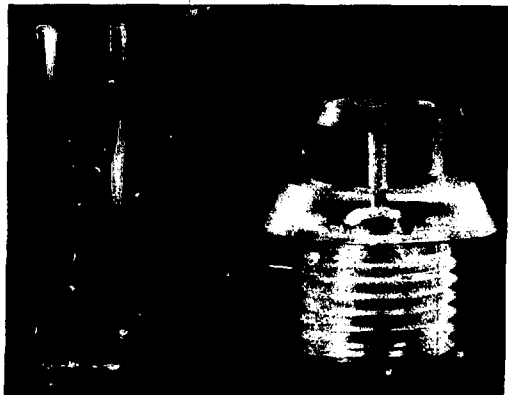


Figure 6. Laval nozzles. A nozzle blown from a glass capillary on the left side and a nozzle made from lucite on the right. The coefficient of magnification is about 3.

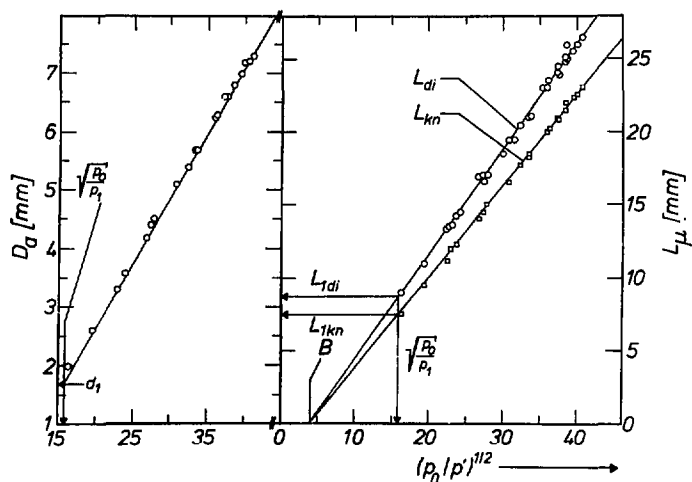


Figure 7. Diameter of the free-jet at its largest extension, and distances of the point of highest density in the focussed flow region  $L_{di}$  and of the head of the knot  $L_{kn}$  from the nozzle exit as a function of the expansion ratio.

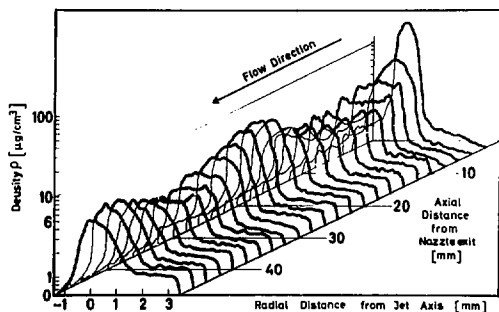


Figure 8. Density distribution of an argon free-jet, measured by the electron large angle scattering method.

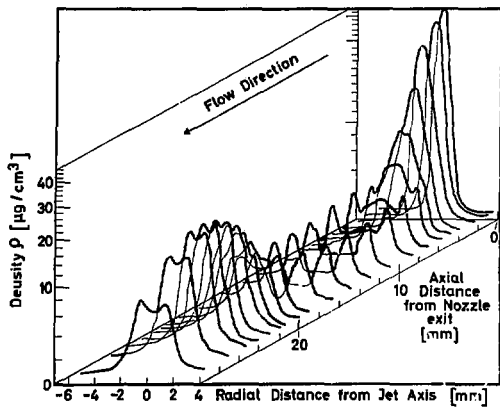


Figure 9. Density profiles of an argon free-jet, received with the fluorescence probe.

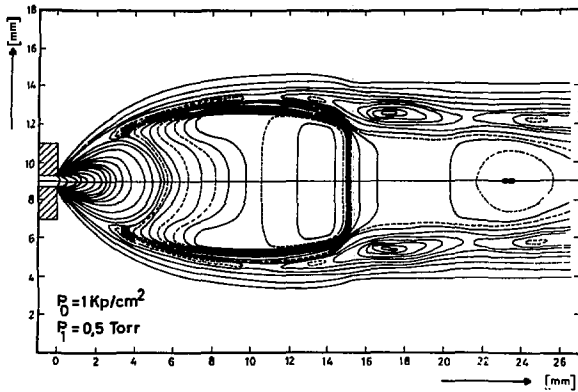


Figure 10. Density distribution of a free-jet produced by a sonic nozzle in a plane which cuts through the jet's centerline.

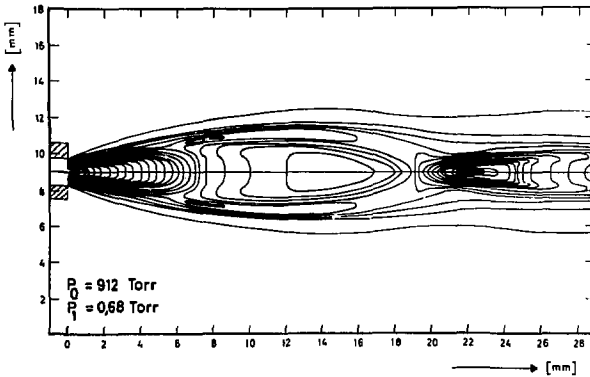


Figure 11. Density distributions of a focussed free-jet produced by a Laval nozzle.

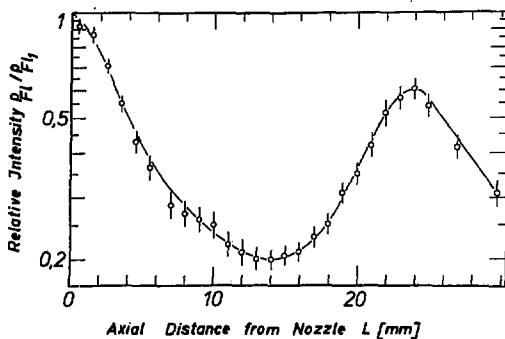


Figure 12. Integrated axial density distribution of a focussed jet, normalized to the density at the nozzle exit.

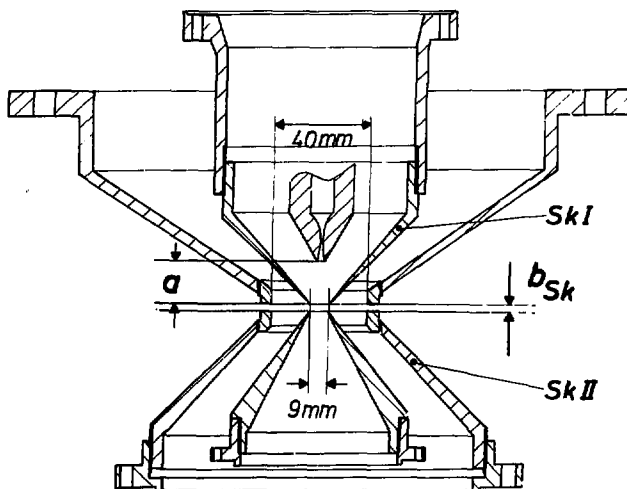


Figure 13. Section of pressure reducing skimmers (sk) of the dynamical pumping system. The distance  $a$  of the Laval nozzle to the slit with the adjustable width  $b_{sk}$  is variable.



Figure 14. Target chamber with mounted pumping ports.

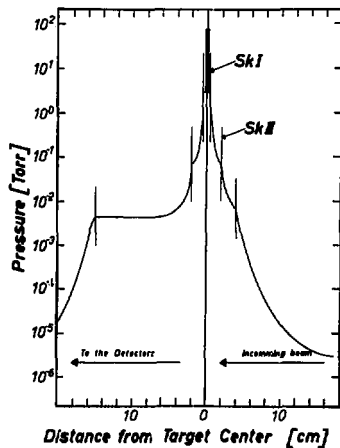


Figure 15. Static pressure along the ion beam line as a function of the radial distance from the target center.



Figure 16. General view of the target.

GALLIUM RICH  $Ga_2O$  TARGETS FOR USE AT ROOM TEMPERATURE  
FROM ISOTOPIC  $Ga_2O_3$  STARTING MATERIAL.

William D. Riel

Department of Physics  
State University of New York  
Stony Brook, New York 11794

ABSTRACT

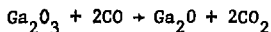
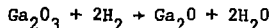
The low melting point of Ga and its ability to supercool render it a difficult target for use in room temperature beam lines. Methods of reducing the sesquioxide are discussed and a technique for reduction-evaporation to obtain the sub-oxide  $Ga_2O$  which is rich in metallic Ga is described.

## DISCUSSION

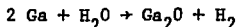
Self-supporting Ga targets of 700  $\mu\text{gs}/\text{cm}^2$  were required for giant resonance studies with the tandem FN Van de Graaff at Stony Brook in a beam-line to be operated at room temperature. Metallic Ga poses formidable obstacles under these circumstances. Even though the melting point ( $29.7^\circ\text{C}$ ) is above room temperature, the pure metal prefers to supercool and remain a liquid down as low as  $0^\circ\text{C}$ .

Should the physics involved tolerate a backing, on which to support the liquid, Ga obliges by alloying with the metals it wets or it beads up into small droplets on those it does not. It fails to wet most non-metals except for pyrex and quartz which are also immune to attack except at very high temperatures. It does not condense on carbon in a vacuum evaporation.

For this particular experiment Ga isotopes of 69 and 71 were required and it was decided that oxygen would not interfere seriously with the experiment. Investigations of the oxides revealed the suboxide  $\text{Ga}_2\text{O}$  to be the best candidate of the three in existence. It is very stable, possesses the highest ratio of metal to oxygen, and sublimes readily above  $500^\circ\text{C}$ . The monoxide is unstable and the sesquioxide  $\text{Ga}_2\text{O}_3$  is stable but has very low notability. The sesquioxide is the form in which the isotopes are supplied by Oak Ridge National Laboratory and is easily reduced by Hydrogen<sup>1)</sup> or carbon monoxide. In fact the reaction favors the right side of the equation so strongly that excessive Ga metal was always produced when attempts were made to limit the reduction by operating at the lowest temperature possible and never exceeding  $500^\circ\text{C}$ .



Another method for producing very pure suboxide proved to be reducing the  $Ga_2O_3$  with  $H_2$  to the Ga metal which is placed in a Ta crucible in a stream of water vapor and heated to  $950^\circ C$ .



The product is sublimed under vacuum from a W boat onto substrates as described later.

This is an excellent procedure when using natural starting materials. The number of steps required however result in high losses of the isotopes. The best technique for these is to heat them in a W boat under vacuum. The suboxide is the main product and since its decomposition temperature is listed at  $700^\circ C$  this was never exceeded at first. These conditions however produce low evaporation rates and poor films. When the temperature is raised to  $1200^\circ C$ , strong, relatively strain free films are produced. X-ray analysis reveals the presence of metallic Ga in films when the boat temperature is raised above  $700^\circ C$ . The mechanism for this is not yet understood. The included Ga results in very tractable films and better statistics for the experiment.

#### PROCEDURE

A polished quartz slide is mounted 8 cm above a commercial .005" W canoe boat charged with 25 mgs of  $Ga_2O_3$  as the isotope required. A Ta canoe boat alongside is charged with a small amount of  $Ba Cl_2$  and the system pumped to  $\sim 10^{-6}$  mm Hg.  $40 \mu g/cm^2$  of  $Ba Cl_2$  is deposited on the slide using a quartz crystal monitor to determine thickness. The W boat is next slowly heated to  $500^\circ C$  till outgassing stops, whereupon the temperature is rapidly raised to  $1275^\circ C$ .  $700 \mu g/cm^2$  requires 3 hrs. and upon completion the temperature must be dropped over a period of 2 hours and the film should remain under vacuum overnight. This will allow the film to anneal and results in a shiny black or dark brown appearance.  $Ga_2O$  films can be mistaken easily for carbon foils and can be handled by the same floating and mounting techniques. Care must

be exercised however with films over  $500 \mu\text{g}/\text{cm}^2$  or where the annealing time may have been shortened. These may curl up on drying and fall from the mounting frame. They should be retained with a target frame cover while still wet. Another method is to dissolve some Canada Balsam in xylene and apply it to the frame. When the solvent has dried, pick the foil up as usual. The Balsam remains tacky and retains foils indefinitely. It also has a low vapor pressure. The suboxide films can be stored in air for years with no ill effects.

#### REFERENCE

1. J. M. Heagney and J. S. Heagney, "Reduction Techniques for Isotopic Materials", Proceedings of International Nuclear Target Development Society, 1976.

PREPARATION OF ISOTOPICALLY ENRICHED, SELF SUPPORTING  
CHROMIUM TARGETS

H. U. Friebe, Dagmar Frischke, R. Großmann and H. J. Maier<sup>†)</sup>

Technologisches Labor der Sektion Physik der Universität München  
Am Coulombwall 1, 8046 Garching, W-Germany

ABSTRACT

The preparation of isotopically enriched, self supporting metallic chromium targets with a thickness between 0,5 and 3 mg/cm<sup>2</sup> is described. Two reduction methods for Cr<sub>2</sub>O<sub>3</sub> to metallic chromium are discussed: a metallothermic reduction -distillation procedure and a reduction with hydrogen gas. Target preparation may be completed without problems by evaporation. Rolling of foils is also possible after a careful pretreatment of the metal, consisting of vacuum-degassing and electron-beam melting.

1. INTRODUCTION

For the investigation of (p, n) reactions on <sup>52</sup>Cr and <sup>54</sup>Cr, of (<sup>3</sup>He, n)-reactions on <sup>53</sup>Cr and of α-induced reactions on <sup>50</sup>Cr

<sup>†)</sup> presented the paper

it was required to prepare self supporting, isotopically enriched metallic chromium targets in the thickness range between 0,5 and 3 mg/cm<sup>2</sup>.

The inventory form of all chromium isotopes offered by the Oak Ridge Isotopes Center and by Technabsexport in Moscow is Chromium-Sesquioxide Cr<sub>2</sub>O<sub>3</sub>. Therefore reduction methods for the conversion of Cr<sub>2</sub>O<sub>3</sub> to metallic chromium had to be developed as well as evaporation and rolling procedures for foil production.

As far as I know there exists only one recent paper dealing with the preparation of self supporting chromium foils. This paper was given at the 1971 Gatlinburg Symposium by Kuehn, O' Donnel and Kobisk (1) and describes an electroplating method. This method is very economic as concerns the waste of isotopic material. However, a large amount of chromiumoxide is necessary to perform the electrolytic deposition of even small quantities of metallic chromium. The authors quote the application of as much as 2.5 grams of CrO<sub>3</sub> for 10 ml of the plating solution. In view of the high cost of enriched isotopes, we looked for methods which do with about 100 mg of material.

## 2. REDUCTION PROCEDURES

Two reduction techniques have been applied successfully for the conversion of Cr<sub>2</sub>O<sub>3</sub> to metallic chromium: first, a reduction distillation method, and - second - the reduction by hydrogen.

## 2.1 Reduction - Distillation

The principle of the reduction-distillation method has been reported by Kobisk and Grisham (2), who used it for the preparation of rare earth metals from their oxides. It is easy to handle and can be done in every target laboratory without buying special equipment. As an example 100 mg of  $\text{Cr}_2\text{O}_3$  are calcined and mixed with about 1,5 times of the stoichiometric amount of Zirconium powder. This mixture is compacted under vacuum and the pellet placed in a tube shaped tantalum crucible, which is heated slowly to  $1500^\circ\text{C}$  and held at that temperature for a period of 15 minutes. The nascent chromium metal is formed by the reaction  $2\text{Cr}_2\text{O}_3 + 3\text{Zr} \rightarrow 4\text{Cr} + 3\text{ZrO}_2$  and condensed in form of a thin layer of about 30 - 50  $\mu\text{m}$  thickness on the inside surface of a quartz hemisphere, which is located 5 mm above the port of the crucible. The collection efficiency is approximately 70%. The chromium layer can be stripped easily from the quartz-surface after cooling.

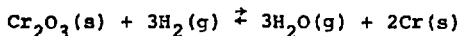
At the reaction temperature, the vapour pressures of Zirconium metal, Zirconium oxide and Chromium-Sesquioxide are low compared to the vapour pressure of Chromium metal (6, 7). This is vital to minimize contamination of the reduction product.

Chromium metal yielded by this procedure is well suited for target preparation by vacuum condensation, but too brittle for a rolling procedure. The reason for this is possibly a silicone contamination introduced by the quartz collecting dome.

## 2.2 Reduction by Hydrogen

More ductile chromium metal can be prepared by hydrogen reduction of  $\text{Cr}_2\text{O}_3$ . This reduction, however, works under special conditions only. Early investigations of Baukloh and Henke (3) showed, that it is important to use dried hydrogen gas and that a high temperature and a long reaction time are necessary to perform the reaction. For instance, an eight hour reduction at  $1000^\circ\text{C}$  has a yield of less than 10% only. For a 100%-yield, a temperature of  $1400^\circ\text{C}$  and a reaction time of 6 hours are necessary.

The theoretical background for this situation must be sought in the unfavourable thermodynamics of the reaction involved:



The equilibrium constant is given by the expression

$$K = \left( \frac{p_{\text{H}_2\text{O}}}{p_{\text{H}_2}} \right)^3$$

which is related to the free energy by

$$\Delta F^\circ = -R \cdot T \cdot \ln K$$

with

$p$  = partial pressure

$T$  = Kelvin-temperature

$R = 1.98 \text{ cal/mole} \cdot ^\circ\text{K} = \text{gas constant.}$

Using the free energy data published by the U. S. Bureau of Mines (4), the ratio of the partial pressures of water and hydrogen in chemical equilibrium has been calculated and compiled in table 1. For example,

T [°K]	1000	1200	1400	1600	1800
$\frac{P_{H_2O}}{P_{H_2}}$	$6.65 \cdot 10^{-6}$	$8.77 \cdot 10^{-5}$	$5.40 \cdot 10^{-4}$	$2.10 \cdot 10^{-3}$	$5.98 \cdot 10^{-3}$

Table 1: Equilibrium conditions for the reduction of  $Cr_2O_3$  by hydrogen.

at  $1000^{\circ}K$ , this ratio is as small as  $6.65 \cdot 10^{-6}$ . At  $1400^{\circ}K$ , which is the maximum temperature we can generate with our tube furnace its value is still  $5.4 \cdot 10^{-4}$ , which means that in equilibrium the maximum tolerable water content of the hydrogen atmosphere is 540 ppm. Moreover, in order to make the reaction come to a completion in a reasonable time we consider a ratio of 10 ppm or less to be favourable.

In order to realize this condition we have set up a special reaction apparatus. Its main part is a tube furnace which is able to heat the sample to a maximum temperature of  $1400^{\circ}K$ . The reaction tube is manufactured of quartz, while the gas conducting system is an all stainless steel construction. Extreme purification of the hydrogen gas is achieved by a palladium diffusion

cell, which guarantees a water- and oxygen content of less than 1 ppm. Operation is started by evacuating the system to a pressure of less than  $10^{-5}$  torr by a turbomolecular pump. Then purified hydrogen is passed through with a flow speed of 1.5 l/min and heating is started. A reaction time of 6 hours at  $1400^{\circ}\text{K}$  turned out to be sufficient to complete the reduction.

### 3. TARGET PREPARATION

#### 3.1 Evaporation Techniques

For target foil preparation by vacuum condensation a collimating tantalum evaporation source of type ME 1, supplied by the Mathis Company, was used. This source yields a collection efficiency of 20% at a distance of 4 cm. Copper sheet with a thickness of 0.01 mm was chosen as a backing. A substrate temperature of  $350^{\circ}\text{C}$  and a deposition rate of  $1 \dots 2 \mu\text{g}/\text{cm}^2 \cdot \text{sec}$  were found best to minimize internal stress of the condensed chromium foil. Etching of the copper backing was performed in the conventional way with a solution consisting of 1 part in weight of trichloroacetic acid, 5 parts of aqueous ammonia of density 0,91 and 5 parts of distilled water. Chromium foils in the thickness range between  $500 \mu\text{g}/\text{cm}^2$  and  $3 \text{mg}/\text{cm}^2$  were produced in this way. Residual copper and chlorine impurities were detected by neutron activation analysis and found to be lower than 500 ppm.

### 3.2 Rolling of target foils

Target preparation by rolling involves some general problems attended with casting and cold working of chromium. Even high purity chromium is brittle at room temperature and can not be rolled to foil without some trouble. Sully and coworkers (5) showed, that small impurities of nearly all metals in the order of magnitude of a few hundred ppm largely enhance the brittleness of the material. This is true also for oxygen, nitrogen and hydrogen. In addition, chromium sublimes to a considerable amount in vacuum at temperatures higher than  $1500^{\circ}\text{C}$ , whereas its melting point is as high as  $1890^{\circ}\text{C}$ . This complicates casting by electron beam melting. Argon-arc melted chromium on the other hand is too brittle to be cold rolled, as shown by Sully. Taking these facts into consideration, the following procedure resulted in usable target foils:

Because of its high degree of purity, it is necessary to use hydrogen reduced chromium. Hydrogen reduction of  $\text{Cr}_2\text{O}_3$  yields powdered metallic chromium. In order to drive out any residual hydrogen, about 100 mg of this metal powder is heated for three hours at  $1300^{\circ}\text{C}$  in an aluminium crucible in a vacuum better than  $5 \cdot 10^{-7}$  torr. After this, a pellet is formed, using a pressure of  $130 \text{ kp/mm}^2$ . This pellet, in turn, is electron beam melted in a water cooled copper crucible, the vacuum again being better than  $5 \cdot 10^{-7}$  torr. Great care has to be taken during

the melting process in order to keep sublimation losses low. An average efficiency of 80% is typical for this step. The resulting chromium bead is still brittle to a certain degree. This manifests itself by fractures during the initial stages of cold rolling. Fragments of about 10 - 15 mg, however, turned out to be ductile enough for rolling down to foils of about 1 mg/cm<sup>2</sup>. Heat treatments at different stages of thickness reduction are of advantage in order to prevent the appearance of pinholes for thicknesses greater than 1 mg/cm<sup>2</sup>. A minimum thickness of 700 µg/cm<sup>2</sup> was achieved by this method.

**Literatur:**

- (1) P. R. Kuehn, F. R. O'Donnel and E. H. Kobisk, NIM 102 (1972), 403
- (2) E. H. Kobisk and W. B. Grisham, Material Research Bull. 4(1969),651
- (3) Baukloh and Henke, Z. anorg.-Chemie 234 (1937), 307
- (4) Bull. 452 of U. S. Bureau of Mines (1954)
- (5) A. H. Sully: Chromium, Butterworth, London 1954
- (6) R. E. Honig and D. A. Cramer, Vapour pressure curves of the elements, RCA-Laboratories, Princeton, N. Y. Fall 1968
- (7) Y. S. Touloukian ed.: Thermophysical properties of high temperature solid materials, Mac Millan, New York 1967

A Dry Powder Technique for the  
Preparation of Carbon Foils\*

W. R. Lozowski

Indiana University Cyclotron Facility  
Milo B. Sampson Lane  
Bloomington, IN 47401

ABSTRACT

One through eight mg/cm<sup>2</sup> carbon foils for use as accelerator targets have been prepared from an air suspension of graphite powder which was allowed to settle and was subsequently pressed. Keys to the process are the use of: 1. a DeVilbiss medicinal powder blower and 2. vacuum-evaporated carbon coated glass slides as the substrate for the settling and pressing operations. In all of several trials, the targets did not stick to the glass slides, could be handled with forceps, trimmed with a razor blade, and mounted over a 20 mm dia. hole. Uniformity was better than 10%.

INTRODUCTION

The method to be described is a successful effort to bridge a nebulous area between processes which produce pure carbon films by vacuum evaporation and those which produce films by straightforward pressing and/or machining. A principal attribute of the method is the short time required to produce

a self-supporting film. Also, potential residues associated with liquid-medium settling techniques are not possible and no binder materials are used. While the use of amorphous carbon is precluded because it is hard and will not bind internally to produce a strong film, in contrast to graphite, additional properties of low thermal conductivity and high electrical resistivity<sup>1)</sup> reveal it to be a poor choice for accelerator targets anyway.

A useful film size from 10 mm x 25 mm to 25 mm square can be routinely produced. All excess carbon remains in the column and is recoverable. The method is therefore economically feasible for isotopically enriched carbon provided it has been graphitized (recrystallized) at 2500°C or more, and enough material for an initial charge of 75 to 300 mg<sup>2)</sup> is available.

Although the dimensional relationships of the settling column components were not found to be at all critical, a fully dimensioned figure has been provided. The DeVilbiss pocket-type powder blower no. 33, the heart of the setup, may be purchased at drugstores and medical supply houses.<sup>3)</sup>

#### PROCEDURE

When the settling column has been assembled as shown in the figure, it is charged with 75 to 300 mg of 325 mesh graphite powder.<sup>4)</sup> One then selects a 20  $\mu\text{g}/\text{cm}^2$  (not a critical thickness) vacuum-evaporated carbon coated glass slide (25 mm x 75 mm) to score and break into two 25 mm square pieces. After one of the pieces is weighed, it is placed on the top disk

(carbon side up) of the removable support wire and lowered into the column. The appropriate height from the bottom of the column can be determined with a few settling trials. Seven centimeters from the bottom of the column (i.e. the top of the funnel) to the top support disk produced an even carbon powder layer with the apparatus described.

A 0.25 mm thick piece of surgical rubber sheet (or similar material) with an appropriate slit for the support rod is used as a top cover. With the cover resting in place and the supply gas or air<sup>5)</sup> adjusted to less than 30 psi, a foot operated free-venting air valve<sup>6)</sup> is tapped lightly and quickly one or more times.

Best results are obtained when the powder is allowed to settle somewhat between these pressure pulses. As each pulse of air in the column reaches the thin rubber cover, it bulges and collapses to provide a gentle brake and reverse pulse. This action discourages suspended powder from being carried out. Also, the free-venting feature of the air valve helps in controlling the carbon powder by providing a controllable pulse of shortened duration. By monitoring the height of the powder in the column with a flashlight and the room lights off, one can avoid blowing any powder out of the top.

Visual inspection is usually adequate to determine when the slide piece should be removed from the column to weigh the deposit. If the coating is too thick or is non-uniform in appearance, the deposit is dumped back into the column and the slide piece is reused for another trial. Of course, if the deposit is too thin, the slide is returned to the column for additional powder. Handling of the coated slide is not particularly difficult.

Having arrived at a satisfactory coating, one transfers the coated slide to a hardened platen and carefully places the mating 25 mm square slide piece (carbon side down) on top of it. This is the most delicate operation in the process. And if it is not done slowly and smoothly, carbon will blow out from the sides or shift on the slide. A mechanical lowering jig may be necessary if one encounters difficulty.

Another hardened platen, added after moving the assembly to a hydraulic press, completes the sandwich for pressing. Fourteen tons/in<sup>2</sup> ( $1.93 \times 10^8$  nt/m<sup>2</sup>) is adequate to compress the graphite powder into a lustrous, somewhat flexible film. The pressure must be released as smoothly as possible.

Noteworthy at this point is the need for "reasonable" parallelism of the press platens. The lack of which, as one might expect, will cause the glass slide pieces to convert to powder with an impressive bang! Surrounding dust shields of cardboard, etc. are highly recommended.

Trimming, measuring and reweighing establish the final dimensions of the film. Any existing non-uniformities of 10% become very evident after pressing. Thicker areas are more reflective of light, thinner areas are dull, and shifted areas are revealed by boundary lines.

#### IMPLICATIONS

One should, hopefully, be able to apply modifications of the above technique in preparing some other desired thin films. Sulfur is one of these. To date, the column has produced good deposits with sifted sulfur powder but a satisfactory releasing substrate for the pressing operation

has not been found. However, if one is willing to sacrifice the completely dry nature of the described process, it should be possible to coat the glass slide pieces (or other temporary substrate) with a substance to be dissolved in a suitable solvent after pressing.

As ever in nuclear target-making, the desire to economically produce thin films from expensive materials precipitates an involving work in an evolving playground.

#### Reference and Footnotes

\*Work supported in part by the National Science Foundation.

1. Coordination and editing by J. F. Hogerton and R. C. Graff, Reactor Handbook - Materials, Tech. Information Service U.S.A.E.C., p. 133, declassified 1955.
2. Larger quantities are easier to work with.
3. Also available from The DeVilbiss Co., P.O. Box 552, Somerset, PA 15501.
4. 99.5% graphite powder is available from Alpha Division of Ventron Corp., 152 Andover St., Danvers, MA 01923.
5. According to the Reactor Handbook - Materials, p. 141, "Graphite will absorb about 0.09 weight-percent of water vapor in a saturated atmosphere at 20°C. Absorption at this temp from an atmosphere of 60-percent relative humidity is negligible."
6. A free-venting air valve is a normally-closed valve of 3-way design that exhausts the down stream line to atmosphere when the valve is unenergized.

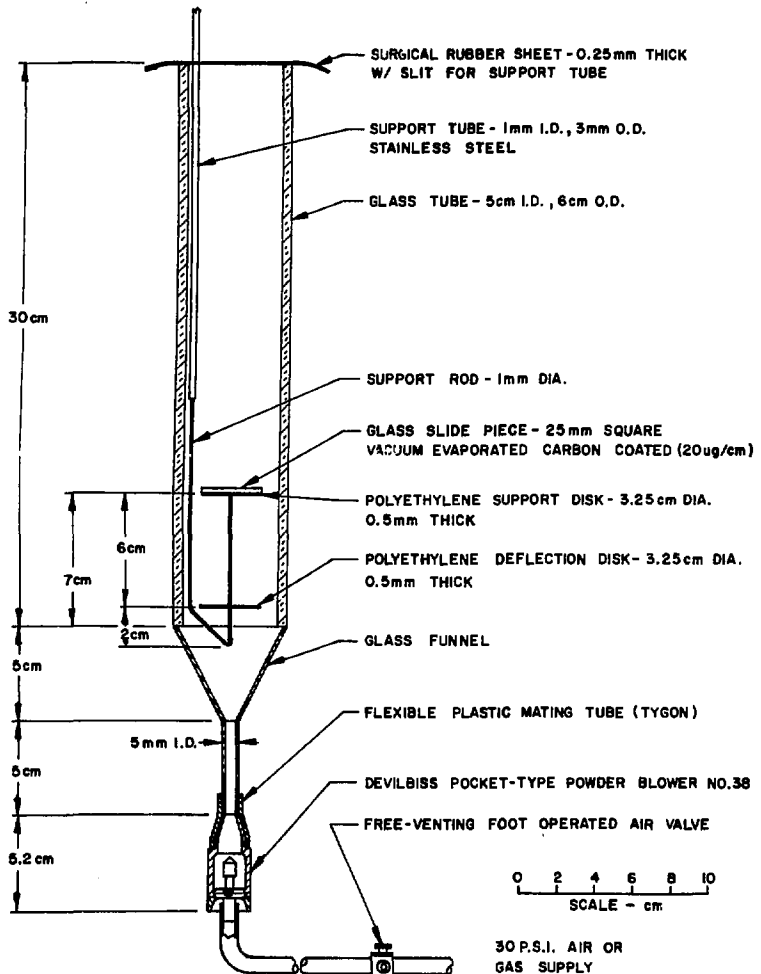


Figure 1. Air suspension/settling column for graphite powder.

A HEAVY ION SPUTTERING SYSTEM WITH A  
PENNING-ION-SOURCE

H. Bauman<sup>+)</sup>  and H.L. Wirth

Max-Planck-Institut für Kernphysik Heidelberg

+)Institut für Kernphysik der Universität Frankfurt/Main

**Abstract:** A Penning-ion-source with end extraction was developed and adapted to a high vacuum sputtering equipment for producing thin films of materials with high melting points.

### Introduction

The preparation of targets for nuclear measurements by using heavy ions for sputtering high melting materials with low vapor pressure has won increasing importance during the last years.

Most of the sputtering systems to our knowledge are equipped with duoplasmatron ion sources. It is well known that some problems arise from operating the duoplasmatron ion source. The ignition is not simple. The lifetime of the filament is not sufficient. Therefore generally targets with a thickness greater  $100\mu\text{gcm}^{-2}$  from materials with low sputtering yield are difficult to be produced in one step. All the interruptions lead to inhomogenous foils because the surface of the substrate is contaminated or oxidized by the vent gas. Furthermore it is impossible to use the duoplasmatron for reactive sputtering with gases like  $\text{O}_2$ ,  $\text{N}_2$ ,  $\text{Cl}_2$  etc. added to the operating gas, because of drastic reduction of the filament lifetime by chemical reaction.

## Description of the system

The mentioned problems prompted us to change the Danfisik duoplasmatron of our sputtering unit for a Penning-ion-source.

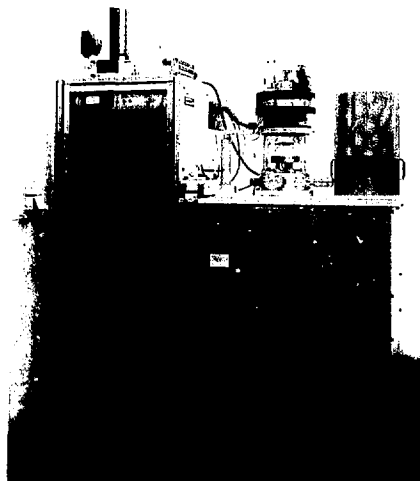
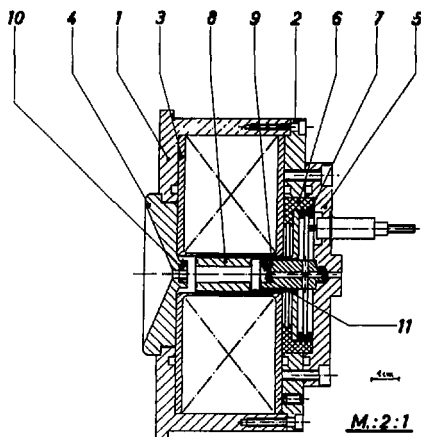


Figure 1. Sputtering system.

Figure 1 shows our sputtering system with the adapted ion-source. The rack on the left side contains the needed power supplies. The ion source we developed has in principle the same construction as described by Baumann<sup>1)</sup>. More over we made use of the experience obtained by operating this source at the single stage Van-de-Graaff-accelerator at Frankfurt/Main.

We reduced the discharge chamber of the source, thus obtaining smaller dimensions, which results in a better handling and maintenance in narrow area like a glove-box. This is important when the source will be used in a sputtering unit for producing radioactive targets.



- 1 = Source housing
- 2 = Upper flange
- 3 = Solenoid
- 4 = Extraction conus
- 5 = Anticathode flange
- 6,7 = Anode isolation
- 8 = Anodecylinder
- 9 = Anticathode holder
- 10 = Cathode
- 11 = Anticathode

Figure 2. Penning-ion-source.

This figure shows a cross-section of the source. The diameter is 120 mm and the height 70 mm. The housing of the source is made of magnetic steel. The magnetic field of the ion source is produced by a solenoid. Cathode with extraction channel, anticathode and anode-cylinder are made of molybdenum. The operating gas is fed into the discharge chamber through the anticathode.

The Penning-ion-source is operated in a high voltage low current discharge mode. The operating values were not changed by the geometrical reduction of the source as described. A total ion beam of argon ions up to 2 mA can be extracted. <sup>1,2)</sup>

The Penning source has a gas consumption of 1 - 5 Ncm<sup>3</sup>/h depending on the ion beam intensity. The quality of the extracted ion beam is characterized by the following data.

Energy spread: 40 - 80 eV  
 Emittance:  $\leq 1$  cm mrad MeV  
 depending on the ion beam intensity <sup>3)</sup>

The total power consumption (discharge and magnetic coil) of the source is smaller than 30 W. Therefore the source can be operated without any cooling system. This facilitates the safety precautions desirable in the preparation of radioactive targets, as no cooling medium of any kind must be lead into the hot area, which can be kept closed during operation.

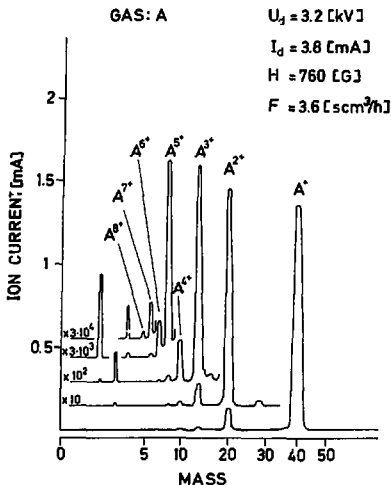


Figure 3. Mass spectrum of total ion beam.

The mass spectrum shows the composition of the extracted ion beam, when the source is operated with Ar-ions. The ion beam consists of single and multiple charged Ar-ions with an intensity of about 99 % of the total ion intensity. The single charge ion component is 90 %. The amount of ions from the residual gases (normally  $O_2$ ,  $N_2$ ,  $H_2O$ ) is totally about 1 %. At optimal operating conditions the portion of metal ions formed inside the source by sputtering of the cathode material can be reduced to a value smaller than 1 %. That means that the contamination of the target material and the resulting layer on the substrate by the ion beam is not significant.

The operating time of the source is essentially limited by sputtering of the cathode material. In a long life test the source ran with a stable ion beam intensity for 165 hours without any trouble. The stability was about 0,2 % by 0,58 mA of ion beam intensity over the whole time.

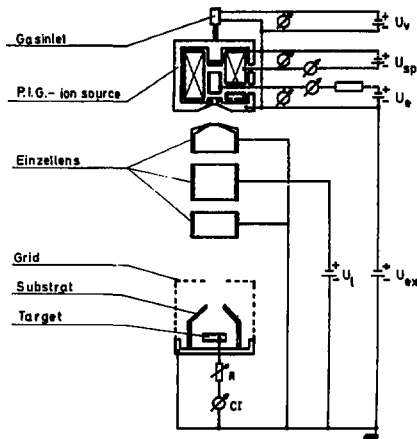


Figure 4. Electrical circuit.

$U_V$ : Gasinlet valve	0,5 V / 70 A
$U_S$ : Solenoid	65 V / 5 A
$U_e$ : Discharge voltage	6 kV / 20 mA
$U_{ex}$ : Extraction voltage	20 kV / 5 mA
$U_1$ : Einzellens	20 kV / 5 mA
CI : Current integrator	
R : Variable resistor	

The source in this sputtering system is on a positive high voltage potential. The secondary electrons, produced on the target material by the ion beam, which falsify the measuring of the ion beam intensity were sup-

pressed by a positive potential of the target of 50 - 100 V together with an earthed grid.

This target potential is produced by a variable resistor which gives us the possibility to check if all secondary electrons are suppressed.

The gas flow into the source is regulated by a thermo-mechanical leak valve with an extremely good stability of flow ratio.

The vacuum system consists of a 30 m<sup>3</sup>/h mechanical pump and a 450 ltr./sec turbomolecular pump. The vacuum in the sputtering chamber is about  $2 \times 10^{-6}$  Torr during the sputtering operation.

Since the energy spread of the ion beam is very low a minimum beam spot of about 1 mm diameter can be achieved. Even with this dimension of the beam spot the halo of the beam is negligible, so that very small amounts (several milligrams) of material can be sputtered without any sputtering of the surrounding material.

To obtain the best geometrical position of the substrate holders in view of sufficiently homogeneous foils we began to measure the angular distribution of the sputtered material. According to the first measurements we have installed an arrangement with geometrical dimensions as shown in Fig. 5.

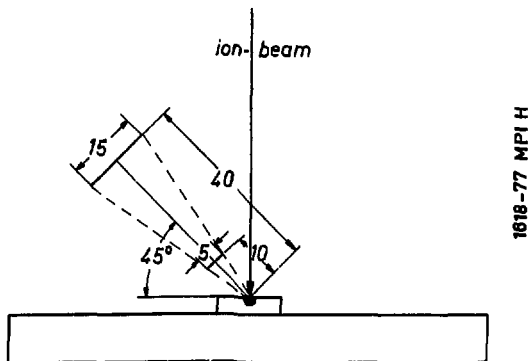


Figure 5. Substrate positions.

The target material is bombarded by the Ar - ion beam at normal incidence and the substrates surround the beam under an angle of  $45^\circ$  in a distance of 40 mm from the beam spot. The area of sufficient homogeneity is about 15 mm. With this arrangement we produced Ta-targets of  $25 \mu\text{g}/\text{cm}^2$  and  $190 \mu\text{g}/\text{cm}^2$  on carbon backings of about  $15 \mu\text{g}/\text{cm}^2$ . The consumption of metallic Tantalum for the production of 8 targets of  $190 \mu\text{g}/\text{cm}^2$  was about 50 mg and about 7 mg for 8 targets of  $25 \mu\text{g}/\text{cm}^2$ .

If only very small amount of materials exists, for example in the case of radioactive or expensive isotopic material, it is possible to reduce the distance of the substrates from the beam spot to 10 mm for producing relatively thick layers. At this distance we prepared Thorium targets on carbon backings with sufficient homogeneous area of  $5 \times 5$  mm.

In the case of the Uranium target production we found that we cannot reproduce the film thickness in spite of the exact measuring of the ion beam intensity. The reason is that Uranium just as several other elements oxidizes very easily at a relatively low temperature. With a mostly used focus diameter (about 2 - 4 mm) and extraction voltage of 10 kV the power density increases to values greater than  $100 \text{ W}/\text{cm}^2$  so that the surface temperature of target material becomes several  $100^\circ\text{C}$  when the heat conduction of the material is relatively low. For that reason a cooling system for the target material post is required.

### Conclusion

We believe that several problems can be avoided by the application of the Penning-ion-source in sputtering systems. The long lifetime of the Penning-source allows one to produce targets of great thickness even from materials with low sputtering yield without interruption of the operation. Also radioactive sputtering operations can be

carried out without any maintenance of the source for a long time. Another point is that the chemical resistance of the cold cathode of the source given us the possibility to operate the source also with chemically active gases. In this way we can achieve that reduction or oxidation of the target material may take place during the sputtering operation. So we can reduce oxides to metal or on the other hand we can form several oxides or nitrides by using isotopic enriched gases.

In account of the high stability of the ion beam it is not necessary to control the sputtering unit during operation.

We believe that with our sputter system we have found a good alternative for preparing targets by sputtering.

Acknowledgements: We wish to thank Mr. B. Schührer for excellently building the mechanical construction of the source and Mrs. V. Träumer for preparing the illustrations.

- 1) H. Baumann, thesis, Heidelberg (1973)
- 2) H. Baumann and K. Bethge, Nucl. Instr. Meth. 122 (1974)517
- 3) H. Baumann, K. Bethge, G. Klein, Trans. Nucl. Sc. NS 23, 2 (1976) 1081

PREPARATION OF SELF-SUPPORTING PLATINUM TARGETS  
BY ELECTRODEPOSITION

M.A. SAETTEL

Centre de Recherches Nucléaires et Université Louis Pasteur  
67037 STRASBOURG Cedex, France

ABSTRACT

The experimental set-up and conditions for preparing self-supporting metallic platinum targets by electrodeposition are described in this paper. Results will be given on the influence of deposition time and current density. The yield of about 20% is better than in the case of evaporated targets.

1. INTRODUCTION

At its melting point, platinum alloys with most refractory materials, and therefore evaporation from a boat raises problems. Electron-guns are more appropriate. However, because platinum has elevated conductivity, melting and boiling points, they must be powerful. Evaporation with a 2 kW gun is very slow.

Electroplating is an alternative method that can be used for preparing metallic platinum targets. This method was successful in the case of self-supporting iron and nickel targets (ref. 1 and 2). Although the platinum electrodeposition does not offer all of the advantages, especially concerning the yield, the method gives good results and strong, pure, self-supporting targets can be readily prepared.

In the following sections, we will describe the experimental set-up, the composition of the electrolytic bath, the conditions of the electroplating, the technique used for preparing self-supporting targets

and the results as a function of deposition time and current density.

## 2. EXPERIMENTAL CONDITIONS

### 2.1. Apparatus

The set-up has been described in detail in the paper concerning the preparation of self-supporting iron targets (ref. 1). Its schematic diagram is shown in fig. 1. The conical plexiglass electrolysis cell is closed at the bottom by a brass disk on which the 10 $\mu$  copper foil is placed. A teflon ring ensures the liquid tightness of the apparatus. The anode is a platinum wire. Both electrodes are connected to a 40V current regulated power supply.

### 2.2. Composition of the bath

The chosen bath is described by Lowenheim in his book "Modern Electroplating" (ref. 3). It is well adapted to small quantities of material. The electrolyte is prepared from the metal, which is an advantage, because the isotopes are often sold in this form. Dissolved in aqua-regia, the platinum is transformed into hexachloroplatinic acid. Potassium hexahydroxoplatinate  $K_2Pt(OH)_6$ , the main component of the electrolytic bath, is then easily prepared from this acid.

The quantitative composition of the bath is as follows : Five mg of platinum are reacted with 2cm<sup>3</sup> of aqua-regia. The solution is evaporated to dryness and the residue dissolved in 10cm<sup>3</sup> of distilled water containing 10mg of potassium chloride. Potassium hydroxide is added in excess in order to precipitate the potassium hexahydroxoplatinate and to make the bath basic : pH 9. The volume of the electrolyte solution is about 10cm<sup>3</sup>. The bath is used at room temperature.

### 2.3. Realization of the targets

A current density of 250mA/cm<sup>2</sup> appears to be the best compromise from the point of view of electrodeposition rate and target quality. Higher

currents tend to produce spongy deposits.

After the platinum is electroplated on the copper foil, the target is rinsed with distilled water and dried. The deposits have a diameter of 10mm. Their thickness is determined by weighing the copper cathode before and after the electrodeposition.

The copper is dissolved in a trichloroacetic acid- ammonia- water solution (ref. 4), and the self-supporting film rinsed with water before placing it on a target holder.

No measurable amount of contamination was observed in the elastic scattering spectrum of 3 MeV protons. The targets have been used in (p,d) and (p,t) experiments (ref. 5). Figure 2 shows a typical deuteron spectrum obtained with a position sensitive detector in the focal plane of the Orsay M.P. split pole spectrometer.

### 3. QUANTITATIVE STUDY OF THE ELECTRODEPOSITION

The thickness of the deposit is dependent on two factors : the deposition time and the current density. We have studied the influence of variation of these two parameters using solutions containing 5mg platinum freshly prepared for each measurement.

#### 3.1. Variation of the deposit thickness as function of the deposition time

The results are given in the following table for a constant current density of  $250\text{mA/cm}^2$

Deposition time min.	Thickness $\mu\text{g/cm}^2$
15	60
30	110
45	170
60	200
90	305

The accuracy is that of the balance :  $\pm 10\mu\text{g}$ . These data are plotted in fig.3. It is seen that the deposition rate is about  $3.6\mu\text{g}/\text{cm}^2$  . min.

### 3.2. Variation of the deposit thickness as function of the current density

The results given in the following table were obtained for a constant deposition time of 30 min.

Current density $\text{mA}/\text{cm}^2$	Thickness $\mu\text{g}/\text{cm}^2$
125	60
250	110
375	170
500	240
625	310

Figure 4 shows the corresponding graph.

## 4. DISCUSSION

As opposed to the 85% efficient electroplating of iron, nickel or zinc, the yield in the case of platinum is about 20%. However, it happens that platinum is lost as a residue in elementary form in the bath. The reason for the reduction could be the presence of platinum ions not oxidized to the +4 state. This valence state is necessary for the precipitation of the platinum with potassium chloride and its complete transformation into potassium hexahydroxoplatinate by addition of an excess of potassium hydroxide. The solution can be evaporated again to dryness and the electrolyte reprepared.

Using the electrodeposition described above and with a bath containing 10mg of platinum, nine deposits, weighing 110 to  $390\mu\text{g}/\text{cm}^2$  have been made. With an electrolyte containing 2mg of platinum, three targets of  $150\mu\text{g}/\text{cm}^2$  were prepared.

There is another bath which gives good deposits of precious metals. The rather acidic electrolyte (pH 2), also described by Lowenheim (ref.2), contains platinum hexachloride and hydrochloric acid. Since this solution attacks the copper foil, an inert material must be used as a cathode.

## 5. CONCLUSION

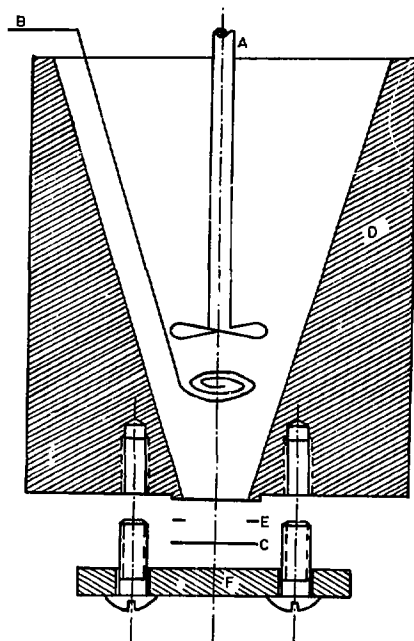
Electroplating furnishes a simple method for preparing self-supporting platinum targets. Even if the yield is low compared to electro-deposition of some other materials, it is much superior to that found in evaporations. In addition, the targets made as we have described are less fragile than those made by evaporation in that they withstand the accelerator beam better. The method is also interesting for isotopically enriched targets, because they can be obtained with little material. This is often difficult in evaporations.

### Acknowledgments

The author would like to thank R. Seltz for checking the purity of the targets and A. Pape for critically reading the manuscript.

## REFERENCES

- 1) S. Gorodetzky and E.S. Drouin. "Preparation of Thin Self-Supporting Enriched Iron Targets", Proceedings of the Seminar on the Preparation and Standardisation of Isotopic Targets and Foils. (Held at A.E.R.E. Harwell, October 20-21, 1965).
- 2) R.S. Drouin and A. Schwentzel. "Préparation de cibles minces auto-supportées de  $^{61}\text{Ni}$ ", IRN Strasbourg, internal report Phys. Nucl. Chev. 6602, January 25, 1966 (unpublished).
- 3) F.A. Lowenheim. Modern Electroplating (Wiley and Sons, New York 1963).
- 4) H.T. Richards. Nuclear Spectroscopy, ed. F. Ajzenberg-Selove (Academic Press, London, 1960) Part A, p.110.
- 5) Orsay report IPNO-PhN-77-13 and R. Seltz, private communication.



Scale : 1cm

Figure 1. Schematic diagram of the electrolysis cell.

- |                   |                            |
|-------------------|----------------------------|
| A. Glass stirrer  | D. Conical plexiglass cell |
| B. Platinum anode | E. Teflon ring             |
| C. Copper foil    | F. Brass disk              |

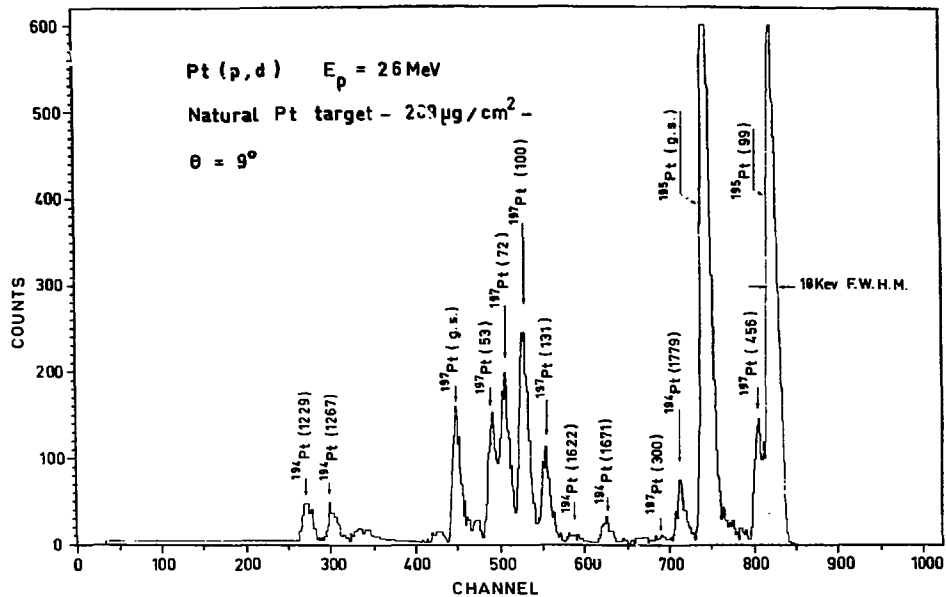


Figure 2. Typical deuteron spectrum. Peaks are labelled by the excitation energy in keV for the final nucleus.

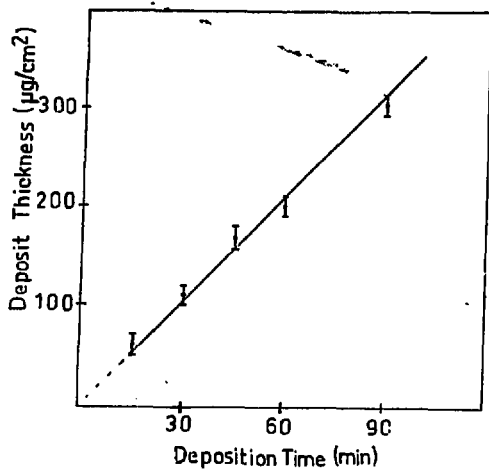


Figure 3. Variation of the deposit thickness as a function of the deposition time.

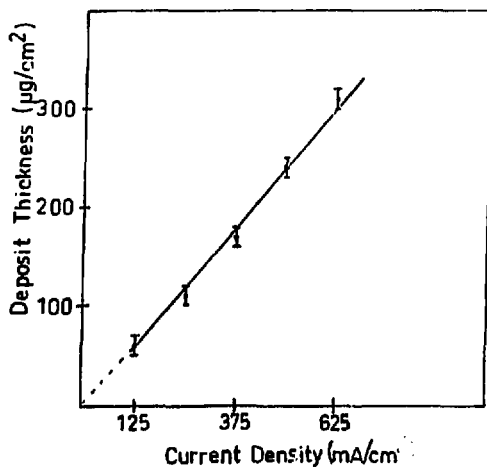


Figure 4. Variation of the deposit thickness as a function of the current density.

## PREPARATION OF TARGETS BY ELECTRODEPOSITION

T. L. Morgan

Schuster Laboratory, University of Manchester  
Manchester, England

Abstract The technique of producing self-supporting ruthenium<sup>96</sup> targets within the range of 200  $\mu\text{g}/\text{cm}^2$  upwards is described.

There are various methods by which the target maker can produce films and foils for the use of the nuclear experimental physicist. Although cost is a significant consideration, the physical properties of the materials are of far greater importance.

In the case of ruthenium 96, the situation is far from flexible: the material is quite expensive and, for the production of a reasonably uniform 3-mg/cm<sup>2</sup> target, evaporation is out of the question. Rolling and pressing were considered but ruthenium is very hard and brittle; therefore, the only other economical method is electroplating. This has proved to be highly successful both in production of the films and in the percentage of the material that is recovered (about 80% to 90%).

Normally, ruthenium is heated to dull red heat for 1 hr in order to volatilize Os which is often present as an impurity. The partially oxidized ruthenium is then reduced in a stream of H<sub>2</sub>. This procedure need not be carried out unless the physics of the Os causes problems in the proposed experiment.

A mixture of 10 mg of the isotope—which is Ru<sup>96</sup> and very pure KOH and K<sub>2</sub>O<sub>3</sub> in a 3: 25: 3 ratio by weight—is prepared and fused in a silica crucible by means of a propane torch. The green melt is kept in the liquid state for a few minutes to ensure complete dissolution of the ruthenium<sup>96</sup>.

The melt is then allowed to cool, and the reaction product is broken into small lumps and dissolved in lukewarm distilled water. This orange-yellow solution is then transferred to a glass beaker, the silica crucible is washed with distilled water and decanted into the glass beaker,

and the volume made up to 20 ml. The volume of concentrated HCl capable of producing a 0.1 N solution with the ruthenium complex is measured into another beaker. Then the orange-yellow solution is poured slowly with stirring into the concentrated HCl to form  $\text{RuCl}_3 \cdot \text{H}_2\text{O}$ , which is normally red in color. It is assumed that if the reverse is applied and the HCl added to the initial solution of ruthenium<sup>96</sup> alkali salts, an insoluble ruthenium hydroxide complex is formed which then renders the solution useless.

In the nuclear physics experiment previously mentioned the target thickness used was  $3\text{-mg/cm}^2$   $\text{Ru}^{96}$  on a gold backing  $3\text{-mg/cm}^2$  thick. A standard tubular cell with a diameter of 1.2 cm was used. The anode used was a Pt mesh, the cathode of course being the  $3\text{-mg/cm}^2$  Au substrate. The current density was  $20\text{ mA/cm}^2$ ; it gave a deposition rate of 1 mg/hr of ruthenium<sup>96</sup> metal. The target thickness required meant an electrolysis of 3 hr at a temperature of  $60^\circ\text{C}$ .

As a result of our research into this method at a temperature of  $60^\circ\text{C}$  and into many other methods of electrolysis, we have drawn the conclusion that it is better if the substance is placed in a plane perpendicular to the anode. The reason is that there is less tendency towards pinholing and stressing of the films produced. Also the removal of the gas bubbles on the surface is far more efficient by a reciprocating solution flow than by spinning the cells.

For the production of self-supporting films of ruthenium the substrate used was a copper film of about  $2\text{-}8\text{ mg/cm}^2$ . These films are best produced by evaporation onto highly polished nickel-chromium plated brass plates. The copper is then peeled off, cut into sections, and mounted into the cell. The cell is washed first with distilled water and then with very dilute  $\text{HNO}_3$  to slightly etch the surface of the copper. The solution is decanted and the cell thoroughly washed with distilled water. The plating solution is then added and the procedure previously described is carried out. When the required amount of material has been deposited the copper is removed with trichloroacetic acid and the target mounted in the manner which is advocated.

A METHOD FOR THE PREPARATION OF CADMIUM  
ISOTOPIC TARGETS

by

J.L. Gallant and D. Yaraskavitch

ABSTRACT

A technique that produces high quality self-supporting isotopic cadmium targets has been developed. Cadmium oxide is dissolved in dilute sulfuric acid and the metal extracted by the electrolysis process. It is then evaporated onto a glass substrate which has been previously coated with a thin film of cadmium chloride. The metal is released from its substrate by immersion in methyl hydrate.

Nuclear Physics Branch  
Atomic Energy of Canada Limited  
Chalk River Nuclear Laboratories  
Chalk River, Ontario, Canada

## INTRODUCTION

Isotopic cadmium targets were used recently at Chalk River in a Coulomb excitation experiment<sup>1)</sup> in which perturbations of the alignment of the 274 keV 84 ns state were studied during recoil in vacuum. In this experiment, uniform flat foils of <sup>111</sup>Cd were bombarded with an oxygen beam.

## PROCEDURE

Stable cadmium isotopes are normally available from suppliers as the oxide CdO. A simple way to convert the oxide to the metal is to dissolve the cadmium oxide in sulfuric acid at concentration of 2 mol/L (4 normal). The cadmium sulfate solution is diluted with distilled water to the required volume. Cadmium is then extracted from the solution by the electrolysis method (Figure 1).

In our apparatus, the isotope is collected as the metal at the cathode (Figure 2) of the electrolytic cell at a current density of  $\sim .5 \text{ A/cm}^2$ . The metal is periodically removed from the cathode and the electrolysis continued until the solution is completely exhausted. By this method cadmium isotope recovery can be as high as 96%. The metal is thoroughly washed in distilled water, rinsed in acetone and dried in an oven at 70°C.

The metallic isotope of cadmium is vacuum deposited at a rapid rate from a tungsten boat onto a glass substrate which has been previously coated with a thin film ( $15 \mu\text{g/cm}^2$ ) of cadmium chloride. Cadmium chloride is used because it has a hexagonal crystal structure similar to that of the metal. Others have used zinc chloride as a parting agent<sup>2)</sup> but the salt of cadmium is preferred because it is not deliquescent. The evaporated cadmium metal is sectioned and immersed in a bath of methyl hydrate, at which time the

foils will release from the surface of the glass (Figure 3). They are then mounted on suitable frames<sup>3)</sup> (Figure 4); rinsed several times with distilled water and finally with ethyl alcohol.

Isotopic cadmium foils were also required with a  $1 \text{ mg/cm}^2$  copper backing. Copper was vacuum evaporated onto the surface of the cadmium. The two layer film was sectioned, stripped in methyl hydrate and mounted as described above.

Analysis showed that the process did not introduce measurable quantities of sulfur or platinum. Rutherford back-scattering of  $2 \text{ MeV } ^4\text{He}$  showed no evidence of platinum impurities. Selective X-ray fluorescence with  $800 \text{ keV Ar}$  beams established a sulfur content of  $< 100 \text{ ppm}$ . A spark source spectrometric analysis of the cadmium indicated  $< 400 \text{ ppm}$  sulfur.

#### ACKNOWLEDGEMENTS

The authors wish to thank Drs. I.V. Mitchell and W.N. Lennard for the back scattering, X-ray fluorescence and Mrs. Solange Armstrong for the spark source spectrometric analysis

REFERENCES

- (1) H.R. Andrews et al, Proceedings of the Fourth International Conference on Hyperfine Interactions, Madison, N.J., 1977.
- (2) D. Ramsay, Proceedings of the 1974 Nuclear Target Development Society Annual Conference, Chalk River Nuclear Laboratories, Page 151 (1974).
- (3) J.L. Gallant, Nuclear Inst. & Meth. 81 (1970) 27-28.

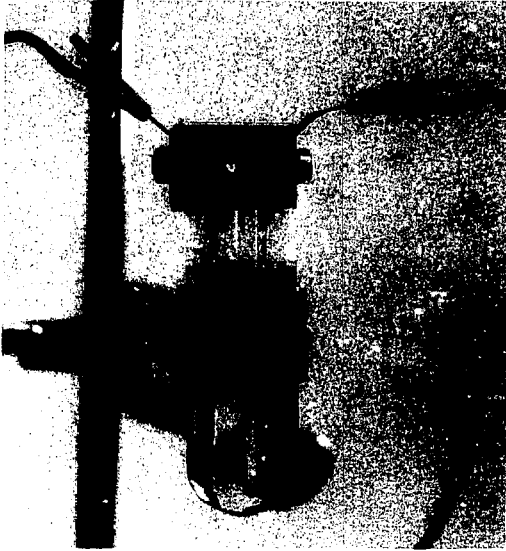


Figure 1. Electrolytic cell with platinum anode and cathode.

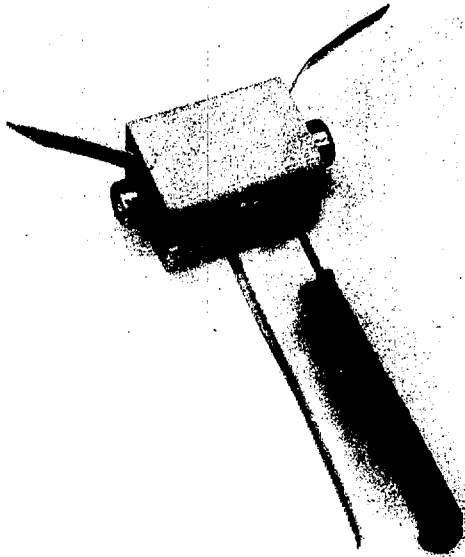


Figure 2. View of cadmium deposit at cathode.

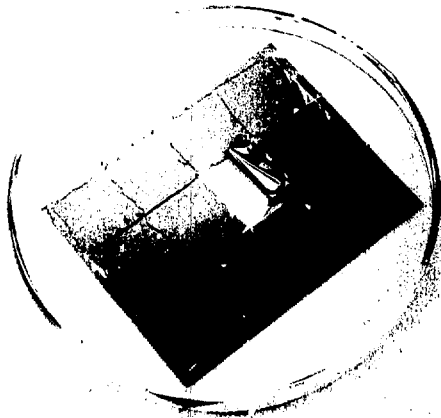


Figure 3. Cadmium foil sectioned and immersed in methyl hydrate bath.



Figure 4. Cadmium film mounted on low mass plunger frame.

## Thin Carbon Foil Breakage Times Under Ion Beam Bombardment

A. E. Livingston, H. G. Berry\* and G. E. Thomas

Argonne National Laboratory, Argonne, Illinois 60439<sup>†</sup>

We have measured the breakage times of thin carbon foils of different thicknesses under bombardment by  $\text{Ar}^+$  ions of 1-3 MeV energy. The breakage times are independent of foil thickness over the areal density range of  $2\text{-}22\mu\text{g,cm}^2$ . Our results are in reasonable agreement with previous measurements of foil breakage. We propose an empirical formula for the foil breakage time  $\tau$  in terms of the ion energy  $E$ :

$$\tau(\mu\text{A}\cdot\text{min}/\text{mm}^2) = A(\sim 10) \cdot E^{1.15} (\text{MeV}/\text{amu}).$$

This article originally appeared in Nuclear Instruments and Methods 148 (1978) 125-127.

Introduction

Carbon foils are frequently employed to excite a distribution of atomic charge states in a monoenergetic fast ion beam. Whether foil excitation is used for measurements of the atomic properties of excited states of the beam ions<sup>1)</sup> or simply to provide multiply ionized beam atoms by electron stripping, as in the high voltage terminal of a tandem accelerator<sup>2)</sup>, the survival time of an individual foil usually represents an important experimental limitation. In the study of excited atomic states, signal normalization is frequently altered by foil breakage. In tandem beams, the efficiency of high-charge-state production decreases as the stripper foil deteriorates following partial breakage.

Only a few investigators<sup>2-5)</sup> have examined foil breakage times under ion bombardment in a systematic manner. In some cases, very different masses, velocities, and current densities of the accelerated ions have been involved, and foil thickness has differed by more than a factor of 10 in different investigations. No attempt has yet been made to establish whether there is a dependence of breakage time upon foil thickness. We report here our results of systematic study of breakage time for carbon foils ranging in areal density from  $2-22\mu\text{g}/\text{cm}^2$ . We also discuss the dependence of foil breakage time upon various ion-beam parameters and compare our results with those of refs. 2-5.

Experiment

The 4 MV Dynamitron accelerator at Argonne National Laboratory was used to provide a magnetically analyzed beam of 3.0 MeV  $Ar^+$  ions. Beam current was uniformly distributed over a 2 mm diameter collimator which preceded normally either 3 mm or 4 mm diameter self-supporting carbon foils mounted perpendicular to the beam axis. Foil condition was monitored in three ways: (1) the fluorescent image of the beam was viewed directly through a quartz beam stop at the end of a Faraday cup; (2) the foil-excited ion beam current was measured from a thin layer of aluminum deposited on the quartz surface; (3) the intensity of light emitted by the excited beam ions following foil excitation was measured with a photomultiplier in photon-counting mode. The digitized beam current and light intensity were monitored continuously and the signals accumulated during preset time intervals were stored in an on-line PDP 11/45 computer. The fluorescent beam image was observed on a television monitor. The occurrence of foil breakage was normally indicated by a sudden drop in both beam current and light intensity, as well as by the appearance of a well-defined fluorescent image of the hole in the foil on the quartz beam stop. We point out that in general the light monitor should be more sensitive than the current monitor since a current change at breakage can exist only if there is a sufficient difference in the observed current with and without a foil being present. In particular, for ion energies where the foil-excited average charge state is similar to the incident ion charge, little current change is observed.

### Results

In fig. 1 we show our results of foil lifetime for 17 foils ranging in areal density from 2 to  $22 \mu\text{g}/\text{cm}^2$ , under bombardment by a  $3 \mu\text{A}/\text{cm}^2$  beam of 3.0 MeV  $\text{Ar}^+$  ions. The results reveal no significant dependence of foil lifetime upon foil thickness, and we can calculate a mean foil lifetime of 22 min for a  $3 \mu\text{A}/\text{cm}^2$  incident ion beam of 3 MeV  $\text{Ar}^+$  ions.

Similar results were also obtained with a  $15 \mu\text{A}/\text{cm}^2$  beam of 3.0 MeV  $\text{Ar}^+$  ions. These measurements are consistent with the results of Dumont et al.<sup>3)</sup> showing the breakage time to depend only on the total number of bombarding ions, independent of beam current. In addition, no foil thickness dependence was found for a  $1 \mu\text{A}/\text{cm}^2$  beam of 1.0 MeV  $\text{Ar}^+$ , and a  $1.4 \mu\text{A}/\text{cm}^2$  beam of 4.0 MeV  $\text{Ni}^+$ . No variation in breakage time was observed for different carbon foil diameters of 2, 3 and 6 mm.

### Discussion

The independence of foil breakage time on the foil thickness is consistent with the picture of the breakage being dependent on the total energy lost per unit volume, or per atom of foil material. Radiation damage and stresses gradually develop up to the breaking time, independent of the rate of energy loss.

However, the results are also consistent with the destructive mechanism being a surface phenomenon, the amount of surface bombarded being the same in all cases. We believe this explanation to be unlikely: the initial breakage for most foils occurs near the perimeter of the beam spot. Here the stresses between bombarded foil, which tends to contract<sup>2, 5)</sup>,

and the unbombarded foil are maximal. For a purely surface phenomenon, the thicker foils would be able to withstand greater stresses and the survival times would be longer.

It seems clear that the stresses are built up throughout the bulk of the thin foil, and that these stresses are maximized in the transition region between the bombarded and unbombarded foil. Then, as observed by Dumont et al.<sup>3)</sup>, there should be little dependence of foil breakage on the surface carbon deposition rate during the ion bombardment. We note that increases in thickness of  $10\mu\text{g}/\text{cm}^2$  foils by 40-100% during heavy-ion bombardment are observed under typical high-vacuum conditions<sup>3,5)</sup>.

Dobberstein and Henke<sup>4)</sup> and Dumont et al.<sup>3)</sup> have noted that the breakage rate should be closely related to the nuclear stopping power  $S_n$ . In fig. 2 we have assembled a large body of data from refs. 2-5 and our own measurements and we plot the reduced foil lifetimes (in  $\mu\text{A}\cdot\text{min}/\text{mm}^2$ ) as a function of ion energy in MeV/amu. We also show theoretical curves corresponding to lifetimes  $\tau = k(S_n)^{-1}$  for  $\text{N}^+$ ,  $\text{Ar}^+$  and  $\text{Kr}^+$  on C. The values for nuclear stopping power,  $S_n$ , have been calculated using the analytical expression of Biersack<sup>6)</sup>. It is clear that the reduced lifetime varies more rapidly than the nuclear stopping power, except possibly at high energy where

$$S_n \approx \frac{1}{E} \ln E + \frac{1}{E}. \quad (1)$$

Data for  $\text{Ar}^+$  ions extend over the largest energy range from  $1.5 \times 10^{-3}$  to more than 1.0 MeV/amu. At the high energy limit,  $\tau$  is

nearly proportional to  $(S_n)^{-1}$ , but a more reasonable fit to all the  $Ar^+$  data is

$$\tau(\rho\mu A \cdot \text{min}/\text{mm}^2) = A \cdot E^{1.15} \text{ (MeV/amu)}, \quad (2)$$

where  $A \approx 20$ . The empirical constant  $A$  varies only slowly with bombarding ion, being larger for lighter ions ( $A \approx 60$  for  $N^+$ ), and being smaller for heavier ions ( $A \approx 5$  for  $Ni^+$ ,  $Br^+$ ). This variation is also similar to the  $Z$ -dependence of  $S_n$  at high energy.

### Conclusions

We have found that the breakage times for thin carbon foils under heavy ion bombardment are independent of the foil thickness for  $Ar^+$  ions of 1 and 3 MeV, and thicknesses of  $2-22\mu\text{g}/\text{cm}^2$ . Consequently, for experiments in which energy and angular dispersions of the ion beam after the carbon foil need to be minimized - for example - in heavy ion accelerator charge strippers and high time resolution experiments, the foils used should be as thin as possible. The usual limitation will be the mechanical problem of producing self-supporting foils over an area corresponding to the beam cross-section. For diameters of a few mm the thinnest self-supporting carbon foils easily produced are of  $2-3\mu\text{g}/\text{cm}^2$ .

We have verified that the foil breakage time is dependent on the total number of bombarding ions, and we suggest the empirical formula [eq. (2)] that the reduced lifetime is nearly proportional to the ion beam energy.

We thank J. Ray for his help in the measurements and J. Yntema for helpful discussions.

Footnotes and References

\*Department of Physics, University of Chicago, Chicago, Illinois 60637

†Work supported in part by the U. S. Department of Energy and N. S. F.

- 1) H. G. Berry, Rep. Progr. Phys. 40 (1977) 155.
- 2) J. L. Yntema, Nucl. Instr. and Meth. 122 (1974) 45; IEEE Trans. Nucl. Sci. NS-23 (1976) 1133 (refs. therein).
- 3) P. D. Dumont, A. E. Livingston, Y. Baudinet-Robinet, G. Weber and L. Quaglia, Physica Scripta 13 (1976) 122.
- 4) P. Dobberstein and L. Henke, Nucl. Instr. and Meth. 119 (1974) 611.
- 5) D. S. Whitmell, B. H. Armitage, D. R. Porter and A. T. G. Ferguson, Int. Conf. on Technology of electrostatic accelerators (Daresbury, England, 1973), DNPL/NSF/R5, p. 265.
- 6) J. P. Biersack, Z. Physik 211 (1968) 495.

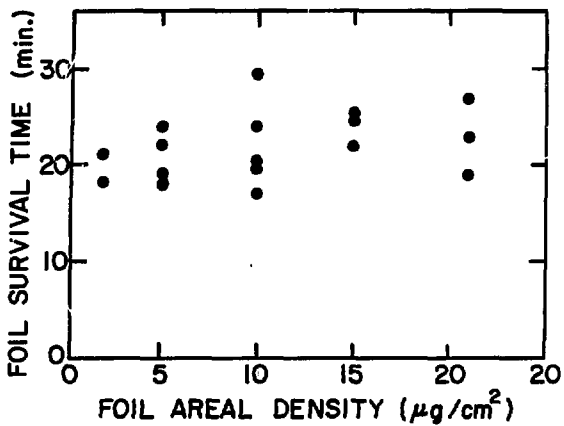


Figure 1. Carbon foil breakage time as a function of foil thickness for a  $3\mu\text{A}/\text{cm}^2$  beam of 3.0 MeV  $\text{Ar}^+$  ions.

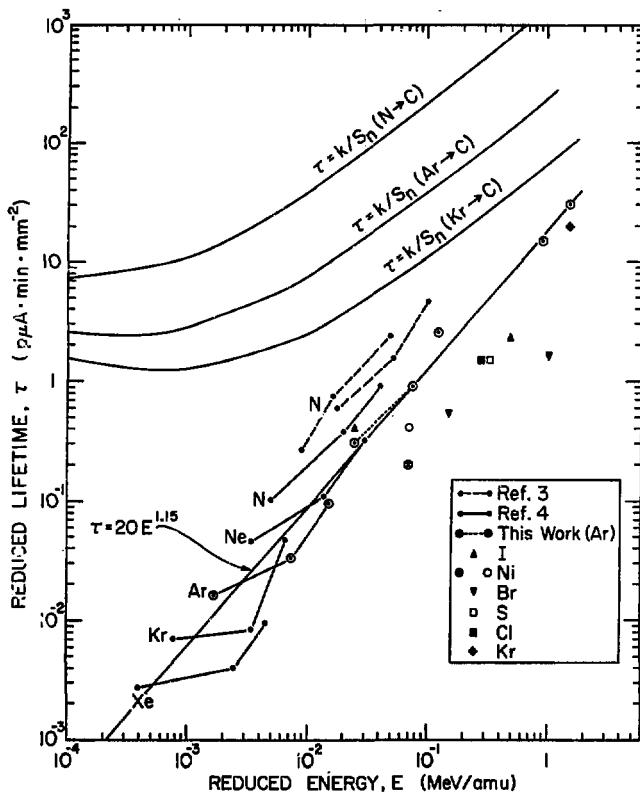


Figure 2. Reduced foil lifetime  $\tau$  as a function of reduced ion energy. Results from Ref. 4 are connected by solid lines; results from Ref. 3 are connected by dashed lines; our results for Ar are connected by the dotted line; and our result for Ni is shown as  $\odot$ . The remaining results are from Ref. 2, where references to unpublished data may be found. Curves of inverse nuclear stopping power,  $\tau = kS_n^{-1}$ , are shown for  $N^+$ ,  $Ar^+$  and  $Kr^+$  in carbon, with  $k = 4.24 \times 10^{-7}$  J/m.

## DISTRIBUTION OF CARBON SURFACE DENSITY EVAPORATED BY A CARBON ARC\*

V. Olivas, J. O. Stoner, Jr., and S. Bashkin  
Department of Physics, University of Arizona, Tucson, AZ 85721

## ABSTRACT

Tests of the angular distribution of carbon evaporated from a carbon arc indicate that such an arc behaves approximately as a cylindrical surface source (a cosine source) with its axis concentric with that of the carbon rods.

- - - - -

Carbon targets were made in a vacuum evaporator by the method developed by Dearnaley.<sup>1</sup> This method was slightly modified (Fig. 1); instead of using springs to force contact between the carbon rods, the rods are aligned vertically and the upper rod, free to move with a weight attached to it, is held by gravity in contact with the lower rod. The arc was pulsed by an automatic circuit. Clean microscope slides were used as substrates. Parameters for the evaporation are listed in Table 1. Thicknesses of the carbon coatings were determined optically.<sup>2</sup> Coatings were made with surface densities in the range of approximately 1 to 50  $\mu\text{g}$  of carbon per  $\text{cm}^2$ .

Table 1

Base pressure	$\leq 2 \times 10^{-6}$ torr
Evaporation pressure	$\leq 3 \times 10^{-5}$ torr initially $\leq 1 \times 10^{-4}$ torr during evap.
Arc voltage	20 V.a.c.
Arc current	200 amps
Arc duration	0.1 - 0.7 sec.
Arc rod diameter	6.2 mm
Taper: tip diameter	2.5 mm
Full cone angle	14°
Shortest distance, arc to Substrate	18.5 cm

To determine the carbon distribution it was found necessary to make some geometrical corrections. This problem was complicated by the fact that the plane, initially horizontal, of the contact surface of the two carbon rods often tilted as the rods burned. Correcting the observed surface density, taken from the microscope slides, to one that gave the density at a constant distance from the carbon rods but at a varying angle from the horizontal, was straightforward when the burning-surface plane remained horizontal during burning. Surface density  $\sigma$  was calculated from:

$$\sigma(\theta) = \frac{\sigma_{\text{obs}}}{\cos \theta} \frac{r^2}{R^2} \quad (1)$$

(See Fig. 1). When Eq. 1 was used to transform  $\sigma_{\text{obs}}$  to  $\sigma(\theta)$  the resulting  $\sigma(\theta)$  was asymmetric about  $\theta = 0$  when the plane of burning

tilted. In such cases however, it was often nearly symmetric about some  $\theta \neq 0$  (Fig. 2). For the thinner coatings it was easy to find runs that exhibited a maximum about some angle near  $\theta = 0$ , since the burning surface usually tilted by angles less than  $20^\circ$ . For thicker coatings, distributing the slides around the circumference of the slide holder ensured that there were always some columns that showed maxima in their distributions.

The observed distributions of surface densities about their line of symmetry are approximately proportional to  $\cos \theta$ , where  $\theta$  is measured from the center of symmetry of the distribution. This implies that the arc acts nearly as a cylindrical surface source with its axis nearly parallel to the rods' axis.

\*Supported in part by NSF, ONR, and CETA.

- 1) G. Dearnaaley, Rev. Sci. Instrum. 31, 197 (1960)
- 2) J. O. Stoner, Jr., J. Appl. Phys. 40, 70 (1969)

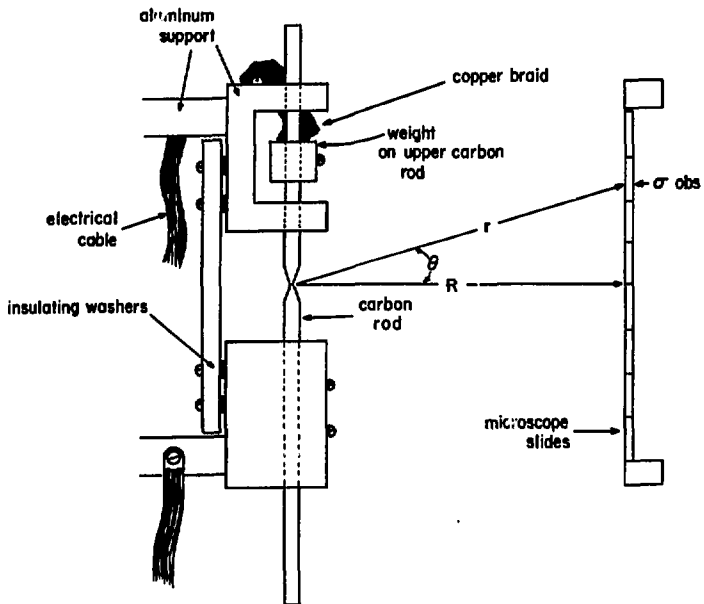


Figure 1. Side view of carbon arc and slide holder (not to scale).

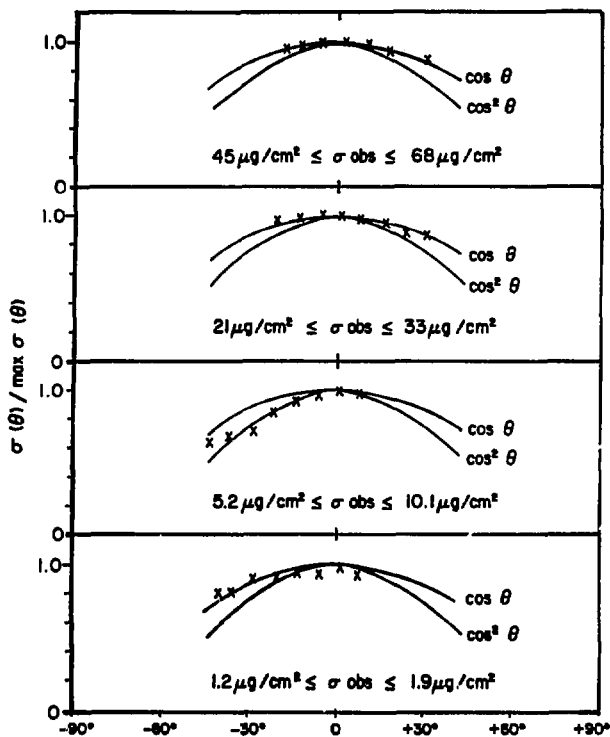


Figure 2. Carbon surface density distributions,  $\sigma(\theta) = \sigma_{\text{obs}}/\cos^3\theta$  normalized to unity maximum and compared with  $\cos\theta$  distributions displaced to fit peak values of the observed data.

## Mounting A Very Large Carbon Foil

John O. Stoner, Jr. and Stanley Bashkin  
Department of Physics, The University of Arizona, Tucson, AZ 85721

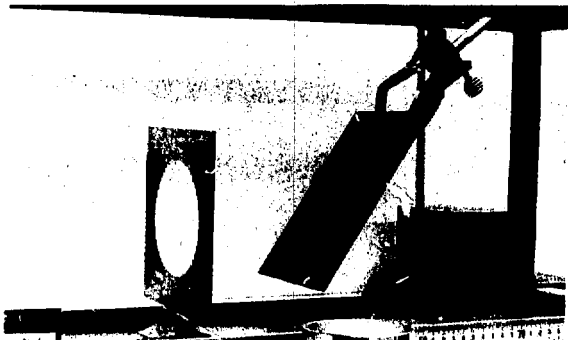
and

The Arizona Carbon Foil Company, 2239 E. Kleindale Rd., Tucson, AZ 85719

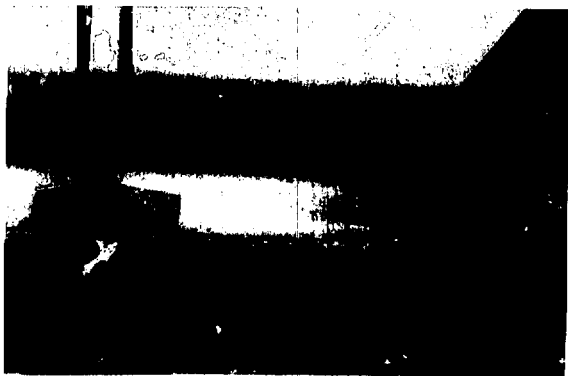
## ABSTRACT

We show pictorially a procedure by which a carbon foil having a surface density of 36 micrograms/centimeter was mounted with a clear unsupported aperture of 102 millimeters (4").

Carbon is evaporated from a carbon arc onto a glass substitute coated with Creme-Cote, a parting agent, in the usual fashion. This substrate, having dimensions 127 mm x 178 mm (5" x 7") is then mounted at a tilt of about 45° in a large tank into which water can be siphoned. Mounted vertically in the tank is a thin flat sheet-metal frame with a hole in it having diameter 102 mm (4 inches).



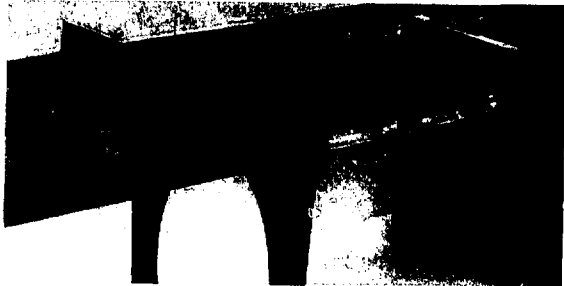
Water is siphoned slowly into the tank. The carbon floats on the water surface.



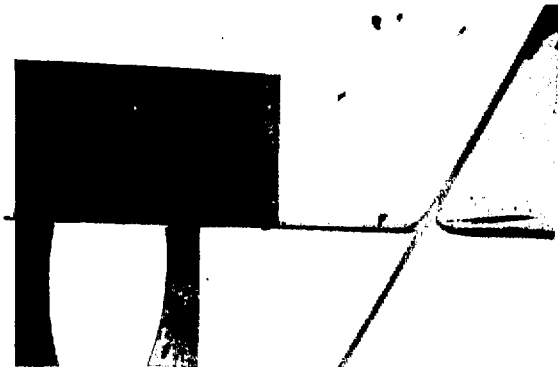
When the carbon coating is completely free of the substrate and the water level is above the frame, the carbon film is carefully moved so that one end of it is above the frame. Caution! The film must not be allowed to get near the walls of the tank! The water is then siphoned out.



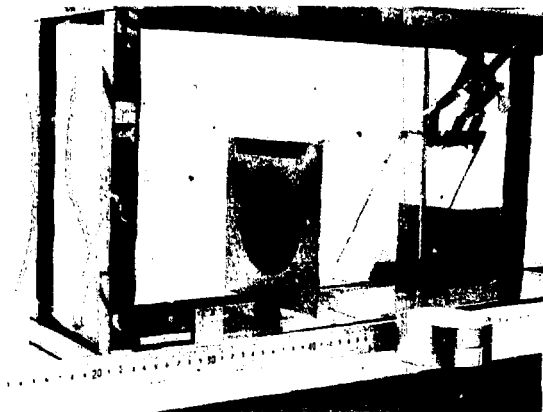
Allowing one end of the carbon film to drape over the edge of the frame ensures that it will not slip off.



If the carbon has no cracks or holes, it will not break at this point. The film stretches itself over the hole with only a few unimportant wrinkles.



When the foil has dried, it is ready for use.



This work was supported by NSF and ONR.

Calibration of Surface Densities of Metal  
Films by Optical Transmittance

Mark Rhoads, John O. Stoner, Jr., and Stanley Bashkin  
Department of Physics, University of Arizona, Tucson, Arizona 85721

ABSTRACT

For evaporated metal coatings (Al, Cr, Cu, Au, Ag, Sn, and Ti) we have developed curves of optical transmittance vs surface density that can be used to estimate surface densities to within about  $\pm 20\%$ .

- - - - -

We have found that calibration curves of optical transmittance of carbon<sup>(1)</sup> and metal films are particularly useful in the preparation of beam-foil targets and ultraviolet filters. We have therefore developed such curves for a number of metals of use to us.

In order to produce such curves, microscope slides were cleaned and weighed, and then metal films were evaporated onto them by conventional techniques. The optical transmittances of the coated slides were then measured at  $\lambda$  5461Å, and the slides were re-weighed to determine the surface densities of the coatings. We found during this procedure that it was not possible to carry out accurate measurements with slides that had been coated with a soap-like parting agent, since these would lose weight upon being placed in vacuo.

Pressures in the vacuum system during evaporation were typically  $1 \times 10^{-5}$  torr. It is certain that all of our coating were contaminated either by oxide layers, burial of residual gas, and/or adsorption of active molecules. The curves indicate such effects by the extent of their non-reproducibility, most serious for the active species Ti, Al,

Cr, and less serious for the other metals. However, the conditions under which these layers were made are typical of those used in the preparation of conventional nuclear targets, and hopefully have some application to such targets.

We wish to acknowledge the cooperation of C. T. Tomizuka who made possible the weighing of our samples.

#### References

- 1) John O. Stoner, Jr., J. Appl. Phys. 40, 707 (1969).

See Also: I. S. McIntock and J. C. Orr, Chemistry and Physics of Carbon, P. L. Walker and P. A. Thrower, editors, Vol. II (Marcel Dekker 1973); John O. Stoner, Jr., and Stanley Bashkin, Proc. INTDS (1976); P. Maier-Komor, Proc. INTDS (1976).

This work was supported by NSF and ONR.

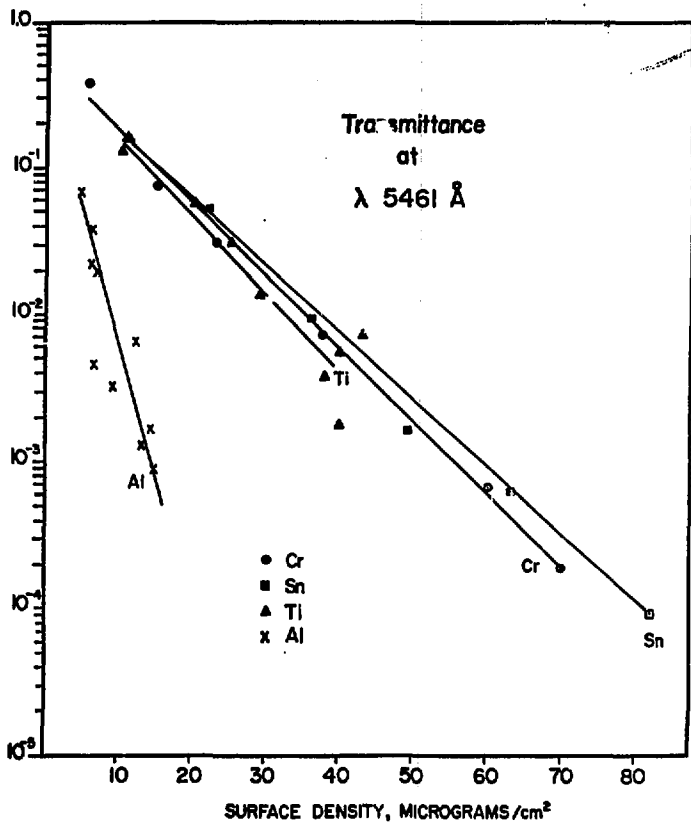


Figure 1. Calibration curves for Al, Cr, Sn, and Ti films deposited on microscope slides by vacuum evaporation.

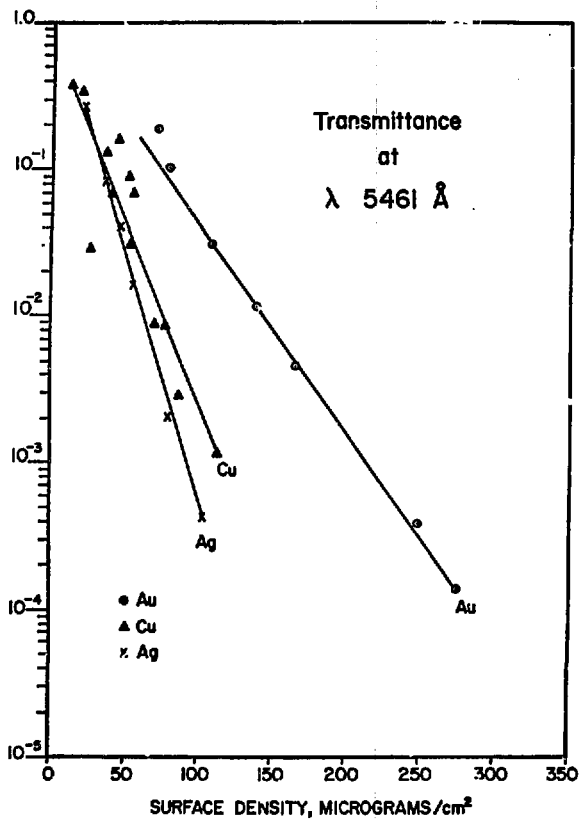


Figure 2. Calibration curves for Ag, Au, and Cu films deposited on microscope slides by vacuum evaporation.

Vacuum Tight  $^{208}\text{Pb}$  Foils

A. MEENS

Centre de Recherches Nucleaires

67037 Strasbourg Cedex , France

## ABSTRACT

Targets of  $^{208}\text{Pb}$  supported on bismuth grids were required as vacuum tight windows for nuclear physics measurements. The foils had to be pinhole free over a surface of  $0.5\text{ cm}^2$ . The fabrication of these pinhole free foils will be described in the first part of the paper. In the second part the results of some yield measurements, made in order to obtain the maximum number of targets from a given amount of isotope, will be given.

## I. FABRICATION OF PINHOLE FREE Pb FOILS

## A. Glass substrate and parting agent

Usually KCl is used as the parting agent for Pb films (Ref. 1) but if KCl and Pb are evaporated without any precautions, the films are full of pinholes (Table 1). All the trials described in the Table 1 were made with a tantalum boat covered with a tantalum screen to strain out projected matter. For each evaporation 3g of Pb was used. The glass slides were placed 15 cm above the boat. The film thickness was monitored with a quartz oscillator, and all of these evaporations were stopped at  $2\text{ mg/cm}^2$ .

The pinhole free films can be removed from the glass slides by floating them onto warm water. Our problem, however, was not yet completely solved, for we needed to glue these films onto a bismuth grid\*. After we tried unsuccessfully to glue the unsupported film, we tried to

---

\* Made in our laboratory by F. Kuntz . See the photograph in fig. 1.

glue the grid to the foil before the flotation step. In this case the film could not be removed from the slide. We finally resorted to evaporating onto Cu substrates.

## B. Copper substrates

The basic method is well-known and consists of evaporating Pb on a thin commercially available Cu foil ( $10 \mu$ ) which is later dissolved with Richard's solution\*\* to leave a self-supporting film. The flaw in this method is that the imperfections in the Cu foil will be reproduced on the Pb films. To reduce this effect, the Cu foil was treated with a direct glow discharge in Ar for about 1h just before the evaporation. The sputtering "leveled" the copper surface. By this method  $1.8 \text{ mg/cm}^2$  Pb foils without any pinholes over  $100 \text{ cm}^2$  were obtained.

The Pb-Cu film was glued (Pb side) on the bismuth grid with Eastman glue. The grid with the Pb-Cu was floated on Richard's solution and washed several times with distilled water. The gas filled target chamber with these supported Pb films as entrance windows lost about 1 torr (air) in 30 min.

## II. YIELD

To make the isotopic Pb targets we had only 200 mg of Pb, and we wanted to make several  $2 \text{ mg/cm}^2$  targets. From experience it is known that the best yield is obtained with a chimney boat at a small boat-substrate distance. However only one or two targets of the maximum thickness can be obtained (Table II), because of the inhomogeneity.

We decided to work at a boat-substrate distance of 5 cm, and in order to determine which type of boat would be the most suitable, we made maps which show the thickness distribution for boats of chimney form (Table III) and central hole form (Table IV).

For each map 200 mg of Pb (nat.) was evaporated on a copper substrate. To protect the substrate from projected matter, and at the same time

---

\*\* To make 1 liter, 100 g  $\text{Cl}_3\text{C}_2\text{OOH}$  and  $500 \text{ cm}^3 \text{ NH}_4\text{OH}$  solution are mixed.

to have a minimum loss of material, the shield placed between the boat and the substrate at the beginning of the evaporation was made of glass, and removed when it began to darken. The areal density of individual squares was determined by weighing each square after Cu dissolution.

#### ACKNOWLEDGMENTS

The author would like to thank J. Gerber for his interest and A. Pape for aid especially during the manuscript preparation.

#### REFERENCES

1. D. Ramsey, Int. Conf. of the Nuclear Target Development Society, Chalk River Nuclear Laboratories, 1974.
2. L. Holland, Vacuum Deposition of Thin Films (Chapman and Hall, Ltd., London, 1961) p. 72.

TABLE I

Summary of information concerning the fabrication of Pb foils.

Glass slides				Parting agent	Results
Cleaning	Protective film	Glow discharge	Heating		
ultra-sound	none	none	none	$50 \mu\text{g}/\text{cm}^2$ evaporated KCl c)	full of pinholes - easy stripping
ultra-sound	none	none	none	Teepol applied with a Kleenex	full of pinholes - easy stripping
ultra-sound	none	10 min indirect glow discharge a)	none	Teepol applied with a Kleenex	some pinholes - difficult stripping
ultra-sound	10% mineral oil, 90% toluene (Ref. 2)	1h direct glow discharge b)	none	none	a few pinholes - stripping impossible
sulfochromic acid bath	10% mineral oil, 90% toluene	1h direct glow discharge	none	none	a few pinholes - stripping impossible
ultra-sound	10% mineral oil, 90% toluene	1h direct glow discharge	at $200^\circ\text{C}$	none	no pinholes - stripping impossible
ultra-sound	Teepol	1h direct glow discharge	at $200^\circ\text{C}$	about $50 \mu\text{g}/\text{cm}^2$ evaporated KCl	a few pinholes - stripping possible on warm water
ultra-sound	Teepol	1h direct glow discharge	at $200^\circ\text{C}$	about $50 \mu\text{g}/\text{cm}^2$ KCl evaporated onto a cold substrate	1 or 2 pinholes on the entire glass slide ( $2\text{x}6 \text{cm}^2$ ) stripping on warm water possible.

- a) Indirect glow discharge is the term we use when the substrate is grounded and the positive high voltage connected to an electrode. This is in opposition to a direct glow discharge when the substrate is connected to a negative high voltage.
- b) The discharge was to remove the protective film on the glass slides in order to have a very clean surface.
- c) The KCl must be preheated separately under vacuum before being put into the boat. This eliminates projected particles during evaporation.

TABLE II

Data on Pb target thickness and homogeneity as a function of boat type and distance.

Type of boat	Boat-substrate distance ( cm )	Thickest target ( $\mu\text{g}/\text{cm}^2$ )	Thickness of a target at 5 cm from the central axis, in percentage of the central target
chimney	1.5	160	( a spot of 1.5 cm diameter - enough for one target)
chimney	5	38	5%
central hole	5	22	20%
central hole	10	2.5	43%
central hole	15	0	80%

TABLE III

Areal density map for 200 mg Pb evaporated from a chimney boat (S19C Mathis Co.) onto a  $8 \times 8$  cm<sup>2</sup> Cu foil. The upper number in the small squares (0.64 cm<sup>2</sup>) are the average thickness in mg/cm<sup>2</sup>. The lower numbers are target thicknesses normalized to 100% for the thickest target.

		0.50 6%	0.75 10%	0.92 12%	1.09 14%	1.03 13%	0.87 11%	0.67 9%	
	0.39 5%	0.84 11%	1.33 17%	1.73 23%	1.90 25%	1.82 24%	1.48 20%	1.15 15%	0.75 10%
0.62 8%		1.30 17%	2.10 27%	2.80 37%	3.50 46%	3.25 43%	2.43 32%		1.06 14%
0.62 8%		2.00 26%	3.33 44%	5.15 68%	5.92 78%	4.32 57%	4.12 54%	2.65 35%	
0.90 12%	1.10 14%	2.96 39%	3.80 50%		5.20 68%	3.68 48%	3.20 42%		1.78 23%
		1.13 15%	3.15 41%	7.60 100%	6.08 80%	5.93 78%	3.82 50%	2.21 29%	
	1.60 21%		3.65 48%	4.50 59%	4.60 60%	3.50 46%	2.00 26%	1.60 21%	0.68 9%
0.62 8%	0.85 11%	1.35 18%	1.76 23%	1.98 26%	2.03 27%	1.38 18%	1.03 14%		
		0.70 9%	0.98 13%	1.23 16%	1.28 17%	1.15 15%	1.03 14%	0.82 11%	
			0.67 9%	0.86 11%	0.79 10%	0.60 8%			

TABLE IV

The same as for Table III, but a central hole boat (type ME4 Mathis Co.).

	0.55 12%	0.78 16%	1.03 22%	1.09 23%	1.18 25%	0.98 21%	0.66 14%	0.59 12%	
0.66 12%	0.70 15%	1.32 28%	1.65 35%	1.90 40%	1.85 39%	1.25 26%	1.09 23%		
	1.10 23%	1.60 34%	2.60 55%	2.78 58%	2.25 47%	2.21 46%	2.20 46%	1.09 23%	0.70 15%
0.75 16%	1.51 32%		3.02 63%	3.84 81%	3.59 75%	2.93 62%	2.10 44%	1.50 32%	0.90 19%
1.01 21%	1.58 33%	2.70 57%	3.80 80%		4.66 98%	3.43 72%	2.30 48%	1.75 37%	1.20 25%
0.93 20%	1.76 37%	2.60 55%	3.80 80%	4.14 87%	4.76 100%	3.70 78%	2.59 54%	1.87 39%	
1.10 23%	1.60 34%	2.56 54%	3.40 71%	4.08 86%	4.07 86%	3.35 70%	2.59 54%	1.60 34%	1.25 26%
0.86 18%	1.22 26%	2.00 42%	2.40 50%	2.60 55%	2.73 57%	2.58 54%	1.90 40%	1.30 27%	0.90 19%
0.70 15%	0.96 20%		1.78 37%	2.03 43%	2.14 45%	1.87 39%	1.42 30%		
	0.70 15%	0.92 19%	1.20 25%	1.35 28%	1.45 30%	1.29 27%	1.10 23%	0.83 17%	

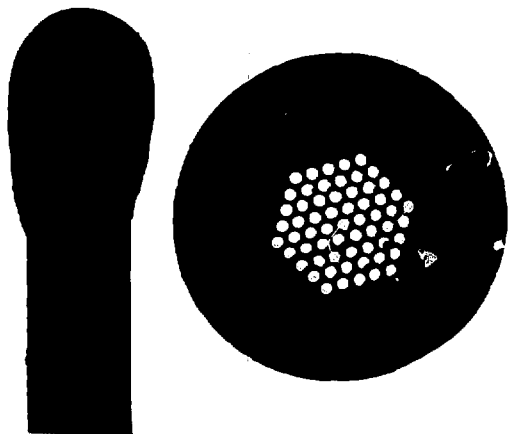


Figure 1. Photograph of the bismuth grid magnified five times. The tip of a safety match is shown for comparison.

SIX ANNUAL CONFERENCE  
INTERNATIONAL NUCLEAR TARGET DEVELOPMENT SOCIETY

Lawrence Berkeley Laboratory

October 19-21, 1977

Registrants

H. L. ADAIR  
Isotopic Research Materials Lab.  
Oak Ridge National Laboratory  
Oak Ridge, Tennessee 37830

DON BLISS  
Lawrence Berkeley Laboratory  
Building 25  
Berkeley, California 94720

CLAUDE ELLSWORTH  
Lawrence Berkeley Laboratory  
Building 88  
Berkeley, California 94720

IRVING FEIGENBAUM  
Brookhaven National Laboratory  
Building 901A, Tandem Van De Graff  
Upton, L.I., New York 11973

HELMUT FOLGER  
GSI, Gesellschaft für  
Schwerionenforschung Planck-Str 1  
D-61 Darmstadt, West Germany

TOM GEF  
Lawrence Berkeley Laboratory  
Building 25  
Berkeley, California 94720

JUDITH GURSKY  
Los Alamos Scientific Laboratory  
MS-458, P. O. Box 1663  
Los Alamos, New Mexico 87545

DON HAMMOND  
Medi-Physics, Inc.  
5801 Christie Avenue  
Emeryville, California 94608

JOE HEAGNEY  
Micro Matter Company  
197-34th East  
Seattle, Washington 98112

JOANNE HEAGNEY  
Micro Matter Company  
197-34th East  
Seattle, Washington 98112

SALLY HOFFMAN  
Nuclear Physics Shop  
University of Washington  
Seattle, Washington 98195

FRANK KARASEK  
Argonne National Laboratory  
MSD 212 H118  
Argonne, Illinois 60439

KURT KENNEDY  
Lawrence Livermore Laboratory  
L-332  
Livermore, California 94550

EDWARD KOBISK  
Isotopic Research Materials Lab.  
Oak Ridge National Laboratory  
Oak Ridge, Tennessee 37830

CHARLES KRIEGER  
Argonne National Laboratory  
Building 326 B002  
Argonne, Illinois 60439

BILL LOZOWSKI  
Indiana University  
Cyclotron Facility, Milo B.  
Sampson Lane  
Bloomington, Indiana 47401

R. H. LEONARD  
Florida State University  
Nuclear Research Building  
Tallahassee, Florida 32306

JEROME LERNER  
Argonne National Laboratory  
CHM 200, MC19  
Argonne, Illinois 60439

ANTHONY LUONGO  
Massachusetts Institute of  
Technology  
6 Vassar Street, 58023B  
Cambridge, Massachusetts 02139

RICHARD J. LEITE  
TRW Systems Group  
Inst. Systems Department  
One Space Park  
Redondo Beach, California 90278

RONALD LOUGHEED  
Lawrence Livermore Laboratory  
P. O. Box 808, L232  
Livermore, California 94550

H. J. MEIER  
Sektion Physik, der  
Universität München  
8046 Garching  
Coulombwall 1, West Germany

PETER MAIER-KOMOR  
Techn. Universität München  
Physik Department  
D 8046 Garching  
West Germany

T. L. MORGAN  
Manchester University  
Schuster Lab., Physics Department  
Manchester M13 9PL, England

DON RAMSEY  
Stanford University  
Physics Department  
Stanford, California 94305

DAN RIEL  
State University of New York  
Physics Department  
Stonybrook, L.I., New York 11790

M. A. SAETTEL  
Lab. de Spectrometrie Nucleair  
23 Rue du Loess  
67037 - Strasbourg Cedex  
France

GORDON STEERS  
Lawrence Berkeley Laboratory  
Building 25  
Berkeley, California 94720

J. D. STINSON  
National Research Council of Canada  
Building M-35 Room X-23  
Montreal Road  
Ottawa, Ontario, Canada K1A 0S1

KARL SCHEU  
Lawrence Berkeley Laboratory  
Building 25  
Berkeley, California 94720

GEORGE THOMAS  
Argonne National Laboratory  
Physics Division, 203, R154  
Argonne, Illinois 60439

W. TIETSCH  
Institut f. Kernphysik  
August-Euler-Str. 6  
D-6000 Frankfurt/M-90 West Germany

HERMANN WIRTH  
Max-Planck-Institut f. Kernphysik,  
Heidelberg  
Postfach 103980  
D6900 Heidelberg, Germany

MARVIN WILLIAMSON  
Lawrence Livermore Laboratory  
P. O. Box 808  
Livermore, California 94550